Science Bulletin 69 (2024) 3005–3035

Contents lists available at ScienceDirect

Science Bulletin

journal homepage: www.elsevier.com/locate/scib

Article

Combination and summary of ATLAS dark matter searches interpreted in a 2HDM with a pseudo-scalar mediator using 139 fb^{-1} of $\sqrt{s} = 13$ TeV pp collision data

The ATLAS Collaboration *

ARTICLE INFO

Article history:
Received 13 June 2023
Received in revised form 3 July 2023
Accepted 27 May 2024
Available online 3 July 2024

Keywords:
High-energy physics
Proton-proton
Beyond Standard Model
Dark matter

ABSTRACT

Results from a wide range of searches targeting different experimental signatures with and without missing transverse momentum ($E_{\mathrm{T}}^{\mathrm{miss}}$) are used to constrain a Two-Higgs-Doublet Model (2HDM) with an additional pseudo-scalar mediating the interaction between ordinary and dark matter (2HDM+a). The analyses use up to 139 fb^{-1} of proton–proton collision data at a centre-of-mass energy $\sqrt{s} = 13$ TeV recorded with the ATLAS detector at the Large Hadron Collider during 2015–2018. The results from three of the most sensitive searches are combined statistically. These searches target signatures with large $E_{\mathrm{T}}^{\mathrm{miss}}$ and a leptonically decaying Z boson; large $E_{\mathrm{T}}^{\mathrm{miss}}$ and a Higgs boson decaying to bottom quarks; and production of charged Higgs bosons in final states with top and bottom quarks, respectively. Constraints are derived for several common and new benchmark scenarios in the 2HDM+a.

1. Introduction

The existence of dark matter (DM) is supported by a plethora of astrophysical measurements, including the rotational speed of stars in galaxies [1–3], precision measurements of the cosmic microwave background [4,5], and gravitational lensing measurements [6–8]. However, little is known of its particle nature, which remains one of the central questions in particle physics. The particle content of the Standard Model (SM) is insufficient to explain these observations; thus, a satisfactory dark matter candidate is a strong consideration in many Beyond-the-SM (BSM) extensions.

Complementary probes of DM are underway in several areas, from indirect searches for the products of dark matter annihilation or decay [9–17], searches for the direct detection of DM scattering elastically off nuclei and electrons [18–33], and recent searches using gravitational-wave interferometers [34,35], to searches for the production of dark matter at collider experiments, such as the ATLAS experiment [36] at the Large Hadron Collider (LHC) [37]. General purpose particle physics experiments are sensitive to a wide variety of potential dark matter candidates, such as axions [38–42] or Weakly Interacting Massive Particles (WIMPs) [43]. The motivation for the latter arises from a paradigm known as the WIMP miracle [43]. Assuming DM to be produced via the freeze-out mechanism, the relic density of non-relativistic matter in the early universe [44], measured in data from the WMAP [4] and Planck [5] missions, can be achieved when the DM mass is close to the electroweak scale and when the DM coupling to SM particles is of the order of the weak interaction. Consequently, WIMP DM particles could be produced and studied at the LHC experiments.

A particular strength of collider searches lies in the fact that the high-energy collisions of SM particles could not only produce DM directly under controlled experimental conditions but also provide access to particles mediating the interactions between DM and the SM sector. A mediator produced in a collision could decay into DM particles, which themselves could not be detected, resulting in a momentum imbalance in the plane tranverse to the collision axis, referred to as missing transverse momentum $\vec{p}_{\mathrm{T}}^{\mathrm{miss}}$, with magnitude $E_{\mathrm{T}}^{\mathrm{miss}}$. Alternatively, a mediator could decay back into SM particles, from which its properties could be reconstructed.

DM searches at the LHC explore both these avenues in the quest to solve the puzzle of DM. Invisible mediator decays can be detected only if the mediator is produced in association with another particle or particles, for example, a quark or gluon from initial-state radiation that results in a hadronic jet (j), leading to a characteristic $E_{\mathrm{T}}^{\mathrm{miss}} + j$ signature [45,46]. These signatures are

* Authors are listed at the end of this paper.

https://doi.org/10.1016/j.scib.2024.06.003
2095-9273/

referred to as $E_{\mathrm{T}}^{\mathrm{miss}}+X$ signatures in the following. Visible mediator decays allow for the reconstruction of the mediator particle from its decay products, for example, in the context of resonance searches, if the mediator is produced in the s-channel [47–51].

The searches mentioned above are traditionally interpreted in the context of simplified models of DM, which rely on a minimal set of new particles and interactions. The most commonly used among these simplified models postulate the existence of a single fermionic DM particle and a single mediator, which, depending on the model, may be a vector, axial-vector, scalar, or pseudo-scalar particle [52–54]. The models are characterised by a minimal set of free parameters, typically the masses and couplings of the DM and mediator particles. While this facilitates the definition of benchmark scenarios that can be used to compare results between experiments, the theoretical incompleteness of simplified models can limit the range of collider signatures realised.

A more complete benchmark model with a rich collider phenomenology is explored in this paper, known as the Two-Higgs-Doublet Model (2HDM) plus pseudo-scalar mediator a, denoted 2HDM+a [55]. In this model, the scalar sector of the SM is extended by an additional complex doublet, an extension that is well motivated by theories beyond the SM addressing, for example, the electroweak hierarchy problem [56–61], baryogenesis [62–68], or the strong CP problem [69]. The model also contains a pseudo-scalar mediator which couples to a fermionic dark matter candidate, χ.

The 2HDM+a is a simple, ultra-violet-complete (UV-complete), gauge-invariant, and renormalisable extension of the pseudo-scalar mediator simplified models [52,70]. A pseudo-scalar mediator is chosen primarily due to the reduced constraints from direct detection experiments, and its ability to reproduce the observed relic abundance across much of the model parameter space, making LHC searches particularly important. Another reason the 2HDM+a is of high interest for the LHC community is the fact that it predicts a wide range of collider signatures with a complex interplay across the model parameter space, including signatures not predicted in the commonly used simplified models. It is promoted by the LHC Dark Matter Working Group as a complete benchmark model [71].

In total, the 2HDM+a adds five new states to the SM scalar sector: a scalar H, pseudo-scalar A, charged Higgs bosons $H^{\pm}$, and the pseudo-scalar mediator a. After the discovery of the Higgs boson h by the LHC experiments [72,73], the exploration of the scalar sector of the SM is another high experimental priority. The results of searches for additional (pseudo-) scalar bosons constrain this model, thus complementing constraints from searches targeting $E_{\mathrm{T}}^{\mathrm{miss}}+X$ signatures.

A comprehensive synopsis is presented of the diverse set of collider signatures of the 2HDM+a benchmark explored through improved ATLAS searches using 139 fb^{-1} of LHC Run 2 data. Compared with earlier summaries, additional signatures are considered, the individual analysis exclusions are improved and a wider range of interpretations are considered. In particular, a statistical combination is performed of three of the most sensitive analyses: a search for large $E_{\mathrm{T}}^{\mathrm{miss}}$ produced in association with a leptonically decaying Z boson, $E_{\mathrm{T}}^{\mathrm{miss}}+Z(\ell\ell)$ [74], a search for large $E_{\mathrm{T}}^{\mathrm{miss}}$ produced in association with a SM Higgs boson decaying into $b\bar{b}$, $E_{\mathrm{T}}^{\mathrm{miss}}+h(b\bar{b})$ [75], and a search for associated production of a top and a bottom quark with a charged Higgs boson decaying into a top and a bottom quark, $tbH^{\pm}(tb)$ [76]. For the first time, constraints from searches targeting the $E_{\mathrm{T}}^{\mathrm{miss}}+j$ [45], $E_{\mathrm{T}}^{\mathrm{miss}}+tW$ [77], $E_{\mathrm{T}}^{\mathrm{miss}}+h(\tau\tau)$ [78], and $h\to aa\to f\bar{f}f'\bar{f}'$ [79–83] signatures are included in the summary, besides constraints from searches targeting the $E_{\mathrm{T}}^{\mathrm{miss}}+h(\gamma\gamma)$ [84], $t\bar{t}t\bar{t}$ [85], and $h\to$ invisible [86] signatures.

In addition to the usual gluon–gluon (gg) initiated processes, $b\bar{b}$-initiated production is considered for all relevant signatures, which is dominant in some regions of the model parameter space. A full set of the benchmark scenarios recommended in Ref. [71] is featured, with an updated definition for the interpretation varying the DM mass motivated by the increased sensitivity of the searches. Finally, a new scenario is introduced, following Ref. [87], to showcase possibilities for lighter pseudo-scalar mediators, and the interplay of light resonance searches with the $E_{\mathrm{T}}^{\mathrm{miss}}$ signatures.

A previous ATLAS summary paper [88] included constraints on the 2HDM+a benchmark from dark matter searches using 36 fb^{-1} of $\sqrt{s}=13$ TeV proton–proton (pp) collision data [89–91]. Constraints on the model have also been placed by the CMS Collaboration using searches in the $E_{\mathrm{T}}^{\mathrm{miss}}+h(b\bar{b})$ [92] and $E_{\mathrm{T}}^{\mathrm{miss}}+Z(\ell\ell)$ [93] final states with 137 fb^{-1} of LHC Run 2 data.

The paper is organised as follows: In Section 2, the theoretical set-up, benchmark model and choice of scenarios are discussed in detail; in Section 3, the ATLAS detector is described; details of the signal and background modelling are given in Section 4. In Section 5, brief overviews of the experimental signatures and the analyses targeting them are described; details of systematic uncertainties and the statistical combination of analyses are given in Sections 6 and 7; the combined results and summaries of the experimental constraints can be found in Section 8; a summary of the findings is given in Section 9.

2. Theoretical framework

The benchmark model used in this publication builds on the assumption of the existence of a second complex Higgs doublet, which is postulated in various UV-complete theories with an extended Higgs sector. The 2HDM sector is assumed to have a CP-conserving potential and a softly broken $\mathbb{Z}_2$ symmetry [94]. After electroweak symmetry breaking, the 2HDM contains five Higgs bosons: a lighter CP-even boson, h, a heavier CP-even boson, H, a CP-odd boson, A, and two charged bosons, $H^{\pm}$. The 2HDM coupling structure is chosen to be of type-II [94] and the alignment and decoupling limits are assumed, so that the lighter CP-even state h can be identified with the SM Higgs boson. In addition, the model includes a fermionic DM particle χ and a pseudo-scalar (CP-odd) mediator a with Yukawa-like couplings to both the SM fermions and the Dirac DM particle χ, thus allowing for interactions between DM and the SM sector. The mediator mixes with the pseudo-scalar A of the 2HDM sector with mixing angle θ.

The 2HDM+a has a particularly rich phenomenology, illustrated by the range of signatures shown in Figs. 1–3, and this paper brings together an unprecedentedly large number of them. The signatures can be grouped into those involving invisible and visible mediator decays, with the former being referred to as $E_{\mathrm{T}}^{\mathrm{miss}}+X$ signatures in the following. At the LHC, the dominant production mode for the majority of signatures is gg-initiated production. In Fig. 1, Feynman diagrams for the relevant signatures arising from gg-initiated production in the 2HDM+a are summarised. The $E_{\mathrm{T}}^{\mathrm{miss}}+Z$ and $E_{\mathrm{T}}^{\mathrm{miss}}+h$ signatures can be resonantly produced (Fig. 1a), and non-resonantly (Fig. 1b), making them particularly relevant in the 2HDM+a interpretation. Additional signatures arising from gg-initiated production are the $E_{\mathrm{T}}^{\mathrm{miss}}$+$j$ signature (Fig. 1c), resonant A/H production with decay into $t\bar{t}$ or $b\bar{b}$ (Fig. 1d), $t\bar{t}$- or $b\bar{b}$-associated resonant A/H production, leading to $t\bar{t}t\bar{t}$, $b\bar{b}b\bar{b}$, $t\bar{t}b\bar{b}$, $E_{\mathrm{T}}^{\mathrm{miss}}+t\bar{t}$, or $E_{\mathrm{T}}^{\mathrm{miss}}+b\bar{b}$ signatures (Fig. 1d), tb-associated production of a charged Higgs boson decaying into tb, $tbH^{\pm}(tb)$ (Fig. 1e), and production of a SM Higgs boson decaying

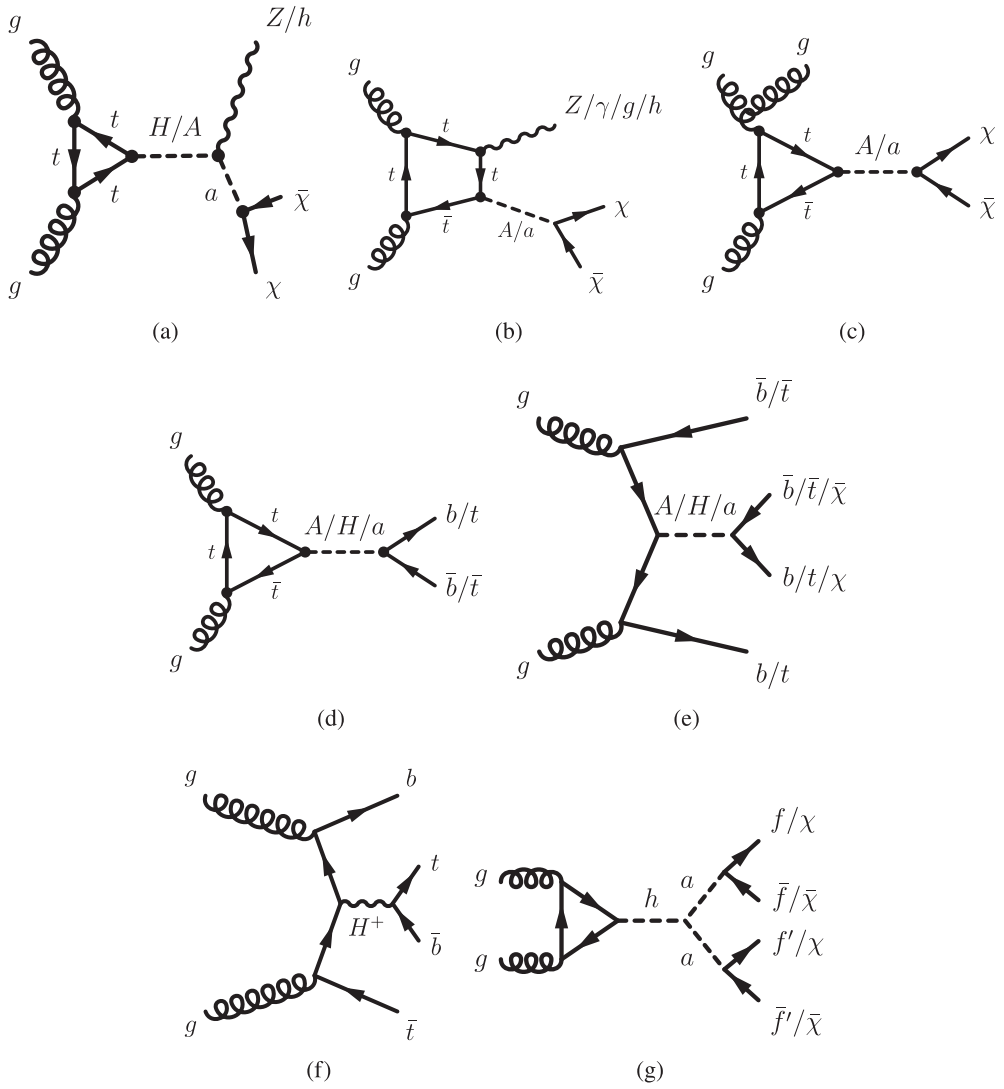

Fig. 1. Representative Feynman diagrams for the dominant gluon-induced production and decay modes in the 2HDM+*a*. (a, b) resonant and non-resonant production of the $E_{\mathrm{T}}^{\mathrm{miss}}+Z$ and $E_{\mathrm{T}}^{\mathrm{miss}}+h$ signatures, (c) production of the $E_{\mathrm{T}}^{\mathrm{miss}}+j$ signature, (d) resonant A/H production with decay into $t\bar{t}$ or $b\bar{b}$, (e) $t\bar{t}$ or $b\bar{b}$ associated resonant A/H production, leading to $t\bar{t}t\bar{t}$, $b\bar{b}b\bar{b}$, $t\bar{t}b\bar{b}$, $E_{\mathrm{T}}^{\mathrm{miss}}+t\bar{t}$, or $E_{\mathrm{T}}^{\mathrm{miss}}+b\bar{b}$ signatures, (f) $tbH^{\pm}(tb)$ production, and (g) production of a SM Higgs boson decaying into a pair of mediators *aa* with subsequent decays into fermions or DM.

into a pair of mediators *aa* with subsequent decays into fermions or DM (Fig. 1f). Production from $b\bar{b}$ initial states for the $E_{\mathrm{T}}^{\mathrm{miss}}+Z$, $E_{\mathrm{T}}^{\mathrm{miss}}+h$, and $E_{\mathrm{T}}^{\mathrm{miss}}+j$ signatures is shown in Fig. 2. Finally, the leading Feynman diagrams for the $E_{\mathrm{T}}^{\mathrm{miss}}+tW$ signature are shown in Fig. 3. The interplay between these signatures is highly dependent on the 2HDM+*a* model parameters.

The phenomenology of the model is fully determined by 14 independent parameters: the masses of the Higgs bosons h, H, A, and $H^{\pm}$; the mass of the mediator a; the mass of the DM particle χ; the Yukawa coupling strength between the mediator and the DM particle, g_{χ}; the electroweak vacuum expectation value (VEV), v; the ratio of the VEVs of the two Higgs doublets, $\tan\beta$; the mixing angles of the CP-even and CP-odd weak eigenstates, α and θ, respectively; the quartic coupling λ_3 of the pure 2HDM potential term and the two quartic couplings of the potential terms connecting the doublet and singlet fields λ_{P1} and λ_{P2}. The values of some of these parameters are heavily constrained by both electroweak and flavour measurements and phenomenological considerations, such as the requirement that the Higgs potential is stable [55,71]. Further parameter choices are driven by the desire to simplify the phenomenology of the model and reduce the space of independent parameters to be scanned by experimental searches. A summary of the parameter choices and the benchmark scenarios shown in this publication is given in the following. A detailed description of the 2HDM+*a* benchmark scenarios recommended by the LHC Dark Matter Working Group is given in Ref. [71].

The following parameter settings are common to all benchmark scenarios described in Section 8. The coupling g_{χ} is set to unity with a negligible effect on the shapes of the kinematic distributions of interest. The alignment and decoupling limits are assumed, hence $m_h = 125$ GeV, $v = 246$ GeV, and $\cos(\beta-\alpha) = 0$. The quartic coupling $\lambda_3 = 3$ is chosen to ensure the stability of the Higgs potential for the choice of the masses of the heavy Higgs bosons. The latter are fixed to the same value ($m_A = m_H = m_{H^{\pm}}$). The choice $m_H = m_{H^{\pm}}$ is made to evade the constraints from electroweak precision measurements [55], while the additional requirement $m_A = m_H$ is made to reduce the number of independent model

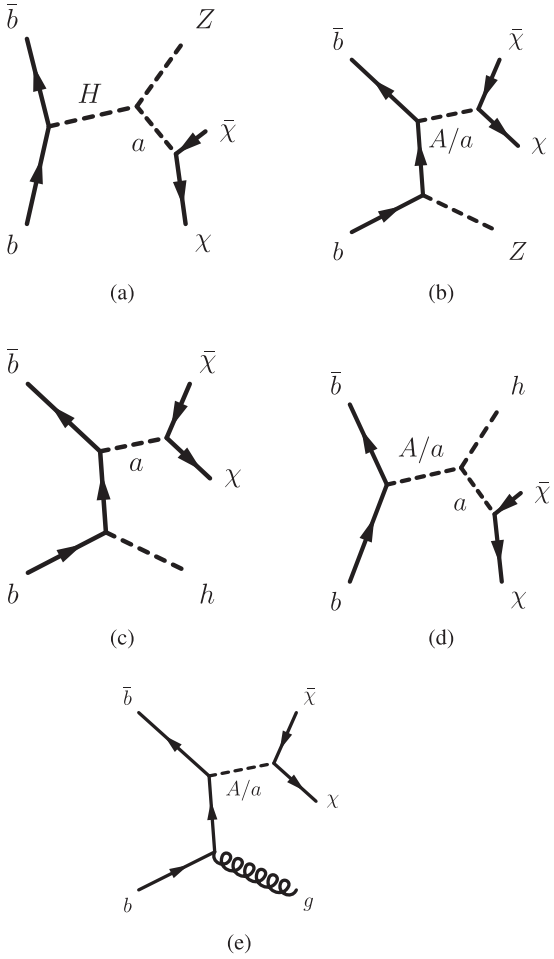

Fig. 2. Representative Feynman diagrams for the $b\bar{b}$-initiated production of (a, b) the $E_{\mathrm{T}}^{\mathrm{miss}} + Z$ signature, (c, d) the $E_{\mathrm{T}}^{\mathrm{miss}} + h$ signature, and (e) the $E_{\mathrm{T}}^{\mathrm{miss}}$+$j$ signature in the 2HDM+a.

parameters [71].[1] The other quartic couplings are also set to 3 to maximise the trilinear couplings between the CP-odd and the CP-even neutral states.

After these considerations, five free parameters remain: the mass of the heavy Higgs bosons, $m_A = m_H = m_{H^{\pm}}$; the mass of the pseudo-scalar mediator, m_a; the mass of the fermionic DM particle, m_χ; the sine of the mixing angle θ between the two CP-odd states a and A, $\sin\theta$; and the VEV ratio, $\tan\beta$.

The constraints on the model are evaluated for some representative benchmark scenarios, in which one or two of the free parameters are varied while the others are kept at fixed values. These benchmark scenarios, summarised in Table 1, are defined with the intention to highlight the diverse phenomenology of the 2HDM+a and to study the interplay and complementarities between different experimental signatures.

2.1. Scenario 1: Exploration of two m_a–m_A planes

Constraints are evaluated as a function of the two pseudo-scalar masses m_a and m_A to highlight the complex dependence of the

[1] The mass differences $|m_A - m_H| \lesssim 200$ GeV are consistent with constraints from electroweak precision measurements and have the largest impact on the $E_{\mathrm{T}}^{\mathrm{miss}} + Z$ and $E_{\mathrm{T}}^{\mathrm{miss}} + h$ signatures due to the possibility of opening up the decay $H \to AZ$, which is not allowed in the mass-degenerate scenario recommended by the LHC Dark Matter Working Group. For further discussions of scenarios with non-zero $|m_A - m_H|$ see Refs. [55,71].

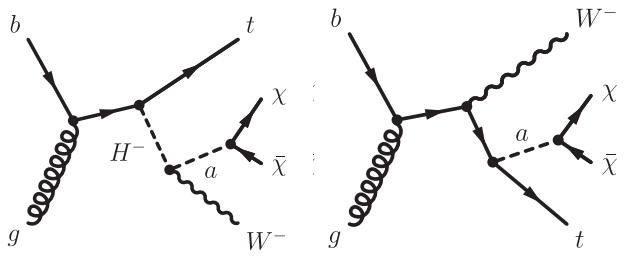

Fig. 3. Representative Feynman diagrams for the dominant production modes for the $E_{\mathrm{T}}^{\mathrm{miss}} + tW$ signature in the 2HDM+a.

2HDM+a phenomenology on the pseudo-scalar mass hierarchy, which determines the production and decay modes that are kinematically accessible and favoured. The value of $\tan\beta$ is fixed to 1.0, favouring couplings to up-type quarks, most notably top quarks. Two choices of the $a - A$ mixing angle, $\sin\theta = 0.35$ and $\sin\theta = 0.7$, are explored. These scenarios correspond to low and almost maximal mixing, respectively, between the pseudo-scalar A belonging to the extended Higgs sector and the pseudo-scalar a mediating the interaction with DM.

2.2. Scenario 2: Exploration of two m_A–$\tan\beta$ planes

The parameters m_A and $\tan\beta$ are varied simultaneously for the two choices of the mixing angle $\sin\theta$. The pseudo-scalar mass is fixed to a value of 250 GeV, such that on-shell decays of the mediator into a pair of top quarks ($t\bar{t}$) are kinematically forbidden. This means that the branching ratio for the invisible mediator decay $a \to \chi\chi$ can be as large as 100%. This benchmark scenario highlights the dependence of the couplings of the pseudo-scalar A on the value of $\tan\beta$ as a function of its mass. Given the type-II Yukawa structure of the 2HDM + a, low values of $\tan\beta$ correspond to a preferred coupling of A (and a) to up-type quarks, while higher values of $\tan\beta$ imply stronger couplings to down-type quarks and charged leptons. This benchmark scenario is evocative of the mass–$\tan\beta$ parameterisation used to summarise constraints on type-II 2HDMs, such as the hMSSM, a Minimal Supersymmetric extension of the SM with a lighter scalar state at a mass of 125 GeV [95]. It also allows an exploration of the interplay between gg-initiated, top-loop induced and $b\bar{b}$-initiated production modes (see below).

2.3. Scenario 3: Exploration of two m_a–$\tan\beta$ planes

This scenario is similar to Scenario 2, with the difference that the mediator mass m_a is varied instead of the mass of the pseudo-scalar m_A, which is fixed to a value of 600 GeV. This means that decays of the pseudo-scalar A into $t\bar{t}$ are kinematically possible and favoured at low values of $\tan\beta$. The choice of m_A is motivated by constraints on the mass of the charged Higgs boson ($m_{H^{\pm}} = m_A$) derived from precision measurements of B-meson decays [55,96]. Similarly to the previous scenarios, two choices of the $a - A$ mixing angle, $\sin\theta = 0.35$ and $\sin\theta = 0.7$, are studied.

2.4. Scenario 4: Variation of the mixing parameter $\sin\theta$

Constraints are evaluated as a function of the $a - A$ mixing parameter $\sin\theta$. This benchmark scenario highlights the interplay between the $E_{\mathrm{T}}^{\mathrm{miss}} + X$ signatures, in particular $E_{\mathrm{T}}^{\mathrm{miss}} + Z$ and $E_{\mathrm{T}}^{\mathrm{miss}} + h$, which arise from invisible mediator decays, and signatures that probe visible mediator decays. This is due to the strong

$\sin\theta$ dependence of the couplings g_{Aha} ($g_{Aha} \propto \sin\theta\cos\theta$) and g_{HZa} ($g_{HZa} \propto \sin\theta$), which affect $E_{\mathrm{T}}^{\mathrm{miss}} + h$ and $E_{\mathrm{T}}^{\mathrm{miss}} + Z$ production in the 2HDM+a (see Figs. 1a and b), and the coupling $g_{at\bar{t}}$, which plays a dominant role in the leading $E_{\mathrm{T}}^{\mathrm{miss}} + X$ production modes ($g_{at\bar{t}} \propto \sin\theta$) (see Fig. 1). As a consequence, for $\sin\theta \to 0$, the sensitivity of the $E_{\mathrm{T}}^{\mathrm{miss}} + X$ signatures vanishes.

2.5. Scenario 5: Variation of the DM mass m_χ

While the value of m_χ has a limited impact on the sensitivity of collider searches for $m_\chi < m_a/2$, it has a strong effect on cosmological parameters, such as the relic density, and on the sensitivity of direct and indirect detection experiments. This benchmark scenario therefore provides a basis for comparing the sensitivity of collider searches to those of non-collider experiments and cosmological observations in the context of the 2HDM+a. Only m_χ is varied, while the other free parameters are fixed to the following values: $\sin\theta = 0.35, m_A = 600$ GeV, $m_a = 400$ GeV, and $\tan\beta = 1.0$. The choice of the two mass parameters differs from that in the equivalent benchmark scenario described in Ref. [71] and explored in a previous ATLAS publication [88], as the latter is fully excluded by the searches discussed in this publication.

2.6. Scenario 6: Exploration of a m_a–m_χ plane

This scenario serves to illustrate the interplay between searches for invisible and exotic decays of the light Higgs boson h in the 2HDM+a. Values of $\sin\theta = 0.35$ and $\tan\beta = 1.0$ are chosen for consistency with the other benchmark scans, while a higher value $m_A = 1200$ GeV is chosen to satisfy the constraint on the coupling g_{haa} from measurements of the total Higgs boson decay width [87]. This is a powerful constraint on the low-m_a region ($m_a < m_h/2$), satisfied only by a relatively narrow range of m_A, for given values of the $\sin\theta, \tan\beta$ and quartic couplings λ.

2.7. Additional parameter choices

In all benchmark scenarios other than Scenarios 5 and 6, $m_\chi = 10$ GeV is chosen. This value ensures a sizeable branching ratio for the decay $a \to \chi\bar{\chi}$ for all values of $m_a > 100$ GeV that are considered. As shown in Section 8.5, the choice of m_χ has a negligible impact on the sensitivity of the searches considered in this publication for $m_\chi < m_a/2$. Thus it is possible to match the observed relic density across a wide range of model parameter space through an appropriate choice of m_χ, without impact on the experimental signatures.

In choosing the ranges for the parameters that are varied in a given benchmark scenario, various theoretical considerations are taken into account. First, in some regions of the probed parameter space, the scalar potential is not bounded from below for large values of m_A. For example, in Scenario 1a, this is the case for $m_A \gtrsim 1250$ GeV ($m_A \gtrsim 1550$ GeV) for $m_a = 100$ GeV ($m_a = 1000$ GeV). However, these constraints can be relaxed substantially if the quartic couplings take a value closer to the perturbative limit or in more general 2HDMs containing additional couplings as discussed in Refs. [55,71,97]. Hence these should not be understood as strong limitations on the validity of the model predictions that were used to derive the exclusion contours. Next, it is worth noting that, given these parameter choices, the aah coupling exceeds the unitarity limit of 4π for large values of m_A. For example, for the mentioned parameter choices $\sin\theta = 0.35$ and $\tan\beta = 1.0$ (Scenario 1a), this is the case for $m_A \gtrsim 1250$ GeV ($m_A \gtrsim 1500$ GeV) for $m_a = 100$ GeV ($m_a = 1000$ GeV). In this context, and for high m_A, the width of the additional heavy Higgs bosons grows substantially and the theoretical predictions are subject to additional theoretical uncertainties from the treatment of the width.[2] Therefore, regions where the relative width Γ/m of at least one of the heavy Higgs bosons or that of the pseudo-scalar mediator exceeds 20% are marked as shaded areas in the summary figures in Section 8.[3] This is a conservative approach to indicate large widths and follows the choice in Ref. [88].

Scenarios 1a, 3a, 4a, 4b, and 5 were recommended by the LHC Dark Matter Working Group [71], and were used in previous ATLAS publications, most notably Ref. [88]. The additional Scenarios 1b, 2a, 2b, 3b, and 6 were motivated by the studies in Refs. [71,87,98]. In particular, the choice of $\sin\theta = 0.7 \approx 1/\sqrt{2}$ ($\theta = \pi/4$) corresponds to maximal mixing in the pseudo-scalar sector and is particularly relevant, for example, for the $E_{\mathrm{T}}^{\mathrm{miss}} + tW$ search, which was designed specifically for 2HDM+a signal processes [98]. Scenario 6 is shown for the first time in this publication to highlight further the rich phenomenology of the model.

Another improvement introduced in this publication concerns the production modes of the various Higgs bosons and the pseudo-scalar mediator. In the previous comprehensive summary publication of ATLAS DM searches [88], only gg-initiated production was considered for the $E_{\mathrm{T}}^{\mathrm{miss}} + Z$ signatures. For the $E_{\mathrm{T}}^{\mathrm{miss}} + h$ signatures, $b\bar{b}$-initiated production was taken into account but only for values of $\tan\beta > 10$. In this publication, $b\bar{b}$-initiated production is taken into account for all $E_{\mathrm{T}}^{\mathrm{miss}} + X$ signatures, which is particularly relevant for the $E_{\mathrm{T}}^{\mathrm{miss}} + Z$ and $E_{\mathrm{T}}^{\mathrm{miss}} + h$ signatures at large values of $\tan\beta$, but also contributes at intermediate values.

3. ATLAS detector

The ATLAS detector [36] is a multipurpose particle detector with a forward–backward symmetric cylindrical geometry and a near 4π coverage in solid angle.[4] It consists of an inner tracking detector surrounded by a thin superconducting solenoid providing a 2 T axial magnetic field, electromagnetic and hadron calorimeters, and a muon spectrometer. The inner-detector (ID) system is immersed in a 2 T axial magnetic field and provides charged-particle tracking in the range of $|\eta| < 2.5$. The high-granularity silicon pixel detector covers the vertex region and typically provides four measurements per track, the first hit normally being in the insertable B-layer (IBL) installed before Run 2 [99,100]. It is followed by the silicon microstrip tracker (SCT), which usually provides eight measurements per track. These silicon detectors are complemented by the transition radiation tracker (TRT), which enables radially extended track reconstruction up to $|\eta| = 2.0$. The TRT also provides electron identification information based on the fraction of hits (typically 30 in total) above a higher energy-deposit threshold corresponding to transition radiation. The calorimeter system covers the pseudorapidity range $|\eta| < 4.9$. Within the region $|\eta| < 3.2$, electromagnetic (EM) calorimetry is provided by barrel and endcap high-granularity lead/liquid-argon (LAr) calorimeters, with an additional

[2] The simulation of the signal processes considers effects due to the off-shell production and decay of the Higgs bosons, but uses a fixed width to describe unstable resonances, thus neglecting variation of the decay width as a function of the Higgs boson virtuality. This can have an impact outside of the resonance region.

[3] These regions are mainly driven by the widths of the heavy Higgs bosons rather than by the typically narrower width of the pseudo-scalar mediator.

[4] ATLAS uses a right-handed coordinate system with its origin at the nominal interaction point in the centre of the detector. The positive x-axis is defined by the direction from the interaction point to the centre of the LHC ring, with the positive y-axis pointing upwards, while the beam direction defines the z-axis. Cylindrical coordinates (r, ϕ) are used in the transverse plane, ϕ being the azimuthal angle around the z-axis. The pseudorapidity η is defined in terms of the polar angle θ by $\eta = -\ln\tan(\theta/2)$, while the rapidity y is defined as $y = 0.5\ln[(E + p_z)/(E - p_z)]$, where E denotes the energy and p_z the component of the momentum along the beam direction. The angular distance ΔR is defined as $\sqrt{(\Delta\eta)^2 + (\Delta\phi)^2}$.

Table 1
Summary of the parameter settings for the different 2HDM+a benchmark scenarios explored in this publication.

Scenario		Fixed parameter values					Varied parameters
		$\sin\theta$	m_A (GeV)	m_a (GeV)	m_χ (GeV)	$\tan\beta$	
1	a	0.35	–	–	10	1.0	(m_a, m_A)
	b	0.70	–	–	10	1.0	
2	a	0.35	–	250	10	–	$(m_A, \tan\beta)$
	b	0.70	–	250	10	–	
3	a	0.35	600	–	10	–	$(m_a, \tan\beta)$
	b	0.70	600	–	10	–	
4	a	–	600	200	10	1.0	$\sin\theta$
	b	–	1000	350	10	1.0	
5		0.35	1000	400	–	1.0	m_χ
6		0.35	1200	–	–	1.0	(m_a, m_χ)

thin LAr presampler covering $|\eta| < 1.8$ to correct for energy loss in material upstream of the calorimeters. Hadron calorimetry is provided by the steel/scintillator-tile calorimeter, segmented into three barrel structures within $|\eta| = 1.7$, and two copper/LAr hadron endcap calorimeters. The solid angle coverage is completed with forward copper/LAr and tungsten/LAr calorimeter modules optimised for electromagnetic and hadronic energy measurements respectively. The muon spectrometer (MS) comprises separate trigger and high-precision tracking chambers measuring the deflection of muons in a magnetic field generated by the superconducting air-core toroidal magnets. The field integral of the toroids ranges between 2.0 and 6.0 T m across most of the detector. Three layers of precision chambers, each consisting of layers of monitored drift tubes, cover the region $|\eta| < 2.7$, complemented by cathode-strip chambers in the forward region, where the background is highest. The muon trigger system covers the range $|\eta| < 2.4$ with resistive-plate chambers in the barrel, and thin-gap chambers in the endcap regions. The ATLAS trigger system consists of a first-level trigger system implemented in custom hardware followed by a software-based high-level trigger [101]. The level-1 trigger uses a subset of the detector information to accept events at a rate below 100 kHz, while the software-based trigger reduces the accepted event rate to 1 kHz on average depending on the data-taking conditions. An extensive software suite [102] is used in the reconstruction and analysis of real and simulated data, in detector operations, and in the trigger and data acquisition systems of the experiment.

4. Data and simulated event samples

All analyses discussed in this publication are based on data from proton–proton collisions at a centre-of-mass energy of $\sqrt{s} = 13$ TeV collected with the ATLAS detector at the LHC in the years 2015–2018, unless otherwise stated. The integrated luminosity of the data sample, after requiring that all detector subsystems were operational and recording good quality data [103], is 139 fb^{-1}.

Simulated data are used to model the background processes and the predictions of the 2HDM+a benchmark. Details of the Monte Carlo (MC) generation for the various background processes considered in the analyses interpreted in this publication are found in the individual analysis publications referenced in Section 5. The 2HDM+a benchmark is implemented in the Universal FeynRules Output (UFO) format [104]. The implementation is referred to as `Pseudoscalar_2HDM` in the following. All signal processes, with the exception of the $tbH^{\pm}(tb)$ process [105] (see Table 2), are generated at leading-order (LO) in the strong coupling constant, where LO means loop-induced gluon-gluon fusion for the $E_{\mathrm{T}}^{\mathrm{miss}} + X$ signatures (Fig. 1).

Events were generated from this UFO implementation using the MadGraph5_aMC@NLO [106] MC generator interfaced with Pythia 8 [107] for the modelling of the parton shower and hadronisation

Table 2
Details of the MadGraph5_aMC@NLO generation set-up used for the 2HDM+a signal samples, for the signatures considered in this publication. The `Pseudoscalar_2HDM` UFO model is used for all simulated samples except those for the $tbH^{\pm}(tb)$ search, which relies on the UFO of Ref. [105]. The $h \to$ invisible and $h \to aa \to ff\bar{f}\bar{f}$ signatures are not listed here as no signal samples required for the re-interpretation, which in those cases relies on the branching ratio limits, as explained in Sections 5.1.7 and 5.2.3, respectively.

Analysis	Generator and Parton Shower	Cross-section	Further details
$E_{\mathrm{T}}^{\mathrm{miss}} + Z(\ell\ell)$	MadGraph5_aMC@NLO 2.4.3 (LO) + Pythia 8.212	LO	
$E_{\mathrm{T}}^{\mathrm{miss}} + h(b\bar{b})$	MadGraph5_aMC@NLO 2.6.0 (LO) + Pythia 8.212[a]	LO	
$E_{\mathrm{T}}^{\mathrm{miss}} + h(\gamma\gamma)$	MadGraph5_aMC@NLO 2.7.3 (LO) + Pythia 8.244	LO	
$E_{\mathrm{T}}^{\mathrm{miss}} + h(\tau\tau)$	MadGraph5_aMC@NLO 2.7.3 (LO) + Pythia 8.244	LO	
$E_{\mathrm{T}}^{\mathrm{miss}} + j$	MadGraph5_aMC@NLO 2.7.3 (LO) + Pythia 8.244	LO	Section 5.1.6
$E_{\mathrm{T}}^{\mathrm{miss}} + tW$	MadGraph5_aMC@NLO 2.7.3 (LO) + Pythia 8.244	LO	
$t\bar{t}t\bar{t}$	MadGraph5_aMC@NLO 2.9.5 (LO) + Pythia 8.245	LO	Ref. [55]
$tbH^{\pm}(tb)$	MadGraph5_aMC@NLO 2.2.2 (NLO) + Pythia 8.212	NLO, 4FS	Section 5.2.1

[a] With the exception of the $m_a - m_\chi$ scan, where MadGraph5_aMC@NLO 2.7.4 (LO) + Pythia 8.244 is used.

with the parameter values set according to the ATLAS tune A14 [108]. MadGraph5_aMC@NLO versions ranging from 2.6.0 to 2.9.5 and Pythia versions ranging from 8.212 to 8.245 were used, depending on the analysis, as summarised in Table 2. No differences between the signal simulations are expected to arise from the different choices of generator versions. The NNPDF3.0NLO [109] set of parton distribution functions (PDF) at next-to-leading-order in the five-flavour scheme was used, which assumes a massless b-quark and $\alpha_s(m_Z) = 0.118$ [109]. For consistency, the five-flavour scheme and $m_b = 0$ GeV were chosen for the matrix element (ME) computation in MadGraph5_aMC@NLO for the $b\bar{b}$-initiated production. For the gg-initiated production the four-flavour scheme was used to include top and bottom quark contributions in the production loop. These modelling choices follow the recommendations of the LHC Dark Matter Working Group [71].

To simulate the effects of additional pp collisions in the same and nearby bunch crossings, additional interactions were simulated using the soft QCD processes of Pythia 8.186 with the A3 tune [110] and the MSTW2008LO PDF [111], and overlaid onto each simulated hard-scatter event. The simulated samples were reweighted to reproduce the instantaneous luminosity spectrum in the data. The simulations include the expected bunch train structure in data and include low-level corrections to account for bunch train effects. Simulated events were processed either

through a detector simulation [112] based on GEANT4 [113] or through a fast simulation [114] with a parameterisation of the calorimeter response and GEANT4 for the other parts of the detector. All simulated samples were reconstructed in the same manner as the data. Corrections derived from data control samples were applied to simulated events to account for differences between data and simulation in the reconstruction efficiencies, the energy/-momentum scale and resolution of reconstructed electrons and muons, and in the efficiency and false positive rate for identifying jets containing b-hadrons. The energy scale and resolution of hadronic jets are also corrected to give the same performance between data and MC.

To produce signal events efficiently across the large multi-dimensional parameter space of the 2HDM+a, the MADGRAPH reweighting module [115] was used to obtain predictions for a range of different signal model parameters from a minimal set of generated events. This was achieved by assigning new event weights based on the ratios of matrix-elements for the input (generated) and target parameter points. The event weights were calculated on-the-fly during the event simulation. This method was validated by comparing weighted distributions with generated ones for a few representative samples. The reweighting immensely reduces the required computing resources as the detector simulation need be run only once.

5. Experimental signatures

A wide range of searches in different final states targeting invisible or visible mediator decays probe the 2HDM+a. No significant deviation from the SM prediction was observed in any of these searches, hence they are used to derive constraints on the 2HDM+a for benchmark scenarios introduced in Section 2. The sensitivity of searches varies across different regions of the 2HDM+a parameter range and not all searches are therefore interpreted in all 2HDM+a benchmark scenarios. In Table 3, an overview of the searches interpreted in the context of different 2HDM+a benchmark scenarios is given. The individual searches are summarised in the following subsections. Further details can be found in the individual publications referenced at the beginning of each subsection. The $E_{\mathrm{T}}^{\mathrm{miss}} + h(b\bar{b})$, $E_{\mathrm{T}}^{\mathrm{miss}} + Z(\ell\ell)$, and $tbH^{\pm}(tb)$ searches enter the statistical combination described in Section 7.

The analyses rely on final-state physics objects that are reconstructed using information from the different subsystems of the ATLAS detector. Jets are reconstructed from particle-flow objects [116] using the anti-k_t algorithm [117,118] with radius parameter $R = 0.4$ (small-R jets) and $R = 1.0$ (large-R jets) [119]. Multivariate algorithms are used to identify small-R jets within $|\eta| = 2.5$ containing b-hadrons (b-jets) [120,121]. Photons are reconstructed from topologically connected clusters of energy deposits in the EM calorimeters [122]. Electrons are reconstructed from topologically connected energy clusters [123] in the EM calorimeters matched to a charged-particle track in the ID [122]. Muons are reconstructed from matching tracks in the ID and MS, refined through a global fit which uses the hits from both the subdetectors [124]. The analyses may implement different lepton and photon selection criteria for particle identification, isolation, and kinematic requirements, for example p_T and η. The reconstruction of τ-leptons depends on the τ-lepton decay (hadronic or leptonic) targeted by a given analysis. The visible part of hadronically decaying τ-leptons [125] is seeded by small-R jets reconstructed from topological clusters, calibrated with a hadronic weighting scheme [126]. The missing transverse momentum $\vec{p}_{\mathrm{T}}^{\,\mathrm{miss}}$ (with magnitude $E_{\mathrm{T}}^{\mathrm{miss}}$) is calculated from the negative vector sum of transverse momenta (p_T) of electrons, muons and jet candidates and an additional soft term [127] which includes activity in the tracking system originating from the primary vertex but not matched with any reconstructed particle. Some analyses may also consider photons and τ-leptons in the $E_{\mathrm{T}}^{\mathrm{miss}}$ reconstruction.

Table 3
Summary of input analyses used in the different benchmark scenarios.

Analysis/Scenario	1a	1b	2a	2b	3a	3b	4a	4b	5	6
$E_{\mathrm{T}}^{\mathrm{miss}} + Z(\ell\ell)$ [74]	x	x	x	x	x	x	x	x	x	
$E_{\mathrm{T}}^{\mathrm{miss}} + h(b\bar{b})$ [75]	x	x	x	x	x	x	x	x	x	x
$E_{\mathrm{T}}^{\mathrm{miss}} + h(\gamma\gamma)$ [84]	x	x			x	x	x	x		
$E_{\mathrm{T}}^{\mathrm{miss}} + h(\tau\tau)$ [78]	x			x						
$E_{\mathrm{T}}^{\mathrm{miss}} + tW$ [77]	x	x	x	x	x	x	x	x		
$E_{\mathrm{T}}^{\mathrm{miss}} + j$ [45]	x	x			x	x	x	x		
$h \to$ invisible [86]	x	x			x					x
$E_{\mathrm{T}}^{\mathrm{miss}} + Z(q\bar{q})$ [89]	x						x	x		
$E_{\mathrm{T}}^{\mathrm{miss}} + b\bar{b}$ [90]							x	x		
$E_{\mathrm{T}}^{\mathrm{miss}} + t\bar{t}$ [90,91]							x	x		
$t\bar{t}t\bar{t}$ [85]	x	x	x	x	x	x	x	x	x	
$tbH^{\pm}(tb)$ [76]	x	x	x	x	x	x	x	x	x	
$h \to aa \to f\bar{f}f'\bar{f}'$ [79–83]										x

5.1. Searches for invisible mediator decays

5.1.1. $E_{\mathrm{T}}^{\mathrm{miss}} + Z(\ell\ell)$

Signal events in this analysis [74] are required to have $E_{\mathrm{T}}^{\mathrm{miss}}$ and a pair of high-p_T leptons ($\ell = e, \mu$). They are required to satisfy a set of single-electron [128] or single-muon [129] triggers which require the presence of an electron (muon) with transverse energy (transverse momentum) above thresholds in the range of 20–26 GeV depending on the lepton flavour and data-taking period [130]. Accordingly, a requirement of $p_T > 30$ GeV is imposed on the leading electron or muon in the event, while the subleading lepton is required to satisfy $p_T > 20$ GeV. The leptons are required to have the same flavour, be oppositely charged, and their invariant mass must be between 76 and 106 GeV, compatible with the Z boson mass. To select events consistent with invisible particles recoiling against the Z boson, events are required to have $E_{\mathrm{T}}^{\mathrm{miss}} > 90$ GeV and $S_{E_{\mathrm{T}}^{\mathrm{miss}}} > 9$, where $S_{E_{\mathrm{T}}^{\mathrm{miss}}}$ denotes the object-based $E_{\mathrm{T}}^{\mathrm{miss}}$ significance [131]. Additionally, a requirement $\Delta R(\ell\ell) < 1.8$ on the angular separation between the two leptons is required. Events with one or more b-jets are removed in all regions to suppress events containing top quarks.

The dominant background is the ZZ background, followed by WZ, Z+jets, and the non-resonant backgrounds (WW, $t\bar{t}$, single top-quark, and $Z \to \tau\tau$). Additional smaller contributions arise from triboson production, $t\bar{t} + V$, and $ZZ \to 4\ell$, where two of the leptons are not reconstructed. The backgrounds from ZZ and WZ production and the sum of the non-resonant backgrounds are estimated from MC simulation and normalised to data in the final likelihood fit using dedicated $4\ell, 3\ell$, and $e\mu$ control regions, which are enriched in the respective background components. The remaining, smaller, backgrounds are estimated from MC simulation. The final analysis result is obtained from a simultaneous profile likelihood fit in the ee and $\mu\mu$ signal and the $4\ell, 3\ell$, and $e\mu$ control regions. The observable of interest in the signal regions and the $e\mu$ control regions is the transverse mass

$$m_{\mathrm{T}}^{\mathrm{lep}} = \sqrt{\left[\sqrt{m_Z^2 + \left(p_T^{\ell\ell}\right)^2} + \sqrt{m_Z^2 + \left(E_{\mathrm{T}}^{\mathrm{miss}}\right)^2}\right]^2 - \left[\vec{p}_{\mathrm{T}}^{\,\ell\ell} + \vec{p}_{\mathrm{T}}^{\,\mathrm{miss}}\right]^2}, \quad (1)$$

which provides a good separation between the 2HDM+a signal and the dominant ZZ background. Only events with $m_{\mathrm{T}}^{\mathrm{lep}} > 200$ GeV are

included in the final fit. In the 4ℓ and 3ℓ control regions, the $E_{\mathrm{T}}^{\mathrm{miss}}$ distribution is fitted.

5.1.2. $E_{\mathrm{T}}^{\mathrm{miss}} + h(b\bar{b})$

The $E_{\mathrm{T}}^{\mathrm{miss}} + h(b\bar{b})$ analysis signature consists of two b-jets and significant $E_{\mathrm{T}}^{\mathrm{miss}}$ coming from the decays of a SM Higgs boson and a light pseudo-scalar to dark matter respectively [75]. Events are required to pass the $E_{\mathrm{T}}^{\mathrm{miss}}$ trigger [132] and to have $E_{\mathrm{T}}^{\mathrm{miss}} > 150$ GeV, with at least two jets identified as b-jets. Selections split the events into categories with exactly two and greater than two b-jets, to give good sensitivity to both the gluon–gluon fusion and $b\bar{b}$-initiated production processes, which are significant at low and high values of $\tan\beta$. The Higgs boson recoils against the pseudo-scalar which decays into dark matter in the signal topology, hence the $E_{\mathrm{T}}^{\mathrm{miss}}$ and Higgs-boson p_T are strongly correlated. For this reason, a $E_{\mathrm{T}}^{\mathrm{miss}} < 500$ GeV requirement is used to separate the resolved topology, in which the b-jets are reconstructed as two separate small-R jets, from the merged one, in which the high momentum of the Higgs boson implies that both the b-quarks can be found within a single large-R jet. Both the topologies are further subdivided into few $E_{\mathrm{T}}^{\mathrm{miss}}$ ranges. The analysis is performed through a simultaneous fit of the observed m_{bb} distribution across all signal regions and the yields of the control regions.

The dominant backgrounds arise from $t\bar{t}$ and Z/W-boson production with jets containing heavy flavour quarks. Smaller contributions from single-top, diboson and SM Vh production are also present. SM processes generating $E_{\mathrm{T}}^{\mathrm{miss}}$ through the leptonic decay of a W boson are reduced by rejecting events containing electron or muons. The contribution from Z+jets processes becomes increasingly dominant for high $E_{\mathrm{T}}^{\mathrm{miss}}$ selections. In the resolved category, events must also satisfy a requirement $S_{E_{\mathrm{T}}^{\mathrm{miss}}} > 12$ which suppresses the multijet background to negligible levels. Additional requirements are made on the transverse mass of the $E_{\mathrm{T}}^{\mathrm{miss}}$ and the b-jets to reduce contamination from $t\bar{t}$ processes. Finally, requirements are made on the reconstructed p_T of the Higgs boson candidate, which increases with $E_{\mathrm{T}}^{\mathrm{miss}}$, and on the number of additional jets in the event. Both of these also serve to reduce background contributions. Control regions requiring one or two leptons are used to normalise and validate the simulations used to model the main background processes for each signal selection.

5.1.3. $E_{\mathrm{T}}^{\mathrm{miss}} + h(\gamma\gamma)$

The $E_{\mathrm{T}}^{\mathrm{miss}} + h(\gamma\gamma)$ analysis targets final states with two photons and significant $E_{\mathrm{T}}^{\mathrm{miss}}$ [84]. Events are selected using a diphoton trigger requiring two reconstructed photon candidates with minimum transverse energies of 35 and 25 GeV for the leading and subleading photons, respectively. Events are required to contain at least two photon candidates and $E_{\mathrm{T}}^{\mathrm{miss}} > 90$ GeV. The two photons with highest energy in the transverse plane are selected to form a Higgs boson candidate if they satisfy the requirements $E_{\mathrm{T}}^{\gamma}/m_{\gamma\gamma} > 0.35$ and 0.25, respectively, where $m_{\gamma\gamma}$ is the invariant mass of the two selected photons. Furthermore, events are required to have 105 GeV $< m_{\gamma\gamma} <$ 160 GeV. The data sideband is defined to use events in this region but excluding the region 120 GeV $< m_{\gamma\gamma} <$ 130 GeV. Following this preselection, a boosted decision tree (BDT) is trained to discriminate between the 2HDM+a signal and the non-resonant diphoton backgrounds, using variables such as $p_T^{\gamma\gamma}$ and $S_{E_{\mathrm{T}}^{\mathrm{miss}}}$ as inputs. Finally, events are separated into low $E_{\mathrm{T}}^{\mathrm{miss}}$ ($E_{\mathrm{T}}^{\mathrm{miss}} < 150$ GeV) and high $E_{\mathrm{T}}^{\mathrm{miss}}$ ($E_{\mathrm{T}}^{\mathrm{miss}} > 150$ GeV) regions. In each region, two categories are defined from two sequential ranges of the BDT score, with the ranges optimised to maximise the combined signal sensitivity in the two chosen categories while discarding the remaining events.

The main backgrounds arise from SM Higgs boson production, QCD-induced non-resonant diphoton production ($\gamma\gamma$ and $V\gamma\gamma$, where V is a W or Z boson), and reducible contributions where an electron or a jet is mis-identified as a photon and $E_{\mathrm{T}}^{\mathrm{miss}}$ is generated either by particles escaping the detector acceptance or by neutrinos ($V\gamma$, γ+jet). An additional background contribution dominating the low $E_{\mathrm{T}}^{\mathrm{miss}}$ region originates from resolution effects when computing the transverse energy from high-energy objects and softer contributions measured in the ID. The background contributions are estimated by fitting analytic functions to the diphoton invariant mass distribution in the range of 105 GeV $< m_{\gamma\gamma} <$ 160 GeV in each of the four signal-region categories.

5.1.4. $E_{\mathrm{T}}^{\mathrm{miss}} + h(\tau\tau)$

The $E_{\mathrm{T}}^{\mathrm{miss}} + h(\tau\tau)$ search targets dark matter produced in association with a Higgs boson in final states with two hadronically decaying τ-leptons and missing transverse momentum [78]. It is optimised specifically to search for the 2HDM+a. Events are required to satisfy a combined di-$\tau_{\mathrm{had-vis}}$ + $E_{\mathrm{T}}^{\mathrm{miss}}$ trigger [101,133], where $\tau_{\mathrm{had-vis}}$ denotes the visible part of a hadronically decaying τ-lepton. They are required to contain exactly two τ-lepton objects that geometrically match the trigger-level τ-lepton candidates activating the di-τ-lepton+$E_{\mathrm{T}}^{\mathrm{miss}}$ trigger. The leading τ-lepton is required to have $p_T >$ 40–65 GeV, depending on the trigger threshold of a given data-taking year, while the sub-leading τ-lepton is required to have $p_T > 30$ GeV. The events also must satisfy $E_{\mathrm{T}}^{\mathrm{miss}} > 150$ GeV to ensure that the trigger is operating at maximum efficiency. Events containing an electron or a muon are vetoed. Events are further required to have at most one b-jet. In addition to these pre-selection requirements, two non-orthogonal signal regions are constructed to target signal model parameter configurations with high and low masses of the heavy pseudo-scalar A, respectively. The signal regions with the stronger expected exclusion for a given signal hypothesis are used to derive the exclusion limits for this hypothesis. Each signal region is further subdivided using the sum of the transverse masses of the two τ-leptons, $m_{\mathrm{T}}^{\tau_1} + m_{\mathrm{T}}^{\tau_2}$, where

$$m_{\mathrm{T}}^{\tau_i} = \sqrt{2 p_T^{\tau_i} E_{\mathrm{T}}^{\mathrm{miss}} \left(1 - \cos\Delta\phi(\tau_i, p_T^{\mathrm{miss}})\right)}. \quad (2)$$

The requirement $m_{\mathrm{T}}^{\tau_1} + m_{\mathrm{T}}^{\tau_2} > 100$ GeV is imposed to suppress events from $Z(\tau\tau)$+jets production, in which the $E_{\mathrm{T}}^{\mathrm{miss}}$ vector is typically collinear with the di-τ-lepton system.

Higgs boson production in association with a Z boson decaying into neutrinos is an irreducible background in this search. Further background contributions arise from Z + jets, VV, $t\bar{t}$, multijet, and Wh production. SM background processes are modelled using a combination of simulated events and data-driven methods. Background processes with only true τ-leptons, mostly Z + jets, VV, and Vh production and most of the $t\bar{t}$ background, are modelled using simulation normalised to the data in the dedicated control regions. Events with at least one fake τ-lepton, i.e., a non-τ-lepton object mis-identified as a τ-lepton, are estimated by data-driven techniques.

5.1.5. $E_{\mathrm{T}}^{\mathrm{miss}} + tW$

The search considers final states with zero or one charged lepton ($\ell = e, \mu$), at least one b-jet and large missing transverse momentum [77]. In addition, a result from a previous search [134] considering final states with two charged leptons is included in the interpretation of the results. The signal regions for the zero-

and one-lepton channels in Ref. [77] are designed to be orthogonal to each other and to the signal region of for the two-lepton channel in Ref. [134] and are statistically combined in the final fit.

The search is optimised specifically for signals arising in the context of the 2HDM+a and is particularly sensitive to on-shell production of the charged Higgs bosons $H^{\pm}$ and their semi-invisible decays via the mediator particle, a: $H^{\pm} \to W^{\pm}a(\chi\bar{\chi})$. Due to the similarity of the experimental signature to $t\bar{t}$ production, the analysis is also sensitive to DM produced in association with two top quarks ($E_{\mathrm{T}}^{\mathrm{miss}} + t\bar{t}$). This final state is not considered in the optimisation of the analysis regions but its contribution is added to the $E_{\mathrm{T}}^{\mathrm{miss}} + tW$ signal, according to the prediction of the 2HDM+a, in the interpretation of the final result. Candidate events were recorded using a combined set of triggers based on the presence of missing transverse momentum or charged leptons and are required to have $E_{\mathrm{T}}^{\mathrm{miss}} > 250$ GeV ($E_{\mathrm{T}}^{\mathrm{miss}} > 200$ GeV for the two-lepton channel). Further event selection criteria differ between analysis channels and are defined based on the number and type of leptons, jets and b-jets, and a number of event variables, such as invariant and transverse masses and the angular separation between selected objects.

The relative importance of SM background processes varies across the different signal regions, although the main sources can be broadly classified by either the presence of genuine $E_{\mathrm{T}}^{\mathrm{miss}}$ produced by neutrinos, or false $E_{\mathrm{T}}^{\mathrm{miss}}$ signals due to the mis-identification of particles, mis-measurements of their properties, due to particles outside the kinematic acceptance of the detector, or pile-up. Examples of the former include the Z + jets background in the zero-lepton channel and the W + jets background in the one-lepton channel. SM $t\bar{t}$ production and W + jets production in the zero-lepton channel are examples of major backgrounds with false $E_{\mathrm{T}}^{\mathrm{miss}}$ signals due to leptons that are either outside of the detector significance or mis-identified as jets. Further backgrounds include those from $t\bar{t}Z$ and single top-quark production. All background components are estimated from MC simulation. Dedicated control regions are used to constrain the normalisation parameters of the five dominant background components in the final likelihood fit.

5.1.6. $E_{\mathrm{T}}^{\mathrm{miss}} + j$

This search targets production of a single jet with large $E_{\mathrm{T}}^{\mathrm{miss}}$ [45]. The data were collected using the $E_{\mathrm{T}}^{\mathrm{miss}}$ trigger. Events are required to have $E_{\mathrm{T}}^{\mathrm{miss}} > 200$ GeV to ensure that the trigger is fully efficient for events passing the analysis selection criteria. They are also required to contain at least one jet with $p_T > 150$ GeV with $|\eta| < 2.4$, up to three additional jets with $p_T > 30$ GeV and $|\eta| < 2.8$, and no reconstructed leptons (e, μ or τ-leptons) or photons. Several signal regions are considered with increasing requirements on the missing transverse momentum starting at 200 GeV. Additional angular requirements on the separation in ϕ between the $E_{\mathrm{T}}^{\mathrm{miss}}$ vector and leading jet are imposed to reduce the contribution from multijet events with mis-measured jet energies.

The dominant SM background for this search arises from $Z(\nu\nu)$ and $W(\ell\nu)$ production with jets, where the W boson decays into either hadronically decaying τ-leptons or undetected electrons or muons. Additional background contributions include $t\bar{t}$ and single-top production, diboson production, as well as non-collision and multijet backgrounds. The estimate of the major SM processes in the analysis selection is based on a profile likelihood fit to the distribution of the p_T of the system recoiling against the jets reconstructed in the event, performed simultaneously in the signal region and in orthogonal control regions enriched with the targeted backgrounds.

Various different signal contributions to the $E_{\mathrm{T}}^{\mathrm{miss}} + j$ signal regions are considered in the re-interpretation of this search in the context of the 2HDM+a. Production of a pair of DM particles with a jet in the matrix element ($pp \to \chi\chi j$) is the dominant signal contribution in the signal regions of the $E_{\mathrm{T}}^{\mathrm{miss}} + j$ analysis for low values of $E_{\mathrm{T}}^{\mathrm{miss}}$ ($E_{\mathrm{T}}^{\mathrm{miss}} \lesssim 500$ GeV) if the mediator mass is not too small ($m_a \gtrsim 150$ GeV). Both the loop-induced, gg-initiated (Fig. 1c) and tree-level, $b\bar{b}$-initiated production (Fig. 2e) are considered, with the latter only being relevant at large values of $\tan\beta$, where the $E_{\mathrm{T}}^{\mathrm{miss}} + j$ analysis is not sensitive for the parameter settings considered in this publication (Section 8). For larger values of $E_{\mathrm{T}}^{\mathrm{miss}}$ and smaller values of m_a, the dominant signal process in the $E_{\mathrm{T}}^{\mathrm{miss}} + j$ signal regions is the production of two pairs of DM particles ($pp \to \chi\bar{\chi}\chi\bar{\chi}$) via invisible decays of the SM Higgs boson into a pair of mediators that each decay into DM ($h \to aa \to \chi\bar{\chi}\chi\bar{\chi}$). Depending on the parameter space, the mediators may be real or virtual. The jet arises from the parton shower. This process is illustrated in Fig. 1f. Additional, though sub-dominant, signal contributions to the $E_{\mathrm{T}}^{\mathrm{miss}} + j$ signal regions arise from $E_{\mathrm{T}}^{\mathrm{miss}} + Z(q\bar{q})$ and $E_{\mathrm{T}}^{\mathrm{miss}} + h(b\bar{b})$ production in parameter regions where invisible decays of the SM Higgs boson are kinematically forbidden. Further, minor contributions arise from the $pp \to t\bar{t} + a$ (Fig. 1d) and $pp \to tW + a$ (Fig. 3) processes.

5.1.7. $h \to$ invisible

A statistical combination of all ATLAS direct searches for invisible decays of the Higgs boson was published in Ref. [86]. It is based on five independent searches relying on 139 fb^{-1} of proton–proton collision data collected with the ATLAS detector at a centre-of-mass energy of $\sqrt{s} = 13$ TeV during LHC Run 2. These searches target Higgs boson production via the vector-boson fusion (VBF), VBF with a photon, gluon-gluon fusion, associated production with a vector boson, and associated production with $t\bar{t}$, respectively in the VBF + $E_{\mathrm{T}}^{\mathrm{miss}}$ [135], VBF + γ + $E_{\mathrm{T}}^{\mathrm{miss}}$ [136], $E_{\mathrm{T}}^{\mathrm{miss}} + j$ [45], $E_{\mathrm{T}}^{\mathrm{miss}} + Z(\ell\ell)$ [74], and $E_{\mathrm{T}}^{\mathrm{miss}} + t\bar{t}$ [137] final states. The results from the Run 2 searches are further combined statistically with the set of constraints on invisible Higgs decays obtained from searches and measurements targeting multiple production and decay channels with up to 4.7 fb^{-1} of pp collision data at $\sqrt{s} = 7$ TeV and 20.3 fb^{-1} at $\sqrt{s} = 8$ TeV [138], yielding the most sensitive direct constraint to invisible Higgs boson decays in ATLAS.

Among the direct searches, the VBF production of Higgs bosons decaying into invisible particles using the full Run 2 data sample is the most sensitive one, setting an observed (expected) upper limit on the invisible branching ratio of 0.145 (0.103) at 95% confidence level (CL). Events are selected using $E_{\mathrm{T}}^{\mathrm{miss}}$ triggers and the analysis requires $E_{\mathrm{T}}^{\mathrm{miss}} > 160$ GeV and two, three or four jets with $p_T > 25$ GeV. The leading and sub-leading jets must have $p_T > 80$ GeV and 50 GeV, respectively. Additional requirements on the angular separation of the two jets are applied to enhance the sensitivity to VBF production. In particular, the two leading jets are required to be well separated in η. Lepton and b-jet vetoes are applied to reduce contamination from W + jets and top-quark backgrounds, respectively. Sixteen orthogonal signal regions are defined based on the values of $E_{\mathrm{T}}^{\mathrm{miss}}$, the jet multiplicity and the two- and three-jet invariant masses in two-jet and three- or four-jet regions, respectively. The dominant background processes are $Z(\nu\nu)$+jets and $W(\ell\nu)$+jets production, where in the latter process the charged lepton ℓ is not detected or mis-identified. These backgrounds are evaluated simultaneously using well populated control regions in the one-lepton and two-leptons channels. Such extrapolation is made possible due to the use of a dedicated theo-

retical calculation at next-to-leading-order in the relevant phase space [139]. The multijet background is directly estimated from data.

An upper limit on the $h \to$ invisible branching ratio of 0.113 $\left(0.080^{+0.031}_{-0.022}\right)$ is observed (expected) at 95% CL. This upper limit is used directly to determine the excluded parameter regions in the 2HDM+a based on the predicted $h \to \chi\bar{\chi}$ branching ratio for each point in the benchmark scenarios in Section 2.

5.1.8. Additional searches using 36 fb^{-1} of $\sqrt{s} = 13$ TeV pp collision data

Results from three searches using 36 fb^{-1} of $\sqrt{s} = 13$ TeV pp collision data, which were already included in the summary of 2HDM+a constraints in Ref. [88], are shown for completeness. The $E_{\text{T}}^{\text{miss}} + Z(q\bar{q})$ search [89] targets final states with $E_{\text{T}}^{\text{miss}} > 150$ GeV and a hadronically decaying W or Z boson candidate. The vector-boson candidate is reconstructed as a single large-R jet with $p_T > 250$ GeV in a boosted topology ($E_{\text{T}}^{\text{miss}} > 250$ GeV) or from two small-R jets with $p_T > 20$ GeV in a resolved topology. In the both cases, a lepton veto is applied. Several signal regions are defined according to the b-jet multiplicity. The normalisations of the dominant backgrounds from $t\bar{t}$ and W/Z+jets production are constrained using a simultaneous fit to the $E_{\text{T}}^{\text{miss}}$ distributions in the signal and dedicated control regions.

The $E_{\text{T}}^{\text{miss}} + b\bar{b}$ search [90] targets events with $E_{\text{T}}^{\text{miss}} > 180$ GeV and at least two b-jets. The azimuthal separations between the b-jets and the $E_{\text{T}}^{\text{miss}}$ direction are exploited to enhance the separation between the signal and the irreducible background from $Z(\nu\bar{\nu}) + b\bar{b}$ events, which is constrained using data in a dedicated control region. The results are extracted from a likelihood fit to the angular observable $\cos\theta^*_{b\bar{b}} = |\tanh\Delta\eta_{b\bar{b}}/2|$, which depends on the pseudorapidity differences $\Delta\eta_{b\bar{b}}$ between the two b-jets.

Searches targeting events with large $E_{\text{T}}^{\text{miss}}$ produced with $t\bar{t}$ are conducted in different final states classified according to the number leptons. A search in zero-lepton final states targets events in which the W bosons from both the top quarks decay hadronically [90]. Events are selected based on the presence of at least four energetic jets, at least two of which are b-tagged, and relatively high $E_{\text{T}}^{\text{miss}}$. Requirements on the invariant mass of reclustered large-R jets are imposed to identify events with a boosted W-boson or top-quark decay. The dominant backgrounds from Z + jets, $t\bar{t}$, and $t\bar{t} + Z$ production are constrained in dedicated control regions. A complementary search in one-lepton final states targets events in which one of the W bosons decays leptonically [91]. Events are required to contain at least four energetic jets, at least one of which is b-tagged, one isolated lepton, and large $E_{\text{T}}^{\text{miss}}$. They are also required to have at least one hadronic top candidate with invariant mass loosely compatible with the mass of the top quark. Requirements on the azimuthal angle between the lepton and $\vec{p}_{\text{T}}^{\text{miss}}$ and on the angular separation $\Delta\phi(\text{jets}, \vec{p}_{\text{T}}^{\text{miss}})$ are used to suppress the background contamination of the signal regions. All background processes involving top quarks are estimated in dedicated control regions.

5.2. Searches for visible mediator decays

5.2.1. $tbH^{\pm}(tb)$

This search targets the production of heavy charged Higgs bosons, $H^{\pm}$, with masses in the range 0.2–2.0 TeV together with a top and a bottom quark with the charged Higgs boson decaying into a top and a bottom quark, $pp \to tbH^{\pm}(tb)$ [76]. Events are pre-selected using single-lepton triggers and are required to contain exactly one electron or muon with $p_T > 27$ GeV and at least five jets with $p_T > 25$ GeV, consistent with the semileptonic decay of one of the top quarks. At least three of the jets are required to be identified as a b-jet to suppress the large backgrounds from multijet production. The selected events are further classified into four separate regions according to the number of reconstructed jets (j) in an event and number of b-jets (b) among them, referred to as $5j3b$, $5j\geqslant 4b$, $\geqslant 6j3b$, and $\geqslant 6j\geqslant 4b$. A neural network is used to enhance the separation between signal and background. The output distributions of the neural network are used in a fit to extract the amount of $tbH^{\pm}(tb)$ signal in data.

The dominant backgrounds for this search are composed of $t\bar{t}$+-jets events, including $t\bar{t}$+ light, $t\bar{t}+\geq 1b$ and $t\bar{t}+\geq 1c$, and single top-quark production in the Wt channel. Both these processes and smaller background contributions are modelled using MC simulation. Data-driven corrections obtained in an additional $\geqslant 5j2b$ region are applied to the simulation for the leading backgrounds via a reweighting procedure to improve the modelling of the transverse momentum distributions of additional jet emissions and of kinematic regions with high jet multiplicities [140,141]. After the reweighting, the final $t\bar{t}+\geq 1b$ and $t\bar{t}+\geq 1c$ normalisation factors are extracted from the fit to data.

Both the model-independent upper limits on the cross-section times branching ratio for the signal process and the model-dependent exclusion contours on specific benchmarks, including a type-II 2HDM in the alignment limit without DM, were derived [76]. These results can be straightforwardly reinterpreted in the context of the 2HDM+a as the dominant production modes and hence the production cross-sections of the charged Higgs bosons are identical in both of the models. This was verified by comparing the simulated predictions of the 2HDM and 2HDM+a benchmarks for a range of relevant kinematic variables. The simulated cross-sections are scaled to their NLO values calculated for the 2HDM+a predictions, in the four-flavour scheme to be consistent with the modelling choices outlined in Section 4. These values are on average 20%–30% smaller than the corresponding NLO cross-sections calculated in the five-flavour scheme used in Ref. [76], in accordance with the results in Ref. [142]. The branching ratios of the charged Higgs bosons differ between the 2HDM+a and the 2HDM without DM due to additional possible decay modes of the charged Higgs bosons in the 2HDM+a. Hence the exclusion limits are rescaled by the ratio of branching ratios in the 2HDM+a and the 2HDM, for which the original exclusion limits are derived, to obtain the exclusion limits for the 2HDM+a.

5.2.2. $t\bar{t}t\bar{t}$

This search specifically targets $t\bar{t}$-associated production of heavy scalar or pseudo-scalar Higgs bosons A/H decaying into $t\bar{t}$ ($t\bar{t} + A/H \to t\bar{t}t\bar{t}$) [85]. It is based on and extends the analysis strategy of Ref. [143] to increase the sensitivity to A/H production. Single-lepton and the dilepton triggers are used to collect the data on which the search is based. Events are required to contain either a same-sign lepton pair or at least three leptons ($\ell = e, \mu$). This includes electron or muons from leptonic τ-lepton decays. Electrons and muons are required to have $p_T > 28$ GeV. A baseline signal region is defined by additionally requiring the presence of at least six jets with $p_T > 25$ GeV, at least two of which must be b-tagged, and $H_T > 500$ GeV, where H_T is defined as the scalar sum of the transverse momenta of all leptons and jets in the event. A multivariate discriminant based on a BDT is used to separate between SM $t\bar{t}t\bar{t}$ production and background processes, using event-level information such as jet and b-jet multiplicity and additional kinematic variables. The BSM search relies on a second BDT to distinguish between BSM and SM four-top production. This second BDT is parameterised as a function of the mass of the heavy

Higgs boson by introducing the mass as a labelled input in the training [144].

The main, irreducible backgrounds arise from the production of a $t\bar{t}$ pair together with a boson and additional jets ($t\bar{t}+W$+jets, $t\bar{t}+Z$+jets, $t\bar{t}+h$+jets). They are estimated by MC simulations with additional data-driven corrections applied in the case of $t\bar{t}+W$+jets production. Smaller, reducible backgrounds arise mostly from $t\bar{t}$+jets and tW+jets production with mis-identified charge, fake and non-prompt leptons. These smaller backgrounds are estimated from data using dedicated control regions.

5.2.3. Exotic Higgs boson decays $h \to aa \to f\bar{f}f'\bar{f}'$

Various complementary searches target decays of the $m_h = 125$ GeV SM Higgs boson to a pair of light pseudo-scalars, which subsequently decay to fermions, $h \to aa \to f\bar{f}f'\bar{f}'$. The searches target final states with different types of fermions and provide sensitivity to different ranges of the pseudo-scalar mass m_a.

A search using 139 fb^{-1} of $\sqrt{s} = 13$ TeV pp collision data in the $b\bar{b}\mu^+\mu^-$ final state targets pseudo-scalars in the range of 16 GeV $\leqslant m_a \leqslant$62 GeV [79]. The di-muon invariant mass is the variable of interest in this search, which is probed for a resonant enhancement over the SM expectation. The dominant backgrounds in the analysis arise from the Drell–Yan di-muon process together with b-quarks and SM $t\bar{t}$ production where each of the W bosons from the two top quarks decays into a muon and a neutrino.

A search using 36 fb^{-1} of $\sqrt{s} = 13$ TeV pp collision data targeting the $b\bar{b}b\bar{b}$ final state provides sensitivity to pseudo-scalars in the mass range 20 GeV $\leqslant m_a \leqslant$60 GeV [80]. It targets Higgs boson production in association with a leptonically decaying W (one-lepton channel) or Z boson (two-lepton channel). Several kinematic variables, including the reconstructed masses in the decay $h \to aa \to 4b$, are used as input to a BDT that is trained to distinguish signal from background events. The dominant background process in the one-lepton signal regions arises from $t\bar{t}$ production with additional jets, while the dominant background component in the signal regions with two leptons is due to Z+jets production. The BDT output distribution is used as the observable of interest in the final likelihood fit. The search is optimised for resolved final states in which the two b-jets from each of the $a \to b\bar{b}$ decays can be reconstructed as two individual small-R jets. This limits the sensitivity of the search for masses $m_a < 30$ GeV, a regime where the two b-jet pairs are increasingly likely to be merged into a single large-R jet. Such merged final states are the target of a complementary search [145] on the same data sample. However, this search provides little additional sensitivity to the 2HDM+a in comparison to the other searches discussed in this section and is therefore not considered in this publication.

The mass range 3.7 GeV $\leqslant m_a \leqslant$50 GeV is probed by a search on 20.3 fb^{-1} of $\sqrt{s} = 8$ TeV pp collision data targeting $\mu^+\mu^-\tau^+\tau^-$ final states [81]. The search probes resonant enhancements in the di-muon invariant mass spectrum.

Finally, masses $m_a \geqslant 1$ GeV are probed by two searches targeting final states with four charged leptons ($\ell = e, \mu$) on 36 fb^{-1} [82] and 139 fb^{-1} [83] of $\sqrt{s} = 13$ TeV pp collision data, respectively, Each search is based on two orthogonal regions: a low-mass region covering the mass range 1 GeV $\leqslant m_a \leqslant$15 GeV, excluding mass ranges around the J/ψ and Υ resonances, and a high-mass region covering the mass range 15 GeV $\leqslant m_a \leqslant$60 GeV. Only the low-mass region is sensitive to the 2HDM+a and hence considered in this publication. For this region, only final states with at least four muons ($\mu^+\mu^-\mu^+\mu^-$) are considered due to their greater branching fraction and the selection efficiency for isolated muons being significantly larger than that for isolated electrons in this mass range. The searches are therefore referred as $h \to aa \to \mu^+\mu^-\mu^+\mu^-$ in the following. The dominant background processes for these searches arise from $ZZ^* \to \mu^+\mu^-\mu^+\mu^-$ and $h \to ZZ^* \to \mu^+\mu^-\mu^+\mu^-$ production. In both the searches, the observable of interest is the average di-muon invariant mass, $< m_{\mu^+\mu^-} >= (m_{12} + m_{34})/2$, where m_{12} and m_{34} are the invariant masses of the two di-muon pairs that minimise the di-muon pair invariant mass difference $|m_{12} - m_{34}|$. In the search conducted on the full 139 fb^{-1} data sample, the di-muon masses are required to satisfy 1.2 GeV $< m_{12}, m_{34} <$20 GeV, excluding the mass ranges of 2.0–4.4 GeV and 8.0–12.0 GeV around the J/ψ and Υ resonances, respectively. Looser requirements are applied in the search conducted on the partial (36 fb^{-1}) data sample, where di-muon invariant masses 0.88 GeV $\leqslant m_{12}, m_{34} \leqslant$20 GeV are allowed. Hence the latter provides sensitivity in the low m_a range where the former is not sensitive.

Model-independent upper limits on the branching ratio of the decay $h \to aa \to f\bar{f}f'\bar{f}'$ are obtained for all searches listed above. This upper limit is used directly to determine the excluded parameter regions in the 2HDM+a based on the predicted $h \to aa \to f\bar{f}f'\bar{f}'$ branching ratio for each point in the benchmark scenarios in Section 2. The branching ratio for the 2HDM+a is calculated at NLO with the $\overline{\text{MS}}$ scheme.

6. Systematic uncertainties

Systematic uncertainties for both the background and signal models are considered in each of the analyses presented in Section 5. These uncertainties and the statistical uncertainties depend on the event selection, the phase space covered by a given analysis, and its background estimation strategy. The systematic uncertainties include experimental and theoretical uncertainties. Details of the latter can be found in the indvidual analysis publications referred to in the previous section. Experimental uncertainties may include uncertainties in the absolute jet energy scales and resolutions, the jet quality requirements, pile-up corrections, b-jet identification efficiencies, and the soft contributions to $E_{\text{T}}^{\text{miss}}$. Uncertainties in lepton identification and reconstruction efficiencies, energy/momentum scale and resolution are included for events with selected or vetoed leptons. Uncertainties due to the finite size of the background MC samples and others related to the modelling of the background processes are also included in the analyses. In all analyses, a luminosity uncertainty of 1.7% [146] is applied to backgrounds derived purely from MC simulation.

The signal modelling is subject to some theoretical uncertainties affecting the production cross-section (normalisation) or the signal acceptance. They include uncertainties related to the PDF, evaluated following the PDF4LHC recommendations [147], and uncertainties related to the choice of renormalisation and factorisation scales. The latter are derived by varying independently such scales by a factor of 2.0 and 0.5 relative to the nominal values used for the MC generation. Additionally, for the $E_{\text{T}}^{\text{miss}} + Z(\ell\ell)$, $E_{\text{T}}^{\text{miss}} + h(b\bar{b})$, and $tbH^{\pm}(tb)$ analyses, which enter the statistical combination, uncertainties in the modelling of initial- and final-state radiation and multi-parton interactions are taken into account.

7. Statistical combination of results

A statistical combination of the $E_{\text{T}}^{\text{miss}} + h(b\bar{b})$, $E_{\text{T}}^{\text{miss}} + Z(\ell\ell)$, and $tbH^{\pm}(tb)$ analyses is performed and described further in this section. These are generally the most constraining signatures and cover complementary regions of the 2HDM+a model parameter space.

The statistical combination is facilitated by the input analyses described in Section 5 being statistically independent. The $E_{\mathrm{T}}^{\mathrm{miss}}+Z(\ell\ell)$ analysis places a veto on the presence of b-jets, whereas signal selections for the $E_{\mathrm{T}}^{\mathrm{miss}}+h(b\bar{b})$ and $tbH^{\pm}(tb)$ analysis require at least two and three b-jets, respectively. Furthermore, the $tbH^{\pm}(tb)$ signal region selections require a charged lepton (e or μ), which is vetoed by the $E_{\mathrm{T}}^{\mathrm{miss}}+h(b\bar{b})$ selections. Thus no overlap between the three analysis signal selections is expected. This was validated on the full data luminosity and additionally by applying the different analysis selections to the simulated signal events of the other two analyses. No overlap between the signal selections was observed in any of these checks. There was a negligible ($\ll 1\%$) event overlap observed between the $tbH^{\pm}(tb)$ signal selection and a background selection used by the $E_{\mathrm{T}}^{\mathrm{miss}}+h(b\bar{b})$ analysis as a leptonic control region, which has no impact on the combination.

7.1. Statistical analysis

The combination of the analyses is performed by constructing their combined likelihood and maximising the corresponding profile likelihood ratio [148]. The common fitted parameter of interest, μ, is the signal strength of a given 2HDM+a signal, defined as the ratio of the observed to the predicted value of the signal cross-section times branching fraction for the specific signal parameter point being tested. The exclusion of $\mu=1$ in the combined fit means that the data globally across the analyses are incompatible with the predictions for the signal hypothesis under consideration. Systematic uncertainties are included in the fit as nuisance parameters (NPs), denoted by $\boldsymbol{\theta}$, and are constrained by Gaussian, Poisson or Log-normal probability density functions. These encode information from auxiliary measurements and measure the effect of systematic uncertainties. The fit model also includes normalisation factors, denoted by $\boldsymbol{\lambda}$, which are floated in the fit without constraints to adjust the agreement with data of background components in their corresponding control region(s).

The likelihood used in the combined fit is given by [149]

$$\mathcal{L}(\mathrm{data}|\mu,\boldsymbol{\lambda}_{\mu},\boldsymbol{\theta}_{\mu})=\prod_{c=1}^{N_{\mathrm{cats}}}\mathcal{L}_{c}(\mathrm{data}|\mu,\boldsymbol{\lambda}_{\mu},\boldsymbol{\theta}_{\mu})\prod_{k=1}^{N_{\mathrm{cons}}}\mathcal{F}\left(\tilde{\theta}_{\mu,k}|\theta_{\mu,k}\right), \tag{3}$$

where $\boldsymbol{\lambda}$ is the vector of normalisation factors, $\boldsymbol{\theta}$ is the vector of nuisance parameters, N_{cats} is the number of categories, N_{cons} is the number of constrained NPs, $\tilde{\theta}_k$ is the global observable corresponding to θ_k, c is the index for the event categories, k is the index for the constrained NPs, and $\mathcal{F}$ denotes a Poisson, a Gaussian or a Log-normal distribution depending on the type of uncertainty.

The 95% CL limits are obtained using the CLs frequentist formalism [150] with the profile likelihood ratio test statistic (q_{μ}) implemented using RooStats [151] and RooFit [152], defined as [148]

$$q_{\mu}=\frac{\mathcal{L}\left(\mu,\hat{\hat{\boldsymbol{\lambda}}}_{\mu},\hat{\hat{\boldsymbol{\theta}}}_{\mu}\right)}{\mathcal{L}\left(\hat{\mu},\hat{\boldsymbol{\lambda}}_{\hat{\mu}},\hat{\boldsymbol{\theta}}_{\hat{\mu}}\right)}, \tag{4}$$

where the numerator indicates the values of $\boldsymbol{\lambda}_{\mu}$ and $\boldsymbol{\theta}_{\mu}$ that maximise $\mathcal{L}$ for a given value of μ, and the denominator is evaluated for the values $\hat{\mu},\hat{\boldsymbol{\lambda}}_{\hat{\mu}},\hat{\boldsymbol{\theta}}_{\hat{\mu}}$ which jointly maximise the likelihood.

7.2. Treatment of uncertainties and their correlations

There are many sources of uncertainty present in the $E_{\mathrm{T}}^{\mathrm{miss}}+h(b\bar{b})$, $E_{\mathrm{T}}^{\mathrm{miss}}+Z(\ell\ell)$, and $tbH^{\pm}(tb)$ analyses; their correlations are treated as follows. Most experimental uncertainties, such as those related to the reconstruction of the physics objects are correlated across search channels, as are the uncertainties in the integrated luminosity and the modelling of pile-up. This includes the uncertainties from electrons, muons, $E_{\mathrm{T}}^{\mathrm{miss}}$, and the jet energy response. The assessment of the correlations of uncertainties stemming from b-jet identification is complicated by differing choices of algorithm and operating point, hence these are not correlated. Finally, a handful of experimental systematic uncertainties that are moderately constrained in a particular analysis are not correlated to avoid introducing any phase-space-specific biases. Different assumptions on the correlation of the uncertainties related to jet, $E_{\mathrm{T}}^{\mathrm{miss}}$, and b-jet indentification and the moderately constrained uncertainties were tested separately to assess their impact on the observed exclusions. The effect on the observed exclusions was found to be negligible.

Uncertainties are assessed on the signal simulation and background modelling for each of the analyses to be combined. Dedicated signal simulations are performed for each of the final states, as they often probe very different kinematic regions of phase space.[5] The resulting theoretical uncertainties are found to be small and often completely negligible, and are considered to be uncorrelated. The uncertainties related to the estimate of the backgrounds are considered to be uncorrelated amongst the analyses. This is motivated by their different sources of leading background, the different kinematic phase space probed, and the wide-spread use of data-derived and analysis-specific methods of background estimation.

7.3. Impact of uncertainties

Inevitably, the contributions of the many uncertainties on the analysis combination vary across the model parameter values, due to the differing signal kinematics and the varying sensitivities of the individual analyses. The contributions to the total uncertainty in the best-fit signal strength from the statistical and systematic uncertanties are shown in Table 4 for m_a = 450 GeV, m_H = 800 GeV, $\tan\beta$ = 1.0 and $\sin\theta=0.35$. This particular signal is narrowly excluded by the combination but is not by any single input analysis, and all three analyses contribute some sensitivity. For this signal, the statistical uncertainty is comparable to (but slightly smaller than) the systematic component, which is broken down into three categories of sources: theoretical, experimental and MC statistical uncertainties. For each category, the uncertainty is assessed by fixing the corresponding uncertainties in a fit and subtracting the resultant uncertainty from the total in quadrature. The theoretical uncertainties, which stem predominantly from uncertainties in the background modelling, are slightly smaller than the experimental ones. The experimental uncertainty is further subdivided into those on each of the reconstructed physics objects, amongst which the largest contributions come from jet and $E_{\mathrm{T}}^{\mathrm{miss}}$ uncertainties.

The most important uncertainties follow directly from those of the individual input analyses. For the background modelling uncertainties, the largest components are ZZ modelling from the $E_{\mathrm{T}}^{\mathrm{miss}}+Z(\ell\ell)$ analysis, $t\bar{t}$ uncertainties affecting $E_{\mathrm{T}}^{\mathrm{miss}}+h(b\bar{b})$, and uncertainties from the production of $t\bar{t}$ with additional b-quarks, which impact the $tbH^{\pm}(tb)$ search. Among the experimental systematic uncertainties, the largest sources are lepton systematic uncertainties impacting $E_{\mathrm{T}}^{\mathrm{miss}}+Z(\ell\ell)$, uncertainties related to jets and $E_{\mathrm{T}}^{\mathrm{miss}}$ affecting $E_{\mathrm{T}}^{\mathrm{miss}}+h(b\bar{b})$, and systematic uncertainties

[5] Each analysis is assessed at each model parameter point, unless the sensitivity of one is known to be negligible in that region of parameter space, in which case it may be omitted and its sensitivity set to zero.

Table 4
Summary of the uncertainties $\Delta\mu$ in the best-fit signal strength on a signal ($m_A = 800$ GeV, $m_a = 450$ GeV, $\tan\beta = 1, \sin\theta = 0.35$), obtained by fixing the corresponding nuisance parameters to their best-fit values, and subtracting the square of the resulting uncertainty from the square of the total uncertainty to evaluate $(\Delta\mu)^2$. The statistical uncertainty component is obtained by fixing all nuisance parameters except free-floating background normalisation factors to their best-fit values, and quantitifes the impact of the limited data yields in the signal and control regions. Note the total uncertainty does not equal the sum of the individual contributions added in quadrature due to correlations between the systematic uncertainties.

Uncertainty source	$\Delta\mu \cdot 100$
Statistical uncertainty	25.0
Systematic uncertainties	27.6
Theory uncertainties	16.2
Signal modelling	2.8
Background modelling	15.9
Experimental uncertainties (excl. MC stat.)	18.8
Luminosity, pile-up	3.9
Jets, $E_{\mathrm{T}}^{\mathrm{miss}}$	12.3
Identification of b-jets	9.1
Electrons, muons	6.1
MC statistical uncertainty	9.3
Total uncertainty	37.2

related to the identification of b-jets in the case of the $tbH^{\pm}(tb)$ analysis.

8. Summary of constraints on the 2HDM+a

8.1. Scenario 1: $m_a - m_A$ planes

The exclusion contours for the $m_A - m_a$ scans with $\sin\theta = 0.35$ and $\sin\theta = 0.7$, which correspond to Scenarios 1a and 1b in Section 2, respectively, are shown in Fig. 4. In the upper sub-figures, the exclusion regions for the statistical combination of the $E_{\mathrm{T}}^{\mathrm{miss}} + h(b\bar{b})$, $E_{\mathrm{T}}^{\mathrm{miss}} + Z(\ell\ell)$, and $tbH^{\pm}(tb)$ searches are shown, along with the exclusion regions from the three individual searches entering the combination. The $E_{\mathrm{T}}^{\mathrm{miss}} + Z(\ell\ell)$ and $E_{\mathrm{T}}^{\mathrm{miss}} + h(b\bar{b})$ searches dominate the sensitivity across a large fraction of the two parameter planes, which is largely due to the resonant production of the (pseudo-) scalars according to the diagram in Fig. 1a. Their sensitivities depend on both the pseudo-scalar Higgs boson and mediator masses. For $\sin\theta = 0.35$ (Scenario 1a), the maximum reach obtained for m_a is up to 560 GeV, if the A boson mass is set to 1.2 TeV, while for $m_a = 150$ GeV values of m_A between 250 and 1.55 TeV are excluded. For both the $\sin\theta$ choices, in the lower left area, the $E_{\mathrm{T}}^{\mathrm{miss}} + Z(\ell\ell)$ limit reaches closer to the $m_A = m_a$ line than the $E_{\mathrm{T}}^{\mathrm{miss}} + h(b\bar{b})$ limit. This is because $E_{\mathrm{T}}^{\mathrm{miss}} + Z(\ell\ell)$ can probe lower $E_{\mathrm{T}}^{\mathrm{miss}}$ values, whereas $E_{\mathrm{T}}^{\mathrm{miss}} + h(b\bar{b})$ requires a higher $E_{\mathrm{T}}^{\mathrm{miss}}$ threshold due to the use of a $E_{\mathrm{T}}^{\mathrm{miss}}$ trigger and due to the mass difference between the Z and Higgs bosons. For both $\sin\theta$ choices, but most notably for $\sin\theta = 0.7$ (Scenario 1b), an increase in the exclusion power of the $E_{\mathrm{T}}^{\mathrm{miss}} + h$ searches is observed at larger values of m_A and low values of m_a. This is due to an increase of the cross-section of the non-resonant $a^* \to ah$ process, without resonant A production. There is no equivalent process for the $E_{\mathrm{T}}^{\mathrm{miss}} + Z$ signature.

The $tbH^{\pm}(tb)$ search provides complementary sensitivity to the $E_{\mathrm{T}}^{\mathrm{miss}} + Z(\ell\ell)$ and $E_{\mathrm{T}}^{\mathrm{miss}} + h(b\bar{b})$ searches, excluding the range $m_A \lesssim 700$ GeV for $\sin\theta = 0.35$. Its exclusion contour shows only a moderate dependence on m_a as this search does not probe the production of the pseudo-scalar mediator directly and is therefore only indirectly affected by the choice of m_a via its effect on the relative branching ratio to tb compared with the branching ratios for other possible decay modes, such as $H^{\pm} \to aW^{\pm}$. The effect of this reduction of the branching ratio to tb is visible in Scenario 1b, where the limits from the $tbH^{\pm}(tb)$ search are slightly weaker at low values of m_a where, for example, the decay into $aW^{\pm}$ is kinematically allowed. The combination of the $tbH^{\pm}(tb)$ with the $E_{\mathrm{T}}^{\mathrm{miss}} + Z(\ell\ell)$ and $E_{\mathrm{T}}^{\mathrm{miss}} + h(b\bar{b})$ searches increases the excluded parameter space, especially the excluded m_a range for $m_A \approx 800$ GeV (Scenario 1a) and for $m_A \approx 700$ GeV (Scenario 1b).

The exclusion regions from other searches not entering the combination are added in the lower sub-figures of Fig. 4. The limit on the branching ratio for invisible Higgs boson decays constrains very low values of m_a, as searches for invisible Higgs boson decays are only sensitive to light a bosons decaying into invisible particles. The $E_{\mathrm{T}}^{\mathrm{miss}} + h(\gamma\gamma)$ search probes a similarly shaped, albeit smaller, region in parameter space compared with the $E_{\mathrm{T}}^{\mathrm{miss}} + h(b\bar{b})$ search due to the smaller branching ratio to $\gamma\gamma$ compared with $b\bar{b}$. However, its sensitivity exceeds that of the $E_{\mathrm{T}}^{\mathrm{miss}} + h(b\bar{b})$ search for low values of m_A because it does not rely on $E_{\mathrm{T}}^{\mathrm{miss}}$ triggers exclusively and hence is able to probe smaller values of $E_{\mathrm{T}}^{\mathrm{miss}}$. Like in the case of the $E_{\mathrm{T}}^{\mathrm{miss}} + h(b\bar{b})$ search, a significant increase in sensitivity for high values of m_A is found due an increase of the cross-section of the $a \to ah$ process. The $E_{\mathrm{T}}^{\mathrm{miss}} + h(\tau\tau)$ search is only interpreted in the scenario with $\sin\theta = 0.35$. Its exclusion contour shows a similar $m_A - m_a$ dependence as that of the $E_{\mathrm{T}}^{\mathrm{miss}} + h(b\bar{b})$ search but its sensitivity is notably lower due to smaller Higgs boson branching ratio to $\tau\tau$ compared with $b\bar{b}$ final states.

The exclusion contour for the $E_{\mathrm{T}}^{\mathrm{miss}} + tW$ search shows a shape similar to those of the $E_{\mathrm{T}}^{\mathrm{miss}} + Z(\ell\ell)$ search for both $\sin\theta$ choices, although the overall exclusion region is smaller. Its observed exclusion is weaker than the expected sensitivity due to a small (less than 2σ) excess in the 2-lepton channel [134]. The sensitivity of the $E_{\mathrm{T}}^{\mathrm{miss}} + tW$ search is greater for larger values of $\sin\theta$ [98].

The sensitivity of the $E_{\mathrm{T}}^{\mathrm{miss}} + j$ search in the $m_a - m_A$ plane is notably different from those of the $E_{\mathrm{T}}^{\mathrm{miss}} + Z$ and $E_{\mathrm{T}}^{\mathrm{miss}} + h$ searches due to the absence of resonant production diagrams for this signature. The signal cross-section for this signature, and hence its sensitivity to the 2HDM+a are affected by interference effects between the non-resonant contributions involving the two pseudo-scalars a and A. The impact of the interference depends notably on the values of both the m_a and m_A and is more pronounced for higher values of $\sin\theta$ due to the larger $a - A$ mixing [55]. In particular for signal hypotheses characterised by a small mass difference between A and a ($m_A \approx m_a$), the interference is destructive, leading to smaller signal cross-sections and hence a reduced sensitivity of the $E_{\mathrm{T}}^{\mathrm{miss}} + j$ signature to the 2HDM+a. This effect is visible for both $\sin\theta = 0.35$ and $\sin\theta = 0.7$. For the scenario with $\sin\theta = 0.35$, the $E_{\mathrm{T}}^{\mathrm{miss}} + j$ search excludes values of m_a up to 600 GeV for $m_A \approx 200$ GeV and values of m_A up to 800 GeV for $m_a \approx 100$ GeV. For the scenario with $\sin\theta = 0.7$, the larger $a - A$ mixing results in higher cross-sections for signal hypotheses with $m_A > m_a$. For $m_A \approx 1300$ GeV, the exclusion power in terms of m_a of the $E_{\mathrm{T}}^{\mathrm{miss}} + j$ search is comparable with that of the $E_{\mathrm{T}}^{\mathrm{miss}} + Z(\ell\ell)$ and $E_{\mathrm{T}}^{\mathrm{miss}} + h(b\bar{b})$ searches. A small region for $m_A < m_a$ is also excluded by the $E_{\mathrm{T}}^{\mathrm{miss}} + j$ search in the high-$\sin\theta$ scenario.

The $t\bar{t}t\bar{t}$ search, like the $tbH^{\pm}(tb)$ search, provides complementary sensitivity to the $E_{\mathrm{T}}^{\mathrm{miss}} + X$ searches, with the main difference that it is only sensitive to the 2HDM+a if either m_A or m_a is above the $t\bar{t}$ production threshold ($m_{A/a} \geqslant 2m_t$). For $\sin\theta = 0.35$, the $t\bar{t}t\bar{t}$ contour shows a behaviour similar to that of the $tbH^{\pm}(tb)$ search. The sensitivity is mostly driven by resonant A/H production and largely independent of m_a. For $\sin\theta = 0.7$, the sensitivity of the

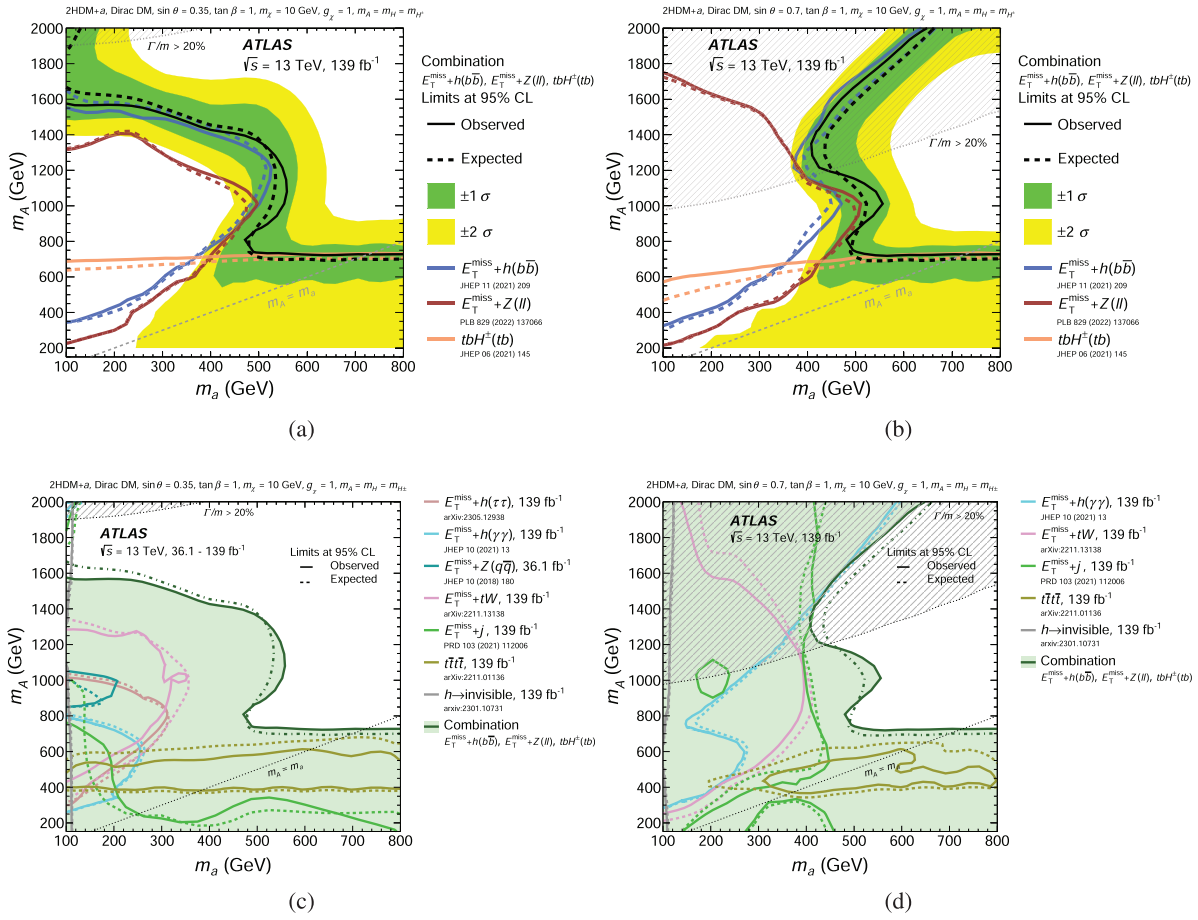

Fig. 4. (Color online) Observed (solid lines) and expected (dashed lines) exclusion regions at 95% C.L. in the (m_a, m_A) plane assuming (a, c) $\sin\theta = 0.35$ (Scenario 1a) and (b, d) $\sin\theta = 0.7$ (Scenario 1b). In the upper sub-figures, the observed (solid lines) and expected (dashed lines) exclusion regions for the statistical combination of the $E_{\mathrm{T}}^{\mathrm{miss}} + h(b\bar{b})$, $E_{\mathrm{T}}^{\mathrm{miss}} + Z(\ell\ell)$, and $tbH^{\pm}(tb)$ searches are shown, along with the observed and expected exclusion regions for the three individual searches entering the combination. The surrounding shaded bands correspond to the ±1 and ±2 standard deviation ($\pm1\sigma$, $\pm2\sigma$) uncertainty in the expected limit of the combined result. In the lower sub-figures, the results are shown for the combination of the $E_{\mathrm{T}}^{\mathrm{miss}} + h(b\bar{b})$, $E_{\mathrm{T}}^{\mathrm{miss}} + Z(\ell\ell)$, and $tbH^{\pm}(tb)$ searches (filled area) and additional individual searches. The individual results from the $E_{\mathrm{T}}^{\mathrm{miss}} + h(b\bar{b})$, $E_{\mathrm{T}}^{\mathrm{miss}} + Z(\ell\ell)$, and $tbH^{\pm}(tb)$ searches are not shown in this case. In all four sub-figures, dashed grey regions indicate the region where the width of any of the Higgs bosons exceeds 20% of its mass.

$t\bar{t}t\bar{t}$ search is smaller for $m_a < 2m_t$ compared with the scenario with $\sin\theta = 0.35$ due to the larger $a - A$ mixing and the fact that in this regime the decay into $a \to t\bar{t}$ is kinematically inaccessible.

For completeness, the observed and expected exclusion contours from a $E_{\mathrm{T}}^{\mathrm{miss}} + Z(q\bar{q})$ search on 36 fb^{-1} are shown for the scenario with $\sin\theta = 0.35$. This result was already included in Ref. [88]. The sensitivity of this search is considerably smaller than that of the $E_{\mathrm{T}}^{\mathrm{miss}} + Z(\ell\ell)$ search due to the larger backgrounds from multijet production in the hadronic decay channel and due to the smaller data sample on which the search is based.

8.2. Scenario 2: $m_A - \tan\beta$ planes

Exclusion limits as a function of the mass of the pseudo-scalar A and $\tan\beta$ (Scenario 2) are summarised in Fig. 5, again for the two scenarios with $\sin\theta = 0.35$ and $\sin\theta = 0.7$. For both the scenarios, a large fraction of the $m_A - \tan\beta$ plane is excluded by the $E_{\mathrm{T}}^{\mathrm{miss}} + Z(\ell\ell)$ search alone. For higher values of m_A, the $E_{\mathrm{T}}^{\mathrm{miss}} + h(b\bar{b})$ search, and hence the combination of the $E_{\mathrm{T}}^{\mathrm{miss}} + Z(\ell\ell)$, $E_{\mathrm{T}}^{\mathrm{miss}} + h(b\bar{b})$, and $tbH^{\pm}(tb)$ searches provides the strongest constraints. The sensitivity of the $E_{\mathrm{T}}^{\mathrm{miss}} + Z(\ell\ell)$ and $E_{\mathrm{T}}^{\mathrm{miss}} + h(b\bar{b})$ searches as a function of $\tan\beta$ is driven by the transition from gg- to $b\bar{b}$-initiated production with a minimum in sensitivity in the transition region around $\tan\beta \approx 5$.

The $E_{\mathrm{T}}^{\mathrm{miss}} + tW$ search probes values of $\tan\beta$ up to 1.5 ($\sin\theta = 0.35$) and 2 ($\sin\theta = 0.7$). Its observed exclusion is weaker than the expected sensitivity due to a small (less than 2σ) excess in the two-lepton channel [134]. Again, the sensitivity of the search is larger for the scenario with $\sin\theta = 0.7$ compared with that with $\sin\theta = 0.35$ [98]. The $E_{\mathrm{T}}^{\mathrm{miss}} + h(\tau\tau)$ search has only been interpreted for the scenario with $\sin\theta = 0.7$. Its sensitivity is notably smaller compared with that of the $E_{\mathrm{T}}^{\mathrm{miss}} + h(b\bar{b})$ search due to the smaller Higgs boson branching ratio to $\tau\tau$ compared with $b\bar{b}$. No exclusion contours are shown for the $E_{\mathrm{T}}^{\mathrm{miss}} + h(\gamma\gamma)$ search.

The sensitivity of the $tbH^{\pm}(tb)$ and $t\bar{t}t\bar{t}$ searches is largest at low values of m_A and $\tan\beta$. This is due to the larger production cross-section for smaller resonance masses and the preference of third-generation couplings at low values of $\tan\beta$.

8.3. Scenario 3: $m_a - \tan\beta$ planes

In Fig. 6, a similar benchmark scenario to that in Fig. 5 is shown with the difference that the mass of the pseudo-scalar mediator m_a rather than m_A is varied (Scenario 3). Again, the exclusion contours are shown for both the $\sin\theta = 0.35$ (Scenario 3a) and $\sin\theta = 0.7$

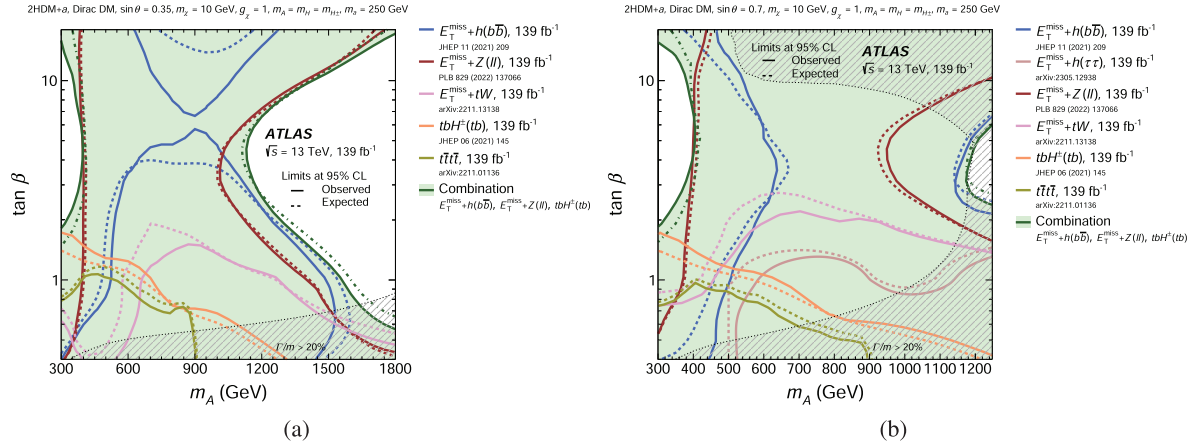

Fig. 5. (Color online) Observed (solid lines and filled area) and expected (dashed lines) exclusion regions at 95% C.L. in the $(m_A, \tan\beta)$ plane assuming (a) $\sin\theta = 0.35$ (Scenario 2a) and (b) $\sin\theta = 0.7$ (Scenario 2b). The results are shown for several individual searches and the combination of the $E_{\mathrm{T}}^{\mathrm{miss}} + h(b\bar{b})$, $E_{\mathrm{T}}^{\mathrm{miss}} + Z(\ell\ell)$, and $tbH^{\pm}(tb)$ searches. The dashed grey regions indicate the region where the width of any of the Higgs bosons exceeds 20% of its mass.

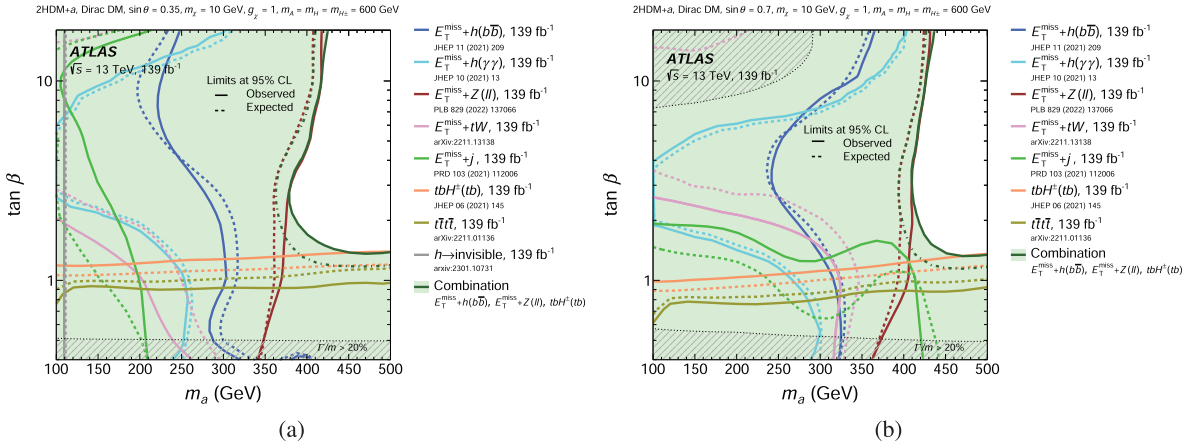

Fig. 6. (Color online) Observed (solid lines and filled area) and expected (dashed lines) exclusion regions at 95% C.L. in the $(m_a, \tan\beta)$ plane assuming (a) $\sin\theta = 0.35$ (Scenario 3a) and (b) $\sin\theta = 0.7$ (Scenario 3b). The results are shown for several individual searches and the combination of the $E_{\mathrm{T}}^{\mathrm{miss}} + h(b\bar{b})$, $E_{\mathrm{T}}^{\mathrm{miss}} + Z(\ell\ell)$, and $tbH^{\pm}(tb)$ searches. The dashed grey regions indicate the region where the width of any of the Higgs bosons exceeds 20% of its mass.

(Scenario 3b). The strongest exclusion is provided by the $E_{\mathrm{T}}^{\mathrm{miss}} + Z(\ell\ell)$ search. Its exclusion varies between $m_a \approx 350$ GeV at $\tan\beta = 0.4$ to above 400 GeV for $\tan\beta \approx 10$. The $E_{\mathrm{T}}^{\mathrm{miss}} + h(b\bar{b})$ and $E_{\mathrm{T}}^{\mathrm{miss}} + h(\gamma\gamma)$ searches exclude a similar $\tan\beta$ range as the $E_{\mathrm{T}}^{\mathrm{miss}} + Z(\ell\ell)$ search but the sensitivity does not reach as high in m_a as that of the $E_{\mathrm{T}}^{\mathrm{miss}} + Z(\ell\ell)$ search. In both the cases, as seen in the $\tan\beta - m_A$ scan for the $E_{\mathrm{T}}^{\mathrm{miss}} + h(b\bar{b})$ search, a decrease in sensitivity is observed for $\tan\beta \approx 5$ due to the transition from gg- to $b\bar{b}$-initiated production.

The $E_{\mathrm{T}}^{\mathrm{miss}} + tW$ search probes the range of low m_a and low $\tan\beta$ values with the sensitivity being slightly higher for the scenario with $\sin\theta = 0.7$. The $E_{\mathrm{T}}^{\mathrm{miss}} + j$ search also excludes signal hypotheses characterised by low values of m_a and $\tan\beta$. The sensitivity of this search is higher for the scenario with $\sin\theta = 0.7$ compared with that with $\sin\theta = 0.35$ due to the higher $a - A$ mixing, which leads to larger signal cross-sections for $m_A > m_a$, as pointed out in Section 8.1. Similarly to the $\tan\beta - m_A$ scan, the branching ratio limit on invisible Higgs boson decay provides constraints at very low values of m_a, independent of the value of $\tan\beta$.

The sensitivity of the $tbH^{\pm}(tb)$ and $t\bar{t}t\bar{t}$ searches is complementary to that of the $E_{\mathrm{T}}^{\mathrm{miss}} + X$ searches. It is mostly limited to the low $\tan\beta$ region and shows only a moderate dependence on m_a.

8.4. Scenario 4: Variation of $\sin\theta$

Exclusion limits as a function of $\sin\theta$ for the 2HDM+a for the low-mass and high-mass mediator hypothesis, respectively, are shown in Fig. 7. In the upper row of this figure, results interpreted for the baseline parameter choice $\tan\beta = 1$ of Scenario 4 are summarised, while in the lower row, additional results derived for the alternative choices $\tan\beta = 0.5$ or $\tan\beta = 50$ are shown. The subfigures on the left correspond to the low-mass hypothesis ($m_A = 0.6$ TeV, $m_a = 200$ GeV, Scenario 4a), while those on the right are derived assuming the high-mass hypothesis ($m_A = 1.0$ TeV, $m_a = 350$ GeV, Scenario 4b). The limits are expressed in terms of the ratio of the excluded cross-section to the nominal cross-section of the model.

For the low-mass hypothesis with $\tan\beta = 1.0$, the strongest limits in the medium and high $\sin\theta$ range are provided by the

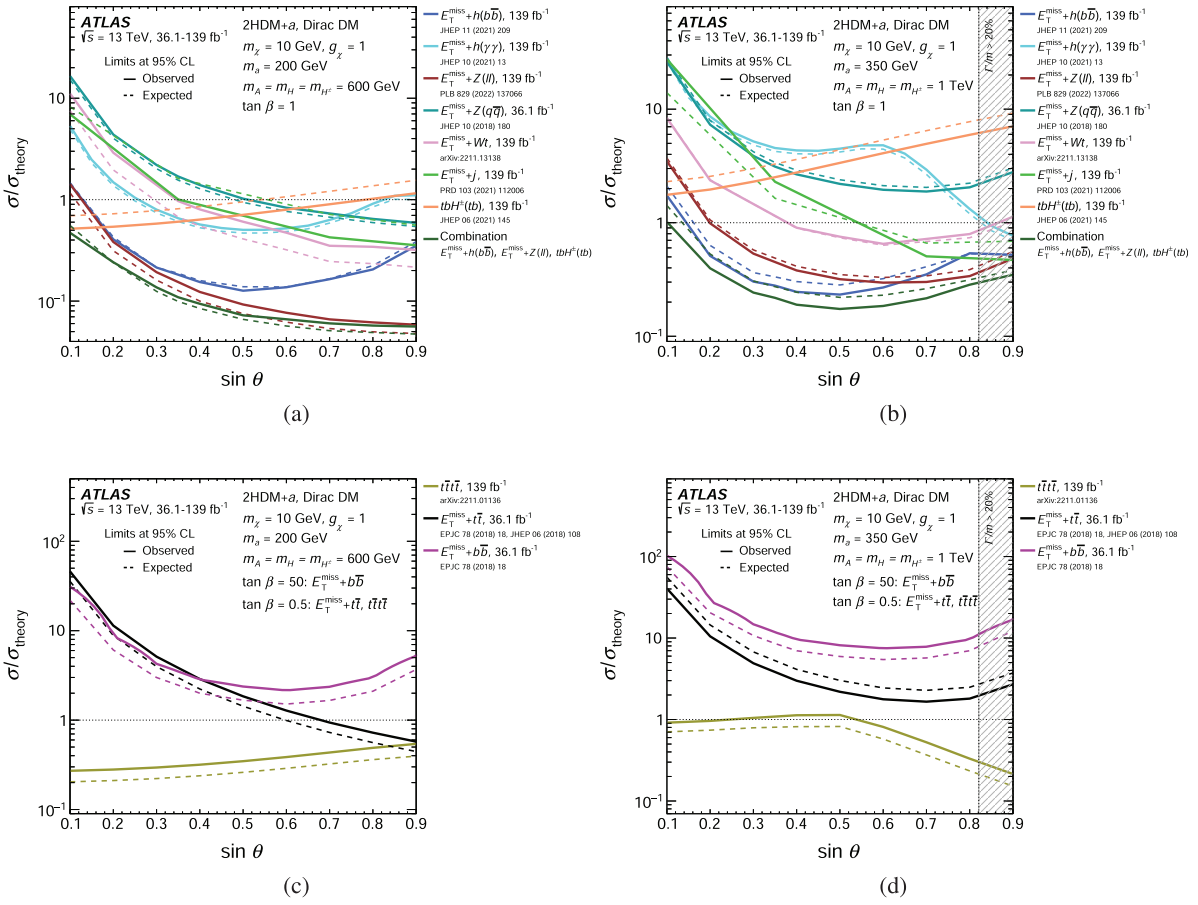

Fig. 7. (Color online) Observed (solid lines) and expected (dashed lines) exclusion limits at 95% C.L. for the 2HDM+a as a function of $\sin\theta$. Results in the subfigures (a) and (b) are derived for the default value $\tan\beta = 1$ of Scenario 4, while those in subfigures (c) and (d) are for alternative values of $\tan\beta = 0.5$ or $\tan\beta = 50$. Subfigures (a) and (c) correspond to $m_A = 0.6$ TeV, $m_a = 200$ GeV (low-mass hypothesis), while (b) and (d) contain results for $m_A = 1.0$ TeV, $m_a = 350$ GeV (high-mass hypothesis). The results are shown for several individual searches and the combination of the $E_{\mathrm{T}}^{\mathrm{miss}} + h(b\bar{b})$, $E_{\mathrm{T}}^{\mathrm{miss}} + Z(\ell\ell)$, and $tbH^{\pm}(tb)$ searches. The dashed grey regions indicate the region where the width of any of the Higgs bosons exceeds 20% of its mass.

$E_{\mathrm{T}}^{\mathrm{miss}} + Z(\ell\ell)$ and $E_{\mathrm{T}}^{\mathrm{miss}} + h(b\bar{b})$ searches. The sensitivity of the former monotonically increases as a function of $\sin\theta$, as the cross-section of the non-resonant and resonant production diagrams, in Figs. 1a and b, respectively, increases with $\sin\theta$. The same production diagrams for the $E_{\mathrm{T}}^{\mathrm{miss}} + h$ signature have very different $\sin\theta$ dependence, as described in Refs. [55,88]. The relative contributions of each diagram are additionally affected by the different $E_{\mathrm{T}}^{\mathrm{miss}} + h(b\bar{b})$ and $E_{\mathrm{T}}^{\mathrm{miss}} + h(\gamma\gamma)$ analysis selections. Both the analyses show a maximum of sensitivity around $\sin\theta \approx 0.5$. The sensitivities of the $E_{\mathrm{T}}^{\mathrm{miss}} + j$ and $E_{\mathrm{T}}^{\mathrm{miss}} + tW$ searches, like that of the $E_{\mathrm{T}}^{\mathrm{miss}} + Z(\ell\ell)$ search, increase monotonically with $\sin\theta$ but remain about an order of magnitude below that of the $E_{\mathrm{T}}^{\mathrm{miss}} + Z(\ell\ell)$ search across the full $\sin\theta$ range due to the overall lower cross-sections for these processes. The $tbH^{\pm}(tb)$ and $t\bar{t}t\bar{t}$ signatures show a different $\sin\theta$ dependence compared with the other signatures as they are not directly sensitive to the neutral boson production. They are particularly sensitive at very small mixing angles, with the $tbH^{\pm}(tb)$ sensitivity exceeding those of the $E_{\mathrm{T}}^{\mathrm{miss}} + h(b\bar{b})$ and $E_{\mathrm{T}}^{\mathrm{miss}} + Z(\ell\ell)$ searches, respectively, for $\sin\theta \lesssim 0.2$. The results from the $E_{\mathrm{T}}^{\mathrm{miss}} + V(q\bar{q})$ search from Ref. [88] are shown for completeness.

For the high-mass hypothesis with $\tan\beta = 1.0$, the mass of the light pseudo-scalar is high enough that the decay $a \to t\bar{t}$ is kinematically allowed, which introduces an additional $\sin\theta$ dependence to the $E_{\mathrm{T}}^{\mathrm{miss}} + Z$ and $E_{\mathrm{T}}^{\mathrm{miss}} + h$ analyses interpreted in this scenario. For this reason, the highest sensitivity for the $E_{\mathrm{T}}^{\mathrm{miss}} + Z$ and $E_{\mathrm{T}}^{\mathrm{miss}} + h$ analyses is found to be around (or slightly below) the maximal mixing condition ($\theta = \pi/4$). However, the $E_{\mathrm{T}}^{\mathrm{miss}} + h$ signatures have a complex $\sin\theta$ dependence due to the different contributions of resonant and non-resonant processes to the final selection in the two analyses. The sensitivity of the $E_{\mathrm{T}}^{\mathrm{miss}} + h(b\bar{b})$ search shows a broad maximum for $\sin\theta$ values below the maximal mixing condition ($\theta = \pi/4$). The $E_{\mathrm{T}}^{\mathrm{miss}} + h(\gamma\gamma)$ search instead shows a local sensitivity minimum around $\sin\theta \simeq 0.6$. The $\sin\theta$ dependence of the $E_{\mathrm{T}}^{\mathrm{miss}} + tW$ search is similar to that of the $E_{\mathrm{T}}^{\mathrm{miss}} + h(b\bar{b})$ and $E_{\mathrm{T}}^{\mathrm{miss}} + Z(\ell\ell)$ searches but its sensitivity is roughly an order of magnitude below that achieved with the combination of the $E_{\mathrm{T}}^{\mathrm{miss}} + h(b\bar{b})$, $E_{\mathrm{T}}^{\mathrm{miss}} + Z(\ell\ell)$, and $tbH^{\pm}(tb)$ searches. In contrast, the $E_{\mathrm{T}}^{\mathrm{miss}} + j$ search shows a monotonic increase in sensitivity with increasing $\sin\theta$ and has a similar sensitivity to the $E_{\mathrm{T}}^{\mathrm{miss}} + h(b\bar{b})$ and $E_{\mathrm{T}}^{\mathrm{miss}} + Z(\ell\ell)$ searches for large values of $\sin\theta$. The $tbH^{\pm}(tb)$ signature, similarly to the low-mass mediator hypothesis, shows a constant sensitivity as a function of $\sin\theta$. Again, the results from the $E_{\mathrm{T}}^{\mathrm{miss}} + V(q\bar{q})$ search from Ref. [88] are shown for completeness.

Alternative choices of $\tan\beta = 0.5$ or $\tan\beta = 50$ for Scenario 4 are explored to highlight the strong $\tan\beta$ dependence of the exclu-

sion power of searches with a strong dependence on the Yukawa couplings of the neutral Higgs bosons and the mediator to fermions in a type-II 2HDM. At low values of $\tan\beta$, the scalars and pseudo-scalars couple preferentially to top quarks, while at high values of $\tan\beta$, couplings to bottom quarks are preferred. Hence, the results of the $t\bar{t}t\bar{t}$ search are shown for $\tan\beta = 0.5$. The sensitivity of the $t\bar{t}t\bar{t}$ search is higher for the low-mass compared with the high-mass scenario primarily due to the lower cross-sections for A/H production at higher values of $m_{A/H}$. In the high-mass scenario, an increase in the $t\bar{t}t\bar{t}$ sensitivity is observed for $\sin\theta > 0.5$ due to the increased $a - A$ mixing and the fact that the mediator mass in this scenario is large enough to allow mediator decays into $t\bar{t}$ and at the same time considerably below the A/H masses, which results in the $t\bar{t}t\bar{t}$ signal cross-section being completely dominated by $t\bar{t} + a(t\bar{t})$ production. For completeness, the results from the $E_{\mathrm{T}}^{\mathrm{miss}} + t\bar{t}$ and $E_{\mathrm{T}}^{\mathrm{miss}} + b\bar{b}$ searches included in Ref. [88] are shown for values of $\tan\beta = 0.5$ and $\tan\beta = 50$, respectively.

8.5. Scenario 5: Variation of m_χ

In Fig. 8, the sensitivity of the different searches is compared as a function of the DM mass m_χ, which is the parameter with the strongest impact on the relic density predicted by the 2HDM+a. This corresponds to benchmark Scenario 5 in Section 2. The sensitivity of the searches is quantified as the observed exclusion limits on the ratio of the excluded cross-section to the nominal cross-section of the model (left vertical axis). The predicted relic density (right vertical axis) for each value of m_χ is overlaid on the plot as a long-dashed line. The region at $m_\chi = m_a/2 = 200$ GeV corresponds to the a-funnel region [71,153,154] where the predicted relic density is depleted by the resonant enhancement of the process $\chi\bar{\chi} \to a \to$ SM. A second funnel region at $m_\chi = m_A/2 = 500$ GeV, corresponding to the resonant enhancement of the process $\chi\bar{\chi} \to A \to$ SM, is not fully included in the probed m_χ range but partially visible as a decrease in the predicted relic density for $m_\chi > 400$ GeV. The plateau for $m_\chi > 200$ GeV is determined by the increase in annihilation cross-section of the DM particles close to threshold for the processes $\chi\bar{\chi} \to t\bar{t}$ (if $m_\chi > m_t$) and $\chi\bar{\chi} \to ah$ (if $m_\chi > (m_a + m_h)/2$). For all signatures shown here, the sensitivity is independent of m_χ as long as the pseudo-scalar mediator, whose mass is fixed at 400 GeV in this benchmark scenario, is allowed to decay into a $\chi\bar{\chi}$ pair. The strongest constraints on this region ($m_\chi < 200$ GeV) from individual searches are provided by the $E_{\mathrm{T}}^{\mathrm{miss}} + Z(\ell\ell)$ search, which, together with the $E_{\mathrm{T}}^{\mathrm{miss}} + h(b\bar{b})$ search, excludes this parameter space. For higher DM masses, the sensitivity of the $E_{\mathrm{T}}^{\mathrm{miss}} + X$ searches decreases rapidly, while that of the $tbH^{\pm}(tb)$ and $t\bar{t}t\bar{t}$ searches remains nearly constant. This is because the corresponding signal processes at LO do not involve the DM particle χ, making the signal cross-sections independent of m_χ. For $m_\chi > m_a/2$, the strongest constraints are obtained from the $tbH^{\pm}(tb)$ search, which probes cross-sections as low as $\sigma/\sigma_{\mathrm{theory}} \approx 2 - 3$. Hence none of the searches excludes the 2HDM+a in this mass region for the chosen benchmark scenario. It is possible to match the observed relic density for $m_\chi \approx 170$ GeV without changing the collider phenomenology, although this value is disfavoured by the searches in this benchmark scenario. It should be noted that the relic density considerations serve as a useful means for putting the 2HDM+a predictions in the context of cosmological observations but should not be understood as strict constraints on the model parameters. This is because the parameter values giving the correct relic density can change either if the model is modified to include additional physics at higher energy scales or if a different cosmological history is assumed.

8.6. Scenario 6: $m_a - m_\chi$ plane

Exclusion limits as a function of m_a and m_χ corresponding to Scenario 6 are shown in Fig. 9. The $h \to aa \to f\bar{f}f'\bar{f}'$ searches target the region characterised by $m_a < m_h/2$, where the decay $h \to aa$ is kinematically allowed, and $m_a < 2m_\chi$ where invisible mediator decays are kinematically forbidden. This region is almost fully excluded by the $h \to aa \to f\bar{f}f'\bar{f}'$ searches under consideration, except for two bands where m_a is close to the masses of the J/ψ and Υ mesons. As discussed in Section 5.2.3, these mass regions

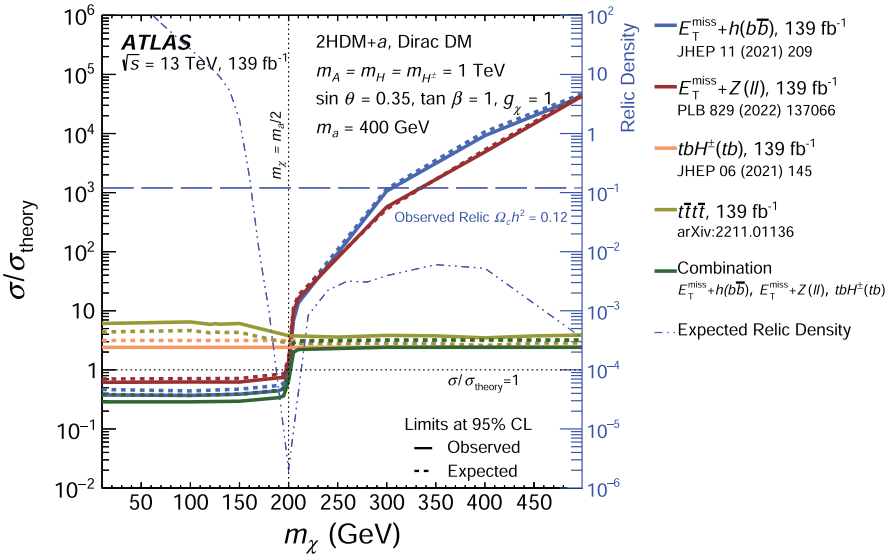

Fig. 8. (Color online) Observed (solid lines) and expected (dashed lines) exclusion limits for the 2HDM+a as a function of m_χ, following the parameter choices of $m_A = 1.0$ TeV, $m_a = 400$ GeV, $\tan\beta = 1.0$, and $\sin\theta = 0.35$ (Scenario 5). The limits are calculated at 95% C.L. and are expressed in terms of the ratio of the excluded cross-section to the nominal cross-section of the model. The results are shown for several individual searches and the combination of the $E_{\mathrm{T}}^{\mathrm{miss}} + Z(\ell\ell)$, $E_{\mathrm{T}}^{\mathrm{miss}} + h(b\bar{b})$, and $tbH^{\pm}(tb)$ searches. The relic density for each m_χ assumption, calculated with MADDM [155], is superimposed in the plot (dashed line) and described by the right vertical axis. The valley at $m_\chi = 200$ GeV indicates the a-funnel region [71,153,154] where the predicted relic density is depleted by the resonant enhancement of the processes $\chi\bar{\chi} \to A/a \to$ SM.

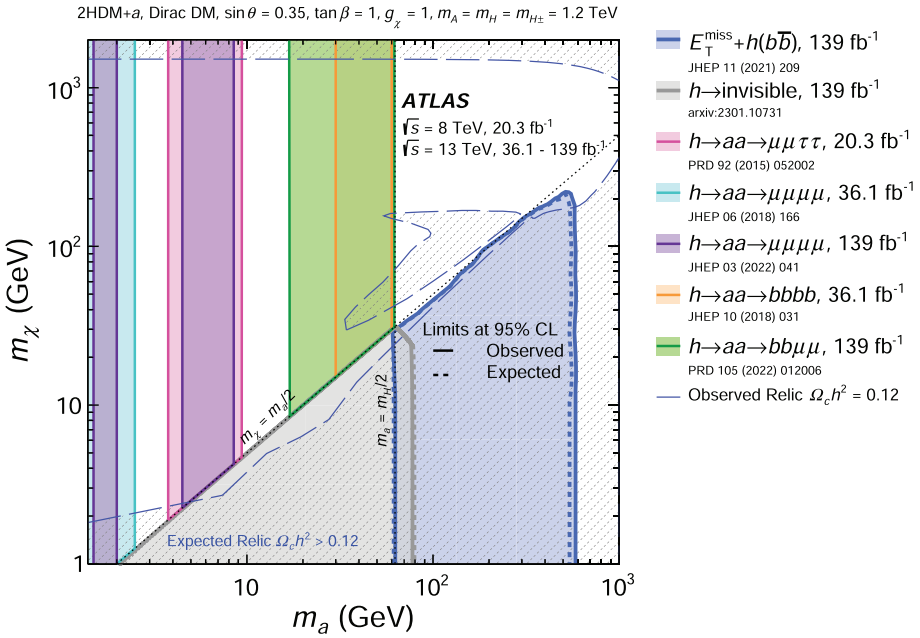

Fig. 9. (Color online) Observed (solid lines) and expected (dashed lines) exclusion regions at 95% C.L. in the (m_a, m_χ) plane following the parameter choices of $m_A = 1.2$ TeV, $\tan\beta = 1.0$, and $\sin\theta = 0.35$ (Scenario 6). The relic density contour for the case $\Omega_c h^2 = 0.12$, calculated with MADDM [155], is superimposed in the plot (long-dashed line). The shaded regions mark parameter values for which the model predict a relic density greater than the observed value $\Omega_c h^2 = 0.12$. The "island" around ($m_\chi \approx 100$ GeV, $m_a \approx 100$ GeV) corresponds to the resonant enhancement of the process $\chi\bar{\chi} \to ah \to$ SM, which depletes the relic density.

are excluded from the searches. Experimentally di-muon searches near the J/ψ mass are challenging, as are $h \to aa \to 4g$ searches. The $\mu^+\mu^-\tau^+\tau^-$ final states [81] have some sensitivity, but are unable to exclude the higher mass region around $m_a = 10$ GeV. Searches for hadronic final states are complicated by the collimation of the quark pairs, and dedicated techniques are often required to make signatures such as $b\bar{b}\tau^+\tau^-$ and $b\bar{b}b\bar{b}$ sensitive. The $h \to aa \to f\bar{f}f'\bar{f}'$ searches are not sensitive for $m_a > m_A/2$, where invisible mediator decays dominate the branching ratio. For $m_a < m_h/2$, this region is excluded by the $h \to$ invisible search. For larger values of m_a, the region $m_a > m_\chi/2$ is excluded by the $E_{\mathrm{T}}^{\mathrm{miss}} + h(b\bar{b})$ search up to $m_a \approx 600$ GeV. The unexcluded high-m_a, high-m_χ region can be probed by searches for the mediator or heavy Higgs boson states in signatures such as $t\bar{t}t\bar{t}$ and $tbH^\pm(tb)$, which are currently unable to exclude $m_A = 1200$ GeV.

The relic density contour for the case $\Omega_c h^2 = 0.12$ is superimposed in the plot (long-dashed line). Regions above this line at low m_χ and below this line at high m_χ, excluding the "island" region around ($m_\chi \approx 100$ GeV, $m_a \approx 150$ GeV), have a predicted relic density $\Omega_c h^2 < 0.12$. Due to the large Yukawa couping, the annihilation process $\chi\bar{\chi} \to t\bar{t}$ is very efficient. For regions with light DM ($m_\chi < m_t$), this is kinematically inaccessible and the predicted relic density is often over-abundant unless alternative annihilation channels are available. The most important of these is resonant annihilation when $m_\chi \simeq m_a/2$, and specific decay channels such as $\chi\bar{\chi} \to aa$ or $\chi\bar{\chi} \to ah$ when allowed or enhanced by kinematics. For low m_a, annihilation to fermions (e.g. $b\bar{b}$, $c\bar{c}$, $\tau^+\tau^-$) can be efficient enough to overcome their smaller couplings and deplete the relic abundance. Larger values of m_χ can also satisfy the observed relic density, as these annihilations become more suppressed.

9. Conclusion

A broad variety of searches for new phenomena performed by the ATLAS Collaboration are summarised and interpreted in the context of a common LHC dark matter benchmark model, namely a 2HDM with an additional pseudo-scalar mediator a (2HDM+a), which couples the dark matter particles to the SM. This model predicts a rich phenomenology of processes resulting in a diverse range of final-state signatures. The searches presented provide sensitivity across a wide range of the model parameter space.

The results are based on up to 139 fb^{-1} of proton-proton collision data at a centre-of-mass energy of $\sqrt{s} = 13$ TeV collected by the ATLAS detector at the LHC in the years 2015–2018, and are in agreement with the SM predictions. Therefore, the results are translated into exclusion limits on the 2HDM+a for a wide selection of representative benchmark scenarios. These include previously explored benchmark scenarios based on the recommendations of the LHC Dark Matter Working Group as well as several new benchmark scenarios that provide further insights into the rich collider phenomenology of the 2HDM+a. All benchmark scenarios rely on the simplifying assumption that the additional Higgs bosons of the 2HDM are mass degenerate ($m_A = m_H = m_{H^\pm}$). The exploration of additional benchmark scenarios in which this assumption is relaxed is left to future publications.

Masses of the pseudo-scalar mediator a are excluded up to 560 GeV for $m_A = m_H = m_{H^\pm} = 1.2$ TeV, $\sin\theta = 0.35$, and $\tan\beta = 1.0$. Values of m_a up to 640 GeV are excluded for $m_A = m_H = m_{H^\pm} = 2.0$ TeV, $\sin\theta = 0.7$, and $\tan\beta = 1.0$. The $E_{\mathrm{T}}^{\mathrm{miss}} + Z(\ell\ell)$ and $E_{\mathrm{T}}^{\mathrm{miss}} + h(b\bar{b})$ searches are the most sensitive analyses in this region of large heavy Higgs boson masses ($m_A = m_H = m_{H^\pm}$). These results mark a significant improvement compared to previous results based on only 36 fb^{-1} of proton-proton collision data at the same centre-of-mass energy, for which the maximum exclusion reach in m_a was up to 340 GeV for $m_A = m_H = m_{H^\pm} = 1.0$ TeV, $\sin\theta = 0.35$, and $\tan\beta = 1.0$. These improvements are not only due to the larger amount of data used in this publication but various improvements in the analysis strategies of the individual searches as well as the statistical combination of the most sensitive individual results.

Additionally, the interpretation of the $tbH^\pm(tb)$ search in the context of the 2HDM+a allows for values of m_A up to 650 GeV to be excluded across the full probed m_a range. The $tbH^\pm(tb)$ search

was not considered in any previous publications but is the most sensitive analysis in this low-m_A region for mediator masses above 400 GeV. It also signficantly extends the exclusion reach in $\tan\beta$ across the full probed m_a range from $\tan\beta \approx 0.6$ achieved via a $t\bar{t}t\bar{t}$ search based on 36 fb^{-1} to $\tan\beta \approx 1.2$ for the same benchmark scenario 3a in this publication. This highlights the importance of searches that are not classically interpreted in the context of DM in constraining more complex models of DM, such as the 2HDM+a. A statistical combination of the $E_{\mathrm{T}}^{\mathrm{miss}} + Z(\ell\ell)$, $E_{\mathrm{T}}^{\mathrm{miss}} + h(b\bar{b})$, and $tbH^{\pm}(tb)$ searches is performed. This combination extends the sensitivity to the 2HDM+a compared with the sensitivities derived from the individual searches across different regions of the 2HDM+a parameter space. Compared with the previous summary of 36 fb^{-1} results, the excluded regions in these benchmark scenarios are considerably extended. Nonetheless, there remains sizeable unexcluded model space, especially if the full parameter space or more general 2HDM+a models are considered. Finally, for the first time the results of searches targeting $h \to aa \to f\bar{f}f'\bar{f}'$ are used to constrain a part of previously unprobed 2HDM+a parameter space. The results in this paper represent the most comprehensive set of constraints on the 2HDM+a obtained by the ATLAS Collaboration to date.

Conflict of interest

The authors declare that they have no conflict of interest.

Acknowledgments

We thank CERN for the very successful operation of the LHC and its injectors, as well as the support staff at CERN and at our institutions worldwide without whom ATLAS could not be operated efficiently.

The crucial computing support from all WLCG partners is acknowledged gratefully, in particular from CERN, the ATLAS Tier-1 facilities at TRIUMF/SFU (Canada), NDGF (Denmark, Norway, Sweden), CC-IN2P3 (France), KIT/GridKA (Germany), INFN-CNAF (Italy), NL-T1 (Netherlands), PIC (Spain), RAL (UK) and BNL (USA), the Tier-2 facilities worldwide and large non-WLCG resource providers. Major contributors of computing resources are listed in Ref. [156].

We gratefully acknowledge the support of ANPCyT, Argentina; YerPhI, Armenia; ARC, Australia; BMWFW and FWF, Austria; ANAS, Azerbaijan; CNPq and FAPESP, Brazil; NSERC, NRC and CFI, Canada; CERN; ANID, Chile; CAS, MOST and NSFC, China; Minciencias, Colombia; MEYS CR, Czech Republic; DNRF and DNSRC, Denmark; IN2P3-CNRS and CEA-DRF/IRFU, France; SRNSFG, Georgia; BMBF, HGF and MPG, Germany; GSRI, Greece; RGC and Hong Kong SAR, China; ISF and Benoziyo Center, Israel; INFN, Italy; MEXT and JSPS, Japan; CNRST, Morocco; NWO, Netherlands; RCN, Norway; MEiN, Poland; FCT, Portugal; MNE/IFA, Romania; MESTD, Serbia; MSSR, Slovakia; ARRS and MIZŠ, Slovenia; DSI/NRF, South Africa; MICINN, Spain; SRC and Wallenberg Foundation, Sweden; SERI, SNSF and Cantons of Bern and Geneva, Switzerland; MOST, Taipei; TENMAK, Türkiye; STFC, United Kingdom; DOE and NSF, United States of America.

Individual groups and members have received support from BCKDF, CANARIE, CRC and DRAC, Canada; CERN-CZ, PRIMUS 21/SCI/017 and UNCE SCI/013, Czech Republic; COST, ERC, ERDF, Horizon 2020, ICSC-NextGenerationEU and Marie Skłodowska-Curie Actions, European Union; Investissements d'Avenir Labex, Investissements d'Avenir Idex and ANR, France; DFG and AvH Foundation, Germany; Herakleitos, Thales and Aristeia programmes co-financed by EU-ESF and the Greek NSRF, Greece; BSF-NSF and MINERVA, Israel; Norwegian Financial Mechanism 2014–2021, Norway; NCN and NAWA, Poland; La Caixa Banking Foundation, CERCA Programme Generalitat de Catalunya and PROMETEO and GenT Programmes Generalitat Valenciana, Spain; Göran Gustafssons Stiftelse, Sweden; The Royal Society and Leverhulme Trust, United Kingdom.

In addition, individual members wish to acknowledge support from Chile: Agencia Nacional de Investigación y Desarrollo (FONDECYT 1190886, FONDECYT 1210400, FONDECYT 1230812, FONDECYT 1230987); China: the National Natural Science Foundation of China (12175119, 12275265, 12075060); Czech Republic: PRIMUS Research Programme (PRIMUS/21/SCI/017); European Union: European Research Council (ERC-948254), Horizon 2020 Framework Programme (MUCCA-CHIST-ERA-19-XAI-00), European Union, Future Artificial Intelligence Research (FAIR-NextGenerationEU PE00000013), Italian Center for High Performance Computing, Big Data and Quantum Computing (ICSC, NextGenerationEU), Marie Sklodowska-Curie Actions (EU H2020 MSC IF GRANT NO 101033496); France: Agence Nationale de la Recherche (ANR-20-CE31-0013, ANR-21-CE31-0013, ANR-21-CE31-0022), Investissements d'Avenir Idex (ANR-11-LABX-0012), Investissements d'Avenir Labex (ANR-11-LABX-0012); Germany: Baden-Württemberg Stiftung (BW Stiftung-Postdoc Eliteprogramme), Deutsche Forschungsgemeinschaft (DFG-CR 312/5–1); Italy: Istituto Nazionale di Fisica Nucleare (FELLINI G.A. n. 754496, ICSC, NextGenerationEU); Japan: Japan Society for the Promotion of Science (JSPS KAKENHI JP21H05085, JSPS KAKENHI JP22H01227, JSPS KAKENHI JP22H04944); Netherlands: Netherlands Organisation for Scientific Research (NWO Veni 2020-VI.Veni.202.179); Norway: Research Council of Norway (RCN-314472); Poland: Polish National Agency for Academic Exchange (PPN/PPO/2020/1/00002/U/00001), Polish National Science Centre (NCN 2021/42/E/ST2/00350, NCN UMO-2019/34/E/ST2/00393, UMO-2020/37/B/ST2/01043, UMO-2021/40/C/ST2/00187); Slovenia: Slovenian Research Agency (ARIS grant J1-3010); Spain: BBVA Foundation (LEO22-1–603), Generalitat Valenciana (Artemisa, FEDER, IDIFEDER/2018/048), La Caixa Banking Foundation (LCF/BQ/PI20/11760025), Ministry of Science and Innovation (MCIN & NextGenEU -PCI2022-135018–2, MICIN & FEDER-PID2021-125273NB, RYC2019-028510-I, RYC2020-030254-I, RYC2021-031273-I, RYC2022-038164-I), PROMETEO and GenT Programmes Generalitat Valenciana (CIDEGENT/2019/023, CIDEGENT/2019/027); Sweden: Swedish Research Council (VR 2018-00482, VR 2022-03845, VR 2022–04683, VR grant 2021-03651), Knut and Alice Wallenberg Foundation (KAW 2017.0100, KAW 2018.0157, KAW 2018.0458, KAW 2019.0447); Switzerland: Swiss National Science Foundation (SNSF-PCEFP2_194658); United Kingdom: Leverhulme Trust (Leverhulme Trust RPG-2020–004); United States of America: Neubauer Family Foundation.

References

[1] Corbelli E, Salucci P. The extended rotation curve and the dark matter halo of M33. Mon Not Roy Astron Soc 2000;311:441.
[2] Rubin VC, Ford WK, Thonnard N. Rotational properties of 21 Sc galaxies with a large range of luminosities and radii, from NGC 4605 (R = 4 kpc) to UGC 2885 (R = 122 kpc). Astrophys J 1980;238:471.
[3] Begeman KG, Broeils AH, Sanders RH. Extended rotation curves of spiral galaxies: Dark haloes and modified dynamics. Mon Not Roy Astron Soc 1991;249:523.
[4] Hinshaw G, Larson D, Komatsu E, et al. Nine-year Wilkinson Microwave Anisotropy Probe (WMAP) observations: Cosmological parameter results. Astrophys J Suppl 2013;208:19.
[5] Planck Collaboration, Aghanim N, et al. Planck 2018 results. I. Overview and the cosmological legacy of Planck. Astron Astrophys 2020;641:A1.
[6] Trimble V. Existence and nature of dark matter in the Universe. Ann Rev Astron Astrophys 1987;25:425.
[7] Bertone G, Hooper D, Silk J. Particle dark matter: Evidence, candidates and constraints. Phys Rept 2005;405:279.

[8] Feng JL. Dark matter candidates from particle physics and methods of detection. Ann Rev Astron Astrophys 2010;48:495.
[9] Acharyya A, Archer A, Bangale P, et al. Search for ultraheavy dark matter from observations of dwarf spheroidal galaxies with VERITAS. Astrophys J 2023;945:101.
[10] H.E.S.S. Collaboration, Abdalla H, et al. Search for dark matter annihilation signals in the H.E.S.S. inner galaxy survey. Phys Rev Lett 2022;129:111101.
[11] MAGIC Collaboration, Acciari VA, et al. Combined searches for dark matter in dwarf spheroidal galaxies observed with the MAGIC telescopes, including new data from Coma Berenices and Draco. Phys Dark Univ 2022;35:100912.
[12] Acharyya A, Archer A, Bangale P, et al. Sensitivity of the Cherenkov Telescope Array to a dark matter signal from the Galactic centre. J Cosmol Astropart Phys 2021;1:057.
[13] Abeysekara AU, Albert AM, Alfaro R, et al. A search for dark matter in the Galactic halo with HAWC. J Cosmol Astropart Phys 2018;02:049.
[14] IceCube Collaboration, Aartsen MG, et al. Search for neutrinos from decaying dark matter with IceCube. Eur Phys J C 2018;78:831.
[15] IceCube Collaboration, Abbasi R, et al. Search for GeV-scale dark matter annihilation in the Sun with IceCube DeepCore. Phys Rev D 2022;105:062004.
[16] Fermi-LAT Collaboration, DES Collaboration, Albert A, et al. Searching for dark matter annihilation in recently discovered Milky Way satellites with Fermi-LAT. Astrophys J 2017;834:110.
[17] Fermi-LAT Collaboration, Albert A, et al. The Fermi galactic center GeV excess and implications for dark matter. Astrophys J 2017;840:43.
[18] Aalbers J, Abe K, Aerne V, et al. A next-generation liquid Xenon observatory for dark matter and neutrino physics. J Phys G 2023;50:013001.
[19] Aalbers J, Akerib D, Akerlof C, et al. First dark matter search results from the LUX-ZEPLIN (LZ) Experiment. Phys Rev Lett 2023;131:041002.
[20] Akerib DS, Alsum S, Araùjo H, et al. Results from a search for dark matter in the complete LUX exposure. Phys Rev Lett 2017;118:021303.
[21] Amole C, Ardid M, Arnquistand IJ, et al. Dark matter search results from the complete exposure of the PICO-60 C3F8 Bubble Chamber. Phys Rev D 2019;100:022001.
[22] PandaX-II Collaboration, Cheng C, et al. Search for light dark matter-electron scatterings in the PandaX-II Experiment. Phys Rev Lett 2021;126:211803.
[23] PandaX-II Collaboration, Cui X, et al. Dark matter results from 54-ton-day exposure of PandaX-II Experiment. Phys Rev Lett 2017;119:181302.
[24] XENON Collaboration, Aprile E, et al. Search for new physics in electronic recoil data from XENONnT. Phys Rev Lett 2022;129:161805.
[25] XENON Collaboration, Aprile E, et al. First dark matter search with nuclear recoils from the XENONnT Experiment. Phys Rev Lett 2023;131:041003.
[26] XENON Collaboration, Aprile E, et al. Constraining the spin-dependent WIMP-nucleon cross sections with XENON1T. Phys Rev Lett 2019;122:141301.
[27] XENON Collaboration, Aprile E, et al. Search for light dark matter interactions enhanced by the Migdal effect or Bremsstrahlung in XENON1T. Phys Rev Lett 2019;123:241803.
[28] DarkSide-50 Collaboration, Agnes P, et al. Search for low-mass dark matter WIMPs with 12 ton-day exposure of DarkSide-50. Phys Rev D 2023;107:063001.
[29] CRESST Collaboration, Angloher G, et al. Results on light dark matter particles with a low-threshold CRESST-II detector. Eur Phys J C 2016;76:25.
[30] Lai M. Recent results from DEAP-3600. J Instrum 2023;18:C02046.
[31] DEAP-3600 Collaboration, Amaudruz P-A, et al. First results from the DEAP-3600 dark matter search with Argon at SNOLAB. Phys Rev Lett 2018;121:071801.
[32] SuperCDMS Collaboration, Agnese R, et al. Results from the Super Cryogenic Dark Matter Search Experiment at Soudan. Phys Rev Lett 2018;120:061802.
[33] SuperCDMS Collaboration, Agnese R, et al. Low-mass dark matter search with CDMSlite. Phys Rev D 2018;97:022002.
[34] LIGO Scientific Collaboration, Virgo Collaboration, KAGRA Collaboration, Abbott R, et al. Constraints on dark photon dark matter using data from LIGO's and Virgo's third observing run. Phys Rev D 2022;105:063030.
[35] Vermeulen SM, Relton P, Grote H. Direct limits for scalar field dark matter from a gravitational-wave detector. Nature 2021;600:424.
[36] ATLAS Collaboration, Aad G, et al. The ATLAS Experiment at the CERN Large Hadron Collider. J Instrum 2008;3:S08003.
[37] Evans L, Bryant P, Machine LHC. J Instrum 2008;3:S08001.
[38] Georgi HM, Kaplan DB, Randall L. Manifesting the invisible axion at low energies. Phys Lett B 1986;169:73.
[39] Choi K, Kang K, Kim JE. Effects of η' in low-energy axion physics. Phys Lett B 1986;181:145.
[40] Preskill J, Wise MB, Wilczek F. Cosmology of the invisible axion. Phys Lett B 1983;120:127.
[41] Abbott LF, Sikivie P. A cosmological bound on the invisible axion. Phys Lett B 1983;120:133.
[42] Dine M, Fischler W. The not so harmless axion. Phys Lett B 1983;120:137.
[43] Steigman G, Turner MS. Cosmological constraints on the properties of weakly interacting massive particles. Nucl Phys B 1985;253:375.
[44] Kolb EW, Turner MS. The Early Universe. Boca Raton:CRC Press;1990.
[45] ATLAS Collaboration, Aad G, et al. Search for new phenomena in events with an energetic jet and missing transverse momentum in pp collisions at $\sqrt{s}$ = 13 TeV with the ATLAS detector. Phys Rev D 2021;103:112006.
[46] CMS Collaboration, Tumasyan A, et al. Search for new particles in events with energetic jets and large missing transverse momentum in proton–proton collisions at $\sqrt{s}$ = 13 TeV. J High Energy Phys 2021;11:153.
[47] ATLAS Collaboration, Aad G, et al. Search for new resonances in mass distributions of jet pairs using 139 fb^{-1} of pp collisions at $\sqrt{s}$ = 13 TeV with the ATLAS detector. J High Energy Phys 2020;03:145.
[48] ATLAS Collaboration, Aad G, et al. Search for high-mass dilepton resonances using 139 fb^{-1} of pp collision data collected at $\sqrt{s}$ = 13 TeV with the ATLAS detector. Phys Lett B 2019;796:68.
[49] CMS Collaboration, Sirunyan AM, et al. Search for narrow and broad dijet resonances in proton–proton collisions at $\sqrt{s}$ = 13 TeV and constraints on dark matter mediators and other new particles. J High Energy Phys 2018;08:130.
[50] CMS Collaboration, Sirunyan AM, et al. Search for high mass dijet resonances with a new background prediction method in proton–proton collisions at $\sqrt{s}$ = 13 TeV. J High Energy Phys 2020;05:033.
[51] CMS Collaboration, Sirunyan AM, et al. Search for resonant and nonresonant new phenomena in high-mass dilepton final states at $\sqrt{s}$ = 13 TeV. J High Energy Phys 2021;07:208.
[52] Abercrombie D, Akchurin N, Akilli E, et al. Dark matter benchmark models for early LHC Run-2 Searches: Report of the ATLAS/CMS Dark Matter Forum. Phys Dark Univ 2020;27:100371.
[53] Boveia A, Buchmueller O, Busoni G, et al. Recommendations on presenting LHC searches for missing transverse energy signals using simplified s-channel models of dark matter. Phys Dark Univ 2020;27:100365.
[54] Albert A, Backovic M, Boveia A, et al. Recommendations of the LHC Dark Matter Working Group: Comparing LHC searches for dark matter mediators in visible and invisible decay channels and calculations of the thermal relic density. Phys Dark Univ 2019;26:100377.
[55] Bauer M, Haisch U, Kahlhoefer F. Simplified dark matter models with two Higgs doublets: I. Pseudoscalar mediators. J High Energy Phys 2017;5:138.
[56] Golfand YA, Likhtman EP. Extension of the algebra of Poincare group generators and violation of p invariance. JETP Lett 1971;13:323.
[57] Volkov DV, Akulov VP. Is the neutrino a goldstone particle? Phys Lett B 1973;46:109.
[58] Wess J, Zumino B. Supergauge transformations in four-dimensions. Nucl Phys B 1974;70:39.
[59] Wess J, Zumino B. Supergauge invariant extension of Quantum Electrodynamics. Nucl Phys B 1974;78:1.
[60] Ferrara S, Zumino B. Supergauge invariant Yang-Mills theories. Nucl Phys B 1974;79:413.
[61] Salam A, Strathdee JA. Supersymmetry and nonabelian gauges. Phys Lett B 1974;51:353.
[62] Dorsch GC, Huber SJ, Konstandin T, et al. A second Higgs doublet in the early universe: Baryogenesis and gravitational waves. J Cosmol Astropart Phys 2017;5:052.
[63] McLerran LD, Shaposhnikov ME, Turok N, et al. Why the baryon asymmetry of the universe is approximately 10^{-10}. Phys Lett B 1991;256:451.
[64] Turok N, Zadrozny J. Electroweak baryogenesis in the two doublet model. Nucl Phys B 1991;358:471.
[65] Cohen AG, Kaplan DB, Nelson AE. Spontaneous baryogenesis at the weak phase transition. Phys Lett B 1991;263:86.
[66] Cline JM, Lemieux P-A. Electroweak phase transition in two Higgs doublet models. Phys Rev D 1997;55:3873.
[67] Fromme L, Huber SJ, Seniuch M. Baryogenesis in the two-Higgs doublet model. J High Energy Phys 2006;11:038.
[68] Cline JM, Kainulainen K, Trott M. Electroweak baryogenesis in two Higgs doublet models and B meson anomalies. J High Energy Phys 2011;11:089.
[69] Kim JE. Light pseudoscalars, particle physics and cosmology. Phys Rept 1987;150:1.
[70] Buckley MR, Feld D, Goncalves D. Scalar simplified models for dark matter. Phys Rev D 2015;91:015017.
[71] Abe T, Afik Y, Albert A, et al. LHC Dark Matter Working Group: Next-generation spin-0 dark matter models. Phys Dark Univ 2020;27:100351.
[72] ATLAS Collaboration, Aad G, et al. Observation of a new particle in the search for the Standard Model Higgs boson with the ATLAS detector at the LHC. Phys Lett B 2012;716:1.
[73] CMS Collaboration, Chatrchyan S, et al. Observation of a new boson at a mass of 125 GeV with the CMS experiment at the LHC. Phys Lett B 2012;716:30.
[74] ATLAS Collaboration, Aad G, et al. Search for associated production of a Z boson with an invisibly decaying Higgs boson or dark matter candidates at $\sqrt{s}$ = 13 TeV with the ATLAS detector. Phys Lett B 2022;829:137066.
[75] ATLAS Collaboration, Aad G, et al. Search for dark matter produced in association with a Standard Model Higgs boson decaying into b-quarks using the full Run 2 dataset from the ATLAS detector. J High Energy Phys 2021;11:209.
[76] ATLAS Collaboration, Aad G, et al. Search for charged Higgs bosons decaying into a top quark and a bottom quark at $\sqrt{s}$ = 13 TeV with the ATLAS detector. J High Energy Phys 2021;06:145.
[77] ATLAS Collaboration, Aad G, et al. Search for dark matter produced in association with a single top quark and an energetic W boson in $\sqrt{s}$ = 13 TeV pp collisions with the ATLAS detector. Eur Phys J C 2023;83:603.
[78] ATLAS Collaboration, Aad G, et al. Search for dark matter produced in association with a Higgs boson decaying to tau leptons at $\sqrt{s}$ = 13 TeV with the ATLAS detector. J High Energy Phys 2023;09:189.

[79] ATLAS Collaboration, Aad G, et al. Search for Higgs boson decays into a pair of pseudoscalar particles in the $ppμμ$ final state with the ATLAS detector in pp collisions at $\sqrt{s}$ = 13 TeV. Phys Rev D 2022;105:012006.
[80] ATLAS Collaboration, Aaboud M, et al. Search for the Higgs boson produced in association with a vector boson and decaying into two spin-zero particles in the $H \to aa \to 4b$ channel in pp collisions at $\sqrt{s}$ = 13 TeV with the ATLAS detector. J High Energy Phys 2018;10:031.
[81] ATLAS Collaboration, Aad G, et al. Search for Higgs bosons decaying to aa in the $μμττ$ final state in pp collisions at $\sqrt{s}$ = 8 TeV with the ATLAS experiment. Phys Rev D 2015;92:052002.
[82] ATLAS Collaboration, Aaboud M, et al. Search for Higgs boson decays to beyond-the-Standard-Model light bosons in four-lepton events with the ATLAS detector at $\sqrt{s}$ = 13 TeV. J High Energy Phys 2018;06:166.
[83] ATLAS Collaboration, Aad G, et al. Search for Higgs bosons decaying into new spin-0 or spin-1 particles in four-lepton final states with the ATLAS detector with 139 fb^{-1} of pp collision data at $\sqrt{s}$ = 13 TeV. J High Energy Phys 2022;03:041.
[84] ATLAS Collaboration, Aad G, et al. Search for dark matter in events with missing transverse momentum and a Higgs boson decaying into two photons in pp collisions at $\sqrt{s}$ = 13 TeV with the ATLAS detector. J High Energy Phys 2021;10:013.
[85] ATLAS Collaboration, Aad G, et al. Search for $t\bar{t}H/A \to t\bar{t}t\bar{t}$ production in the multilepton final state in proton–proton collisions at $\sqrt{s}$ = 13 TeV with the ATLAS detector. J High Energy Phys 2023;07:203.
[86] ATLAS Collaboration, Aad G, et al. Combination of searches for invisible decays of the Higgs boson using 139 fb^{-1} of proton–proton collision data at $\sqrt{s}$ = 13 TeV collected with the ATLAS experiment. Phys Lett B 2023;842:137963.
[87] Argyropoulos S, Haisch U. Benchmarking LHC searches for light 2HDM+a pseudoscalars. SciPost Phys 2022;13:007.
[88] ATLAS Collaboration, Aaboud M, et al. Constraints on mediator-based dark matter and scalar dark energy models using $\sqrt{s}$ = 13 TeV pp collision data collected by the ATLAS detector. J High Energy Phys 2019;05:142.
[89] ATLAS Collaboration, Aaboud M, et al. Search for dark matter in events with a hadronically decaying vector boson and missing transverse momentum in pp collisions at $\sqrt{s}$ = 13 TeV with the ATLAS detector. J High Energy Phys 2018;10:180.
[90] ATLAS Collaboration, Aad G, et al. Search for dark matter produced in association with bottom or top quarks in $\sqrt{s}$ = 13 TeV pp collisions with the ATLAS detector. Eur Phys J C 2018;78:18.
[91] ATLAS Collaboration, Aaboud M, et al. Search for top-squark pair production in final states with one lepton, jets, and missing transverse momentum using 36 fb^{-1} of $\sqrt{s}$ = 13 TeV pp collision data with the ATLAS detector. J High Energy Phys 2018;06:108.
[92] CMS Collaboration, Sirunyan AM, et al. Search for dark matter particles produced in association with a Higgs boson in proton–proton collisions at $\sqrt{s}$ = 13 TeV. J High Energy Phys 2020;03:025.
[93] CMS Collaboration, Sirunyan AM, et al. Search for dark matter produced in association with a leptonically decaying Z boson in proton–proton collisions at $\sqrt{s}$ = 13 TeV. Eur Phys J C 2021;81:13.
[94] Gunion JF, Haber HE. The CP conserving two Higgs doublet model: The approach to the decoupling limit. Phys Rev D 2003;67:075019.
[95] Djouadi A, Maiani L, Moreau G, et al. The post-Higgs MSSM scenario: Habemus MSSM? Eur Phys J C 2013;73:2650.
[96] Misiak M, Steinhauser M. Weak radiative decays of the B meson and bounds on $M_{H^\pm}$ in the two-Higgs-doublet model. Eur Phys J C 2017;77:201.
[97] Haisch U, Polesello G. Searching for heavy Higgs bosons in the $t\bar{t}Z$ and tbW final states. J High Energy Phys 2018;09:151.
[98] Pani P, Polesello G. Dark matter production in association with a single top-quark at the LHC in a two-Higgs-doublet model with a pseudoscalar mediator. Phys Dark Univ 2018;21:8.
[99] ATLAS Collaboration, Aad G, et al. ATLAS Insertable B-Layer: Technical Design Report, ATLAS-TDR-19, CERN-LHCC-2010-013, 2010, https: //cds.cern.ch/record/1291633, Addendum: ATLAS-TDR-19-ADD-1, CERN-LHCC-2012-009, 2012, https://cds.cern.ch/record/1451888.
[100] Abbott B, Albert J, Alberti F, et al. Production and integration of the ATLAS insertable B-layer. J Instrum 2018;13:T05008.
[101] ATLAS Collaboration, Aaboud M, et al. Performance of the ATLAS trigger system in 2015. Eur Phys J C 2017;77:317.
[102] ATLAS Collaboration, Aad G et al. The ATLAS Collaboration software and firmware. ATL-SOFT-PUB-2021-001, 2021. https://cds.cern.ch/record/2767187.
[103] ATLAS Collaboration, Aad G, et al. ATLAS data quality operations and performance for 2015–2018 data-taking. J Instrum 2020;15:P04003.
[104] Degrande C, Duhr C, Fuks B, et al. UFO—The Universal FeynRules Output. Comput Phys Commun 2012;183:1201.
[105] Degrande C, Ubiali M, Wiesemann M, et al. Heavy charged Higgs boson production at the LHC. J High Energy Phys 2015;10:145.
[106] Alwall J, Frederix R, Frixione S, et al. The automated computation of tree-level and next-to-leading order differential cross sections, and their matching to parton shower simulations. J High Energy Phys 2014;7:079.
[107] Sjöstrand T, Ask S, Christiansen JR, et al. An introduction to PYTHIA 8.2. Comput Phys Commun 2015;191:159.
[108] ATLAS Collaboration, G. Aad et al. ATLAS Pythia 8 tunes to 7 TeV data, ATL-PHYS-PUB-2014-021, 2014, https://cds.cern.ch/record/1966419.
[109] NNPDF Collaboration, Ball RD, et al. Parton distributions for the LHC run II. J High Energy Phys 2015;4:040.
[110] ATLAS Collaboration, G. Aad et al. Summary of ATLAS Pythia 8 tunes, ATL-PHYS-PUB-2012-003, 2012, https://cds.cern.ch/record/1474107.
[111] Martin AD, Stirling WJ, Thorne RS, et al. Parton distributions for the LHC. Eur Phys J C 2009;63:189.
[112] ATLAS Collaboration, Aad G, et al. The ATLAS simulation infrastructure. Eur Phys J C 2010;70:823.
[113] Agostinelli S. Allison J, Amako K, et al. Geant4—a simulation toolkit. Nucl Instrum Meth A 2003;506:250.
[114] ATLAS Collaboration, Aad G, et al. The simulation principle and performance of the ATLAS fast calorimeter simulation. FastCaloSim, ATL-PHYS-PUB-2010-013, 2010. https://cds.cern.ch/record/1300517.
[115] Mattelaer O. On the maximal use of Monte Carlo samples: Re-weighting events at NLO accuracy. Eur Phys J C 2016;76:674.
[116] ATLAS Collaboration, Aad G, et al. Jet reconstruction and performance using particle flow with the ATLAS Detector. Eur Phys J C 2017;77:466.
[117] Cacciari M, Salam GP, Soyez G. The anti-k_t jet clustering algorithm. J High Energy Phys 2008;04:063.
[118] Cacciari M, Salam GP, Soyez G. FastJet user manual. Eur Phys J C 2012;72:1896.
[119] ATLAS Collaboration, Aad G, et al. Jet energy scale and resolution measured in proton–proton collisions at $\sqrt{s}$ = 13 TeV with the ATLAS detector. Eur Phys J C 2021;81:689.
[120] ATLAS Collaboration, Aad G, et al. ATLAS flavour-tagging algorithms for the LHC Run 2 pp collision dataset. Eur Phys J C 2023;83:681.
[121] ATLAS Collaboration, Aad G, et al. ATLAS b-jet identification performance and efficiency measurement with $t\bar{t}$ events in pp collisions at $\sqrt{s}$ = 13 TeV. Eur Phys J C 2019;79:970.
[122] ATLAS Collaboration, Aad G, et al. Electron and photon performance measurements with the ATLAS detector using the 2015–2017 LHC proton-proton collision data. J Instrum 2019;14:P12006.
[123] ATLAS Collaboration, Aad G, et al. Electron and photon reconstruction and performance in ATLAS using a dynamical, topological cell clustering-based approach. ATL-PHYS-PUB-2017-022, 2017, https://cds.cern.ch/record/2298955.
[124] ATLAS Collaboration, Aad G, et al. Muon reconstruction performance of the ATLAS detector in proton–proton collision data at $\sqrt{s}$ = 13 TeV. Eur Phys J C 2016;76:292.
[125] ATLAS Collaboration, Aad G, et al. Reconstruction, energy calibration, and identification of hadronically decaying tau leptons in the ATLAS Experiment for Run-2 of the LHC. ATL-PHYS-PUB-2015-045, 2015. https://cds.cern.ch/record/2064383.
[126] ATLAS Collaboration. Local hadronic calibration. ATL-LARG-PUB-2009-001-2, ATL-COM-LARG-2008-006, ATL-LARG-PUB-2009-001, 2008. https://cds.cern.ch/record/1112035.
[127] ATLAS Collaboration, Aad G, et al. Performance of missing transverse momentum reconstruction with the ATLAS detector using proton–proton collisions at $\sqrt{s}$ = 13 TeV. Eur Phys J C 2018;78:903.
[128] ATLAS Collaboration, Aad G, et al. Performance of electron and photon triggers in ATLAS during LHC Run 2. Eur Phys J C 2020;80:47.
[129] ATLAS Collaboration, Aad G, et al. Performance of the ATLAS muon triggers in Run 2. J Instrum 2020;15:P09015.
[130] ATLAS Collaboration, Aad G, et al. The ATLAS inner detector trigger performance in pp collisions at 13 TeV during LHC Run 2. Eur Phys J C 2022;82:206.
[131] ATLAS Collaboration, Aad G, et al. Object-based missing transverse momentum significance in the ATLAS. Detector ATLAS-CONF-2018-038, 2018. https://cds.cern.ch/record/2630948.
[132] ATLAS Collaboration, Aad G. et al.Performance of the missing transverse momentum triggers for the ATLAS detector during Run-2 data taking. J High Energy Phys 2020;8:080.
[133] ATLAS Collaboration. The ATLAS tau trigger in Run 2. ATLAS-CONF-2017-061, 2017. https://cds.cern.ch/record/2274201.
[134] ATLAS Collaboration, Aad G, et al. Search for dark matter produced in association with a single top quark in $\sqrt{s}$ = 13 TeV pp collisions with the ATLAS detector. Eur Phys J C 2021;81:860.
[135] ATLAS Collaboration, Aad G, et al. Search for invisible Higgs-boson decays in events with vector-boson fusion signatures using 139 fb^{-1} of proton–proton data recorded by the ATLAS experiment. J High Energy Phys 2022;8:104.
[136] ATLAS Collaboration, Aad G, et al. Observation of electroweak production of two jets in association with an isolated photon and missing transverse momentum, and search for a Higgs boson decaying into invisible particles at 13 TeV with the ATLAS detector. Eur Phys J C 2022;82:105.
[137] ATLAS Collaboration, Aad G, et al. Constraints on spin-0 dark matter mediators and invisible Higgs decays using ATLAS 13 TeV pp collision data with two top quarks and missing transverse momentum in the final state. Eur Phys J C 2023;83:503.
[138] ATLAS Collaboration, Aad G, et al. Constraints on new phenomena via Higgs boson couplings and invisible decays with the ATLAS detector. J High Energy Phys 2015;11:206.
[139] Lindert JM, Pozzorini S, Schönherr M. Precise predictions for V + 2 jet backgrounds in searches for invisible Higgs decays. J High Energy Phys 2023;1:070.
[140] ATLAS Collaboration, Aad G, et al. Improvements in $t\bar{t}$ modelling using NLO +PS Monte Carlo generators for Run 2. ATL-PHYS-PUB-2018-009, 2018. https://cds.cern.ch/record/2630327.

[141] ATLAS Collaboration, Aad G, et al. Measurements of top-quark pair single- and double-differential cross-sections in the all-hadronic channel in pp collisions at $\sqrt{s}$ = 13 TeV using the ATLAS detector. J High Energy Phys 2021;01:033.
[142] de Florian D, Grojean C, Maltoni F, et al. Handbook of LHC Higgs cross sections: 4. In: Deciphering the nature of the Higgs sector. CERN-2017-002-M, 2017.
[143] ATLAS Collaboration, Aad G, et al. Evidence for $t\bar{t}t\bar{t}$ production in the multilepton final state in proton–proton collisions at $\sqrt{s}$ = 13TeV with the ATLAS detector. Eur Phys J C 2020;80:1085.
[144] Baldi P, Cranmer K, Faucett T, et al. Parameterized neural networks for high-energy physics. Eur Phys J C 2016;76:235.
[145] ATLAS Collaboration, Aad G, et al. Search for Higgs boson decays into two new low-mass spin-0 particles in the 4b channel with the ATLAS detector using pp collisions at $\sqrt{s}$13 TeV. Phys Rev D 2020;102:112006.
[146] ATLAS Collaboration, Aad G, et al. Luminosity determination in pp collisions at $\sqrt{s}$ = 13 TeV using the ATLAS detector at the LHC. ATLAS-CONF-2019-021, 2019. https://cds.cern.ch/record/2677054.
[147] Butterworth J, Carrazza S, Cooper-Sarkar A, et al. PDF4LHC recommendations for LHC Run II. J Phys G 2016;43:023001.
[148] Cowan G, Cranmer K, Gross E, et al. Asymptotic formulae for likelihood-based tests of new physics. Eur Phys J C 2011;71:1554 [Erratum: Eur Phys J C 2013;73:2501].
[149] Cranmer K, Lewis G, Moneta L, et al. HistFactory: A tool for creating statistical models for use with RooFit and RooStats. CERN-OPEN-2012-016, 2012. https://cds.cern.ch/record/1456844.
[150] Read AL. Presentation of search results: The CL_S technique. J Phys G 2002;28:2693.
[151] Moneta L, Belasco K, Cranmer K, et al. The RooStats project 2001. arXiv: 1009.1003, 2011.
[152] Verkerke W, Kirkby D. The RooFit toolkit for data modeling arXiv: 0306116, 2003.
[153] Djouadi A, Drees M, Kneur JL. Neutralino dark matter in mSUGRA: Reopening the light Higgs pole window. Phys Lett B 2005;624:60.
[154] Bagnaschi EA, Buchmueller O, Cavanaugh R, et al. Supersymmetric dark matter after LHC Run 1. Eur Phys J C 2015;75:500.
[155] Ambrogi F, Arina C, Backovic M, et al. MadDM vol 3.0: A comprehensive tool for dark matter studies. Phys Dark Univ 2019;24:100249.
[156] ATLAS Collaboration, Aad G, et al. ATLAS computing acknowledgements. ATL-SOFT-PUB-2023-001, 2023. https://cds.cern.ch/record/2869272.

The ATLAS experiment

ATLAS is one of the four large experiments at CERN's Large Hadron Collider (LHC). The ATLAS experiment is a multipurpose particle detector with a forward–backward symmetric cylindrical geometry and nearly 4π coverage in solid angle. It consists of an inner tracking detector surrounded by a thin superconducting solenoid, high-granularity sampling electromagnetic and hadronic calorimeters, and a muon spectrometer with three superconducting air-core toroidal magnets. The ATLAS Collaboration consists of more than 5900 members from 253 institutes in 42 countries on 6 continents, including physicists, engineers, students, and technical staff.

G. Aad [102], B. Abbott [120], K. Abeling [55], N.J. Abicht [49], S.H. Abidi [29], A. Aboulhorma [35e], H. Abramowicz [151], H. Abreu [150], Y. Abulaiti [117], A.C. Abusleme Hoffman [137a], B.S. Acharya [69a,69b,r], C. Adam Bourdarios [4], L. Adamczyk [86a], L. Adamek [155], S.V. Addepalli [26], M.J. Addison [101], J. Adelman [115], A. Adiguzel [21c], T. Adye [134], A.A. Affolder [136], Y. Afik [36], M.N. Agaras [13], J. Agarwala [73a,73b], A. Aggarwal [100], C. Agheorghiesei [27c], A. Ahmad [36], F. Ahmadov [38,ai], W.S. Ahmed [104], S. Ahuja [95], X. Ai [62a], G. Aielli [76a,76b], A. Aikot [163], M. Ait Tamlihat [35e], B. Aitbenchikh [35a], I. Aizenberg [169], M. Akbiyik [100], T.P.A. Åkesson [98], A.V. Akimov [37], D. Akiyama [168], N.N. Akolkar [24], K. Al Khoury [41], G.L. Alberghi [23b], J. Albert [165], P. Albicocco [53], G.L. Albouy [60], S. Alderweireldt [52], M. Aleksa [36], I.N. Aleksandrov [38], C. Alexa [27b], T. Alexopoulos [10], F. Alfonsi [23b], M. Algren [56], M. Alhroob [120], B. Ali [132], H.M.J. Ali [91], S. Ali [148], S.W. Alibocus [92], M. Aliev [145], G. Alimonti [71a], W. Alkakhi [55], C. Allaire [66], B.M.M. Allbrooke [146], J.F. Allen [52], C.A. Allendes Flores [137f], P.P. Allport [20], A. Aloisio [72a,72b], F. Alonso [90], C. Alpigiani [138], M. Alvarez Estevez [99], A. Alvarez Fernandez [100], M. Alves Cardoso [56], M.G. Alviggi [72a,72b], M. Aly [101], Y. Amaral Coutinho [83b], A. Ambler [104], C. Amelung [36], M. Amerl [101], C.G. Ames [109], D. Amidei [106], S.P. Amor Dos Santos [130a], K.R. Amos [163], V. Ananiev [125], C. Anastopoulos [139], T. Andeen [11], J.K. Anders [36], S.Y. Andrean [47a,47b], A. Andreazza [71a,71b], S. Angelidakis [9], A. Angerami [41,am], A.V. Anisenkov [37], A. Annovi [74a], C. Antel [56], M.T. Anthony [139], E. Antipov [145], M. Antonelli [53], F. Anulli [75a], M. Aoki [84], T. Aoki [153], J.A. Aparisi Pozo [163], M.A. Aparo [146], L. Aperio Bella [48], C. Appelt [18], A. Apyan [26], N. Aranzabal [36], C. Arcangeletti [53], A.T.H. Arce [51], E. Arena [92], J.-F. Arguin [108], S. Argyropoulos [54], J.-H. Arling [48], O. Arnaez [4], H. Arnold [114], G. Artoni [75a,75b], H. Asada [111], K. Asai [118], S. Asai [153], N.A. Asbah [61], J. Assahsah [35d], K. Assamagan [29], R. Astalos [28a], S. Atashi [160], R.J. Atkin [33a], M. Atkinson [162], H. Atmani [35f], P.A. Atmasiddha [106], K. Augsten [132], S. Auricchio [72a,72b], A.D. Auriol [20], V.A. Austrup [101], G. Avolio [36], K. Axiotis [56], G. Azuelos [108,au], D. Babal [28b], H. Bachacou [135], K. Bachas [152,x], A. Bachiu [34], F. Backman [47a,47b], A. Badea [61], P. Bagnaia [75a,75b], M. Bahmani [18], A.J. Bailey [163], V.R. Bailey [162], J.T. Baines [134], L. Baines [94], C. Bakalis [10], O.K. Baker [172], E. Bakos [15], D. Bakshi Gupta [8], V. Balakrishnan [120], R. Balasubramanian [114], E.M. Baldin [37], P. Balek [86a], E. Ballabene [23b,23a], F. Balli [135], L.M. Baltes [63a], W.K. Balunas [32], J. Balz [100], E. Banas [87], M. Bandieramonte [129], A. Bandyopadhyay [24], S. Bansal [24], L. Barak [151], M. Barakat [48], E.L. Barberio [105], D. Barberis [57b,57a], M. Barbero [102], K.N. Barends [33a], T. Barillari [110], M.-S. Barisits [36], T. Barklow [143], P. Baron [122], D.A. Baron Moreno [101], A. Baroncelli [62a], G. Barone [29], A.J. Barr [126], J.D. Barr [96], L. Barranco Navarro [47a,47b], F. Barreiro [99], J. Barreiro Guimarães da Costa [14a], U. Barron [151], M.G. Barros Teixeira [130a], S. Barsov [37], F. Bartels [63a], R. Bartoldus [143], A.E. Barton [91], P. Bartos [28a], A. Basan [100], M. Baselga [49], A. Bassalat [66,b], M.J. Basso [156a], C.R. Basson [101], R.L. Bates [59], S. Batlamous [35e], J.R. Batley [32], B. Batool [141], M. Battaglia [136], D. Battulga [18], M. Bauce [75a,75b], M. Bauer [36], P. Bauer [24], L.T. Bazzano Hurrell [30], J.B. Beacham [51], T. Beau [127], P.H. Beauchemin [158], F. Becherer [54], P. Bechtle [24], H.P. Beck [19,v], K. Becker [167], A.J. Beddall [82], V.A. Bednyakov [38], C.P. Bee [145], L.J. Beemster [15], T.A. Beermann [36], M. Begalli [83d], M. Begel [29], A. Behera [145], J.K. Behr [48], J.F. Beirer [55], F. Beisiegel [24], M. Belfkir [159], G. Bella [151], L. Bellagamba [23b], A. Bellerive [34], P. Bellos [20], K. Beloborodov [37], N.L. Belyaev [37], D. Benchekroun [35a], F. Bendebba [35a], Y. Benhammou [151], M. Benoit [29], J.R. Bensinger [26], S. Bentvelsen [114], L. Beresford [48], M. Beretta [53], E. Bergeaas Kuutmann [161], N. Berger [4], B. Bergmann [132], J. Beringer [17a], G. Bernardi [5], C. Bernius [143], F.U. Bernlochner [24], F. Bernon [36,102], T. Berry [95], P. Berta [133], A. Berthold [50], I.A. Bertram [91], S. Bethke [110], A. Betti [75a,75b], A.J. Bevan [94], M. Bhamjee [33c], S. Bhatta [145], D.S. Bhattacharya [166], P. Bhattarai [143], V.S. Bhopatkar [121], R. Bi [29,aw], R.M. Bianchi [129], G. Bianco [23b,23a], O. Biebel [109], R. Bielski [123], M. Biglietti [77a], T.R.V. Billoud [132], M. Bindi [55], A. Bingul [21b], C. Bini [75a,75b], A. Biondini [92], C.J. Birch-sykes [101], G.A. Bird [20,134], M. Birman [169], M. Biros [133], T. Bisanz [49], E. Bisceglie [43b,43a], D. Biswas [141], A. Bitadze [101], K. Bjørke [125], I. Bloch [48], C. Blocker [26], A. Blue [59], U. Blumenschein [94], J. Blumenthal [100], G.J. Bobbink [114], V.S. Bobrovnikov [37], M. Boehler [54], B. Boehm [166], D. Bogavac [36], A.G. Bogdanchikov [37], C. Bohm [47a], V. Boisvert [95], P. Bokan [48], T. Bold [86a], M. Bomben [5], M. Bona [94], M. Boonekamp [135], C.D. Booth [95], A.G. Borbély [59,ar], I.S. Bordulev [37], H.M. Borecka-Bielska [108], L.S. Borgna [96], G. Borissov [91], D. Bortoletto [126], D. Boscherini [23b], M. Bosman [13], J.D. Bossio Sola [36], K. Bouaouda [35a], N. Bouchhar [163], J. Boudreau [129],

E.V. Bouhova-Thacker[91], D. Boumediene[40], R. Bouquet[5], A. Boveia[119], J. Boyd[36], D. Boye[29], I.R. Boyko[38], J. Bracinik[20], N. Brahimi[62d], G. Brandt[171], O. Brandt[32], F. Braren[48], B. Brau[103], J.E. Brau[123], R. Brener[169], L. Brenner[114], R. Brenner[161], S. Bressler[169], D. Britton[59], D. Britzger[110], I. Brock[24], G. Brooijmans[41], W.K. Brooks[137f], E. Brost[29], L.M. Brown[165,o], L.E. Bruce[61], T.L. Bruckler[126], P.A. Bruckman de Renstrom[87], B. Brüers[48], A. Bruni[23b], G. Bruni[23b], M. Bruschi[23b], N. Bruscino[75a,75b], T. Buanes[16], Q. Buat[138], D. Buchin[110], A.G. Buckley[59], M.K. Bugge[125], O. Bulekov[37], B.A. Bullard[143], S. Burdin[92], C.D. Burgard[49], A.M. Burger[40], B. Burghgrave[8], O. Burlayenko[54], J.T.P. Burr[32], C.D. Burton[11], J.C. Burzynski[142], E.L. Busch[41], V. Büscher[100], P.J. Bussey[59], J.M. Butler[25], C.M. Buttar[59], J.M. Butterworth[96], W. Buttinger[134], C.J. Buxo Vazquez[107], A.R. Buzykaev[37], S. Cabrera Urbán[163], L. Cadamuro[66], D. Caforio[58], H. Cai[129], Y. Cai[14a,14e], V.M.M. Cairo[36], O. Cakir[3a], N. Calace[36], P. Calafiura[17a], G. Calderini[127], P. Calfayan[68], G. Callea[59], L.P. Caloba[83b], D. Calvet[40], S. Calvet[40], T.P. Calvet[102], M. Calvetti[74a,74b], R. Camacho Toro[127], S. Camarda[36], D. Camarero Munoz[26], P. Camarri[76a,76b], M.T. Camerlingo[72a,72b], D. Cameron[36,h], C. Camincher[165], M. Campanelli[96], A. Camplani[42], V. Canale[72a,72b], A. Canesse[104], J. Cantero[163], Y. Cao[162], F. Capocasa[26], M. Capua[43b,43a], A. Carbone[71a,71b], R. Cardarelli[76a], J.C.J. Cardenas[8], F. Cardillo[163], T. Carli[36], G. Carlino[72a], J.I. Carlotto[13], B.T. Carlson[129,y], E.M. Carlson[165,156a], L. Carminati[71a,71b], A. Carnelli[135], M. Carnesale[75a,75b], S. Caron[113], E. Carquin[137f], S. Carrá[71a,71b], G. Carratta[23b,23a], F. Carrio Argos[33g], J.W.S. Carter[155], T.M. Carter[52], M.P. Casado[13,k], M. Caspar[48], E.G. Castiglia[172], F.L. Castillo[4], L. Castillo Garcia[13], V. Castillo Gimenez[163], N.F. Castro[130a,130e], A. Catinaccio[36], J.R. Catmore[125], V. Cavaliere[29], N. Cavalli[23b,23a], V. Cavasinni[74a,74b], Y.C. Cekmecelioglu[48], E. Celebi[21a], F. Celli[126], M.S. Centonze[70a,70b], V. Cepaitis[56], K. Cerny[122], A.S. Cerqueira[83a], A. Cerri[146], L. Cerrito[76a,76b], F. Cerutti[17a], B. Cervato[141], A. Cervelli[23b], G. Cesarini[53], S.A. Cetin[82], Z. Chadi[35a], D. Chakraborty[115], J. Chan[170], W.Y. Chan[153], J.D. Chapman[32], E. Chapon[135], B. Chargeishvili[149b], D.G. Charlton[20], T.P. Charman[94], M. Chatterjee[19], C. Chauhan[133], S. Chekanov[6], S.V. Chekulaev[156a], G.A. Chelkov[38,a], A. Chen[106], B. Chen[151], B. Chen[165], H. Chen[14c], H. Chen[29], J. Chen[62c], J. Chen[142], M. Chen[126], S. Chen[153], S.J. Chen[14c], X. Chen[62c,135], X. Chen[14b,at], Y. Chen[62a], C.L. Cheng[170], H.C. Cheng[64a], S. Cheong[143], A. Cheplakov[38], E. Cheremushkina[48], E. Cherepanova[114], R. Cherkaoui El Moursli[35e], E. Cheu[7], K. Cheung[65], L. Chevalier[135], V. Chiarella[53], G. Chiarelli[74a], N. Chiedde[102], G. Chiodini[70a], A.S. Chisholm[20], A. Chitan[27b], M. Chitishvili[163], M.V. Chizhov[38], K. Choi[11], A.R. Chomont[75a,75b], Y. Chou[103], E.Y.S. Chow[114], T. Chowdhury[33g], K.L. Chu[169], M.C. Chu[64a], X. Chu[14a,14e], J. Chudoba[131], J.J. Chwastowski[87], D. Cieri[110], K.M. Ciesla[86a], V. Cindro[93], A. Ciocio[17a], F. Cirotto[72a,72b], Z.H. Citron[169,p], M. Citterio[71a], D.A. Ciubotaru[27b], B.M. Ciungu[155], A. Clark[56], P.J. Clark[52], J.M. Clavijo Columbie[48], S.E. Clawson[48], C. Clement[47a,47b], J. Clercx[48], L. Clissa[23b,23a], Y. Coadou[102], M. Cobal[69a,69c], A. Coccaro[57b], R.F. Coelho Barrue[130a], R. Coelho Lopes De Sa[103], S. Coelli[71a], H. Cohen[151], A.E.C. Coimbra[71a,71b], B. Cole[41], J. Collot[60], P. Conde Muiño[130a,130g], M.P. Connell[33c], S.H. Connell[33c], I.A. Connelly[59], E.I. Conroy[126], F. Conventi[72a,av], H.G. Cooke[20], A.M. Cooper-Sarkar[126], A. Cordeiro Oudot Choi[127], F. Cormier[164], L.D. Corpe[40], M. Corradi[75a,75b], F. Corriveau[104,ag], A. Cortes-Gonzalez[18], M.J. Costa[163], F. Costanza[4], D. Costanzo[139], B.M. Cote[119], G. Cowan[95], K. Cranmer[170], D. Cremonini[23b,23a], S. Crépé-Renaudin[60], F. Crescioli[127], M. Cristinziani[141], M. Cristoforetti[78a,78b], V. Croft[114], J.E. Crosby[121], G. Crosetti[43b,43a], A. Cueto[99], T. Cuhadar Donszelmann[160], H. Cui[14a,14e], Z. Cui[7], W.R. Cunningham[59], F. Curcio[43b,43a], P. Czodrowski[36], M.M. Czurylo[63b], M.J. Da Cunha Sargedas De Sousa[57b,57a], J.V. Da Fonseca Pinto[83b], C. Da Via[101], W. Dabrowski[86a], T. Dado[49], S. Dahbi[33g], T. Dai[106], D. Dal Santo[19], C. Dallapiccola[103], M. Dam[42], G. D'amen[29], V. D'Amico[109], J. Damp[100], J.R. Dandoy[128], M.F. Daneri[30], M. Danninger[142], V. Dao[36], G. Darbo[57b], S. Darmora[6], S.J. Das[29,aw], S. D'Auria[71a,71b], C. David[156b], T. Davidek[133], B. Davis-Purcell[34], I. Dawson[94], H.A. Day-hall[132], K. De[8], R. De Asmundis[72a], N. De Biase[48], S. De Castro[23b,23a], N. De Groot[113], P. de Jong[114], H. De la Torre[115], A. De Maria[14c], A. De Salvo[75a], U. De Sanctis[76a,76b], A. De Santo[146], J.B. De Vivie De Regie[60], D.V. Dedovich[38], J. Degens[114], A.M. Deiana[44], F. Del Corso[23b,23a], J. Del Peso[99], F. Del Rio[63a], F. Deliot[135], C.M. Delitzsch[49], M. Della Pietra[72a,72b], D. Della Volpe[56], A. Dell'Acqua[36], L. Dell'Asta[71a,71b], M. Delmastro[4], P.A. Delsart[60], S. Demers[172], M. Demichev[38], S.P. Denisov[37], L. D'Eramo[40], D. Derendarz[87], F. Derue[127], P. Dervan[92], K. Desch[24], C. Deutsch[24], F.A. Di Bello[57b,57a], A. Di Ciaccio[76a,76b], L. Di Ciaccio[4], A. Di Domenico[75a,75b], C. Di Donato[72a,72b], A. Di Girolamo[36], G. Di Gregorio[5], A. Di Luca[78a,78b], B. Di Micco[77a,77b], R. Di Nardo[77a,77b], C. Diaconu[102], M. Diamantopoulou[34], F.A. Dias[114], T. Dias Do Vale[142], M.A. Diaz[137a,137b], F.G. Diaz Capriles[24], M. Didenko[163], E.B. Diehl[106], L. Diehl[54], S. Díez Cornell[48], C. Diez Pardos[141], C. Dimitriadi[161,24,161], A. Dimitrievska[17a], J. Dingfelder[24], I.-M. Dinu[27b], S.J. Dittmeier[63b], F. Dittus[36], F. Djama[102], T. Djobava[149b], J.I. Djuvsland[16], C. Doglioni[101,98], A. Dohnalova[28a], J. Dolejsi[133], Z. Dolezal[133], M. Donadelli[83c], B. Dong[107], J. Donini[40], A. D'Onofrio[77a,77b], M. D'Onofrio[92], J. Dopke[134], A. Doria[72a], N. Dos Santos Fernandes[130a], P. Dougan[101], M.T. Dova[90], A.T. Doyle[59], M.A. Draguet[126], E. Dreyer[169], I. Drivas-koulouris[10], A.S. Drobac[158], M. Drozdova[56], D. Du[62a], T.A. du Pree[114], F. Dubinin[37], M. Dubovsky[28a], E. Duchovni[169], G. Duckeck[109], O.A. Ducu[27b], D. Duda[52], A. Dudarev[36], E.R. Duden[26], M. D'uffizi[101], L. Duflot[66], M. Dührssen[36], C. Dülsen[171], A.E. Dumitriu[27b], M. Dunford[63a], S. Dungs[49], K. Dunne[47a,47b], A. Duperrin[102], H. Duran Yildiz[3a], M. Düren[58], A. Durglishvili[149b], B.L. Dwyer[115], G.I. Dyckes[17a], M. Dyndal[86a], S. Dysch[101], B.S. Dziedzic[87], Z.O. Earnshaw[146], G.H. Eberwein[126], B. Eckerova[28a], S. Eggebrecht[55], E. Egidio Purcino De Souza[127], L.F. Ehrke[56], G. Eigen[16], K. Einsweiler[17a], T. Ekelof[161], P.A. Ekman[98], S. El Farkh[35b], Y. El Ghazali[35b], H. El Jarrari[35e,148], A. El Moussaouy[35a], V. Ellajosyula[161], M. Ellert[161], F. Ellinghaus[171], A.A. Elliot[94], N. Ellis[36], J. Elmsheuser[29], M. Elsing[36], D. Emeliyanov[134], Y. Enari[153], I. Ene[17a], S. Epari[13], J. Erdmann[49], P.A. Erland[87], M. Errenst[171], M. Escalier[66], C. Escobar[163], E. Etzion[151], G. Evans[130a], H. Evans[68], L.S. Evans[95], M.O. Evans[146], A. Ezhilov[37], S. Ezzarqtouni[35a], F. Fabbri[59], L. Fabbri[23b,23a], G. Facini[96], V. Fadeyev[136], R.M. Fakhrutdinov[37], S. Falciano[75a], L.F. Falda Ulhoa Coelho[36], P.J. Falke[24], J. Faltova[133], C. Fan[162], Y. Fan[14a], Y. Fang[14a,14e], M. Fanti[71a,71b], M. Faraj[69a,69b], Z. Farazpay[97], A. Farbin[8], A. Farilla[77a], T. Farooque[107], S.M. Farrington[52], F. Fassi[35e], D. Fassouliotis[9], M. Faucci Giannelli[76a,76b], W.J. Fawcett[32], L. Fayard[66], P. Federic[133], P. Federicova[131], O.L. Fedin[37,a], G. Fedotov[37], M. Feickert[170], L. Feligioni[102], D.E. Fellers[123], C. Feng[62b], M. Feng[14b], Z. Feng[114], M.J. Fenton[160], A.B. Fenyuk[37], L. Ferencz[48], R.A.M. Ferguson[91], S.I. Fernandez Luengo[137f], M.J.V. Fernoux[102], J. Ferrando[48], A. Ferrari[161], P. Ferrari[114,113], R. Ferrari[73a], D. Ferrere[56], C. Ferretti[106], F. Fiedler[100], A. Filipčič[93], E.K. Filmer[1], F. Filthaut[113], M.C.N. Fiolhais[130a,130c,d], L. Fiorini[163], W.C. Fisher[107], T. Fitschen[101], P.M. Fitzhugh[135], I. Fleck[141], P. Fleischmann[106], T. Flick[171], M. Flores[33d,an], L.R. Flores Castillo[64a], L. Flores Sanz De Acedo[36], F.M. Follega[78a,78b], N. Fomin[16], J.H. Foo[155], B.C. Forland[68], A. Formica[135], A.C. Forti[101], E. Fortin[36], A.W. Fortman[61], M.G. Foti[17a], L. Fountas[9,l], D. Fournier[66], H. Fox[91],

P. Francavilla[74a,74b], S. Francescato[61], S. Franchellucci[56], M. Franchini[23b,23a], S. Franchino[63a], D. Francis[36], L. Franco[113], L. Franconi[48], M. Franklin[61], G. Frattari[26], A.C. Freegard[94], W.S. Freund[83b], Y.Y. Frid[151], J. Friend[59], N. Fritzsche[50], A. Froch[54], D. Froidevaux[36], J.A. Frost[126], Y. Fu[62a], M. Fujimoto[118,ao], E. Fullana Torregrosa[163,**], K.Y. Fung[64a], E. Furtado De Simas Filho[83b], M. Furukawa[153], J. Fuster[163], A. Gabrielli[23b,23a], A. Gabrielli[155], P. Gadow[36], G. Gagliardi[57b,57a], L.G. Gagnon[17a], E.J. Gallas[126], B.J. Gallop[134], K.K. Gan[119], S. Ganguly[153], J. Gao[62a], Y. Gao[52], F.M. Garay Walls[137a,137b], B. Garcia[29,aw], C. García[163], A. Garcia Alonso[114], A.G. Garcia Caffaro[172], J.E. García Navarro[163], M. Garcia-Sciveres[17a], G.L. Gardner[128], R.W. Gardner[39], N. Garelli[158], D. Garg[80], R.B. Garg[143,u], J.M. Gargan[52], C.A. Garner[155], S.J. Gasiorowski[138], P. Gaspar[83b], G. Gaudio[73a], V. Gautam[13], P. Gauzzi[75a,75b], I.L. Gavrilenko[37], A. Gavrilyuk[37], C. Gay[164], G. Gaycken[48], E.N. Gazis[10], A.A. Geanta[27b], C.M. Gee[136], C. Gemme[57b], M.H. Genest[60], S. Gentile[75a,75b], S. George[95], W.F. George[20], T. Geralis[46], P. Gessinger-Befurt[36], M.E. Geyik[171], M. Ghani[167], M. Ghneimat[141], K. Ghorbanian[94], A. Ghosal[141], A. Ghosh[160], A. Ghosh[7], B. Giacobbe[23b], S. Giagu[75a,75b], T. Giani[114], P. Giannetti[74a], A. Giannini[62a], S.M. Gibson[95], M. Gignac[136], D.T. Gil[86b], A.K. Gilbert[86a], B.J. Gilbert[41], D. Gillberg[34], G. Gilles[114], N.E.K. Gillwald[48], L. Ginabat[127], D.M. Gingrich[2,au], M.P. Giordani[69a,69c], P.F. Giraud[135], G. Giugliarelli[69a,69c], D. Giugni[71a], F. Giuli[36], I. Gkialas[9,l], L.K. Gladilin[37], C. Glasman[99], G.R. Gledhill[123], G. Glemža[48], M. Glisic[123], I. Gnesi[43b,g], Y. Go[29,aw], M. Goblirsch-Kolb[36], B. Gocke[49], D. Godin[108], B. Gokturk[21a], S. Goldfarb[105], T. Golling[56], M.G.D. Gololo[33g], D. Golubkov[37], J.P. Gombas[107], A. Gomes[130a,130b], G. Gomes Da Silva[141], A.J. Gomez Delegido[163], R. Gonçalo[130a,130c], G. Gonella[123], L. Gonella[20], A. Gongadze[149c], F. Gonnella[20], J.L. Gonski[41], R.Y. González Andana[52], S. González de la Hoz[163], S. Gonzalez Fernandez[13], R. Gonzalez Lopez[92], C. Gonzalez Renteria[17a], M.V. Gonzalez Rodrigues[48], R. Gonzalez Suarez[161], S. Gonzalez-Sevilla[56], G.R. Gonzalvo Rodriguez[163], L. Goossens[36], B. Gorini[36], E. Gorini[70a,70b], A. Gorišek[93], T.C. Gosart[128], A.T. Goshaw[51], M.I. Gostkin[38], S. Goswami[121], C.A. Gottardo[36], S.A. Gotz[109], M. Gouighri[35b], V. Goumarre[48], A.G. Goussiou[138], N. Govender[33c], I. Grabowska-Bold[86a], K. Graham[34], E. Gramstad[125], S. Grancagnolo[70a,70b], M. Grandi[146], C.M. Grant[1,135], P.M. Gravila[27f], F.G. Gravili[70a,70b], H.M. Gray[17a], M. Greco[70a,70b], C. Grefe[24], I.M. Gregor[48], P. Grenier[143], C. Grieco[13], A.A. Grillo[136], K. Grimm[31], S. Grinstein[13,ac], J.-F. Grivaz[66], E. Gross[169], J. Grosse-Knetter[55], C. Grud[106], J.C. Grundy[126], L. Guan[106], W. Guan[29], C. Gubbels[164], J.G.R. Guerrero Rojas[163], G. Guerrieri[69a,69c], F. Guescini[110], R. Gugel[100], J.A.M. Guhit[106], A. Guida[18], T. Guillemin[4], E. Guilloton[167,134], S. Guindon[36], F. Guo[14a,14e], J. Guo[62c], L. Guo[48], Y. Guo[106], R. Gupta[48], S. Gurbuz[24], S.S. Gurdasani[54], G. Gustavino[36], M. Guth[56], P. Gutierrez[120], L.F. Gutierrez Zagazeta[128], C. Gutschow[96], C. Gwenlan[126], C.B. Gwilliam[92], E.S. Haaland[125], A. Haas[117], M. Habedank[48], C. Haber[17a], H.K. Hadavand[8], A. Hadef[100], S. Hadzic[110], J.J. Hahn[141], E.H. Haines[96], M. Haleem[166], J. Haley[121], J.J. Hall[139], G.D. Hallewell[102], L. Halser[19], K. Hamano[165], M. Hamer[24], G.N. Hamity[52], E.J. Hampshire[95], J. Han[62b], K. Han[62a], L. Han[14c], L. Han[62a], S. Han[17a], Y.F. Han[155], K. Hanagaki[84], M. Hance[136], D.A. Hangal[41,am], H. Hanif[142], M.D. Hank[128], R. Hankache[101], J.B. Hansen[42], J.D. Hansen[42], P.H. Hansen[42], K. Hara[157], D. Harada[56], T. Harenberg[171], S. Harkusha[37], M.L. Harris[103], Y.T. Harris[126], J. Harrison[13], N.M. Harrison[119], P.F. Harrison[167], N.M. Hartman[110], N.M. Hartmann[109], Y. Hasegawa[140], A. Hasib[52], S. Haug[19], R. Hauser[107], C.M. Hawkes[20], R.J. Hawkings[36], Y. Hayashi[153], S. Hayashida[111], D. Hayden[107], C. Hayes[106], R.L. Hayes[114], C.P. Hays[126], J.M. Hays[94], H.S. Hayward[92], F. He[62a], M. He[14a,14e], Y. He[154], Y. He[127], N.B. Heatley[94], V. Hedberg[98], A.L. Heggelund[125], N.D. Hehir[94], C. Heidegger[54], K.K. Heidegger[54], W.D. Heidorn[81], J. Heilman[34], S. Heim[48], T. Heim[17a], J.G. Heinlein[128], J.J. Heinrich[123], L. Heinrich[110,as], J. Hejbal[131], L. Helary[48], A. Held[170], S. Hellesund[16], C.M. Helling[164], S. Hellman[47a,47b], R.C.W. Henderson[91], L. Henkelmann[32], A.M. Henriques Correia[36], H. Herde[98], Y. Hernández Jiménez[145], L.M. Herrmann[24], T. Herrmann[50], G. Herten[54], R. Hertenberger[109], L. Hervas[36], M.E. Hesping[100], N.P. Hessey[156a], H. Hibi[85], S.J. Hillier[20], J.R. Hinds[107], F. Hinterkeuser[24], M. Hirose[124], S. Hirose[157], D. Hirschbuehl[171], T.G. Hitchings[101], B. Hiti[93], J. Hobbs[145], R. Hobincu[27e], N. Hod[169], M.C. Hodgkinson[139], B.H. Hodkinson[32], A. Hoecker[36], J. Hofer[48], T. Holm[24], M. Holzbock[110], L.B.A.H. Hommels[32], B.P. Honan[101], J. Hong[62c], T.M. Hong[129], B.H. Hooberman[162], W.H. Hopkins[6], Y. Horii[111], S. Hou[148], A.S. Howard[93], J. Howarth[59], J. Hoya[6], M. Hrabovsky[122], A. Hrynevich[48], T. Hryn'ova[4], P.J. Hsu[65], S.-C. Hsu[138], Q. Hu[41], Y.F. Hu[14a,14e], S. Huang[64b], X. Huang[14c], Y. Huang[139,n], Y. Huang[14a], Z. Huang[101], Z. Hubacek[132], M. Huebner[24], F. Huegging[24], T.B. Huffman[126], C.A. Hugli[48], M. Huhtinen[36], S.K. Huiberts[16], R. Hulsken[104], N. Huseynov[12,a], J. Huston[107], J. Huth[61], R. Hyneman[143], G. Iacobucci[56], G. Iakovidis[29], I. Ibragimov[141], L. Iconomidou-Fayard[66], P. Iengo[72a,72b], R. Iguchi[153], T. Iizawa[126,s], Y. Ikegami[84], N. Ilic[155], H. Imam[35a], M. Ince Lezki[56], T. Ingebretsen Carlson[47a,47b], G. Introzzi[73a,73b], M. Iodice[77a], V. Ippolito[75a,75b], R.K. Irwin[92], M. Ishino[153], W. Islam[170], C. Issever[18,48], S. Istin[21a,ay], H. Ito[168], J.M. Iturbe Ponce[64a], R. Iuppa[78a,78b], A. Ivina[169], J.M. Izen[45], V. Izzo[72a], P. Jacka[131,132], P. Jackson[1], R.M. Jacobs[48], B.P. Jaeger[142], C.S. Jagfeld[109], P. Jain[54], G. Jäkel[171], K. Jakobs[54], T. Jakoubek[169], J. Jamieson[59], K.W. Janas[86a], M. Javurkova[103], F. Jeanneau[135], L. Jeanty[123], J. Jejelava[149a,aj], P. Jenni[54,i], C.E. Jessiman[34], S. Jézéquel[4], C. Jia[62b], J. Jia[145], X. Jia[61], X. Jia[14a,14e], Z. Jia[14c], Y. Jiang[62a], S. Jiggins[48], J. Jimenez Pena[13], S. Jin[14c], A. Jinaru[27b], O. Jinnouchi[154], P. Johansson[139], K.A. Johns[7], J.W. Johnson[136], D.M. Jones[32], E. Jones[48], P. Jones[32], R.W.L. Jones[91], T.J. Jones[92], R. Joshi[119], J. Jovicevic[15], X. Ju[17a], J.J. Junggeburth[103,w], T. Junkermann[63a], A. Juste Rozas[13,ac], M.K. Juzek[87], S. Kabana[137e], A. Kaczmarska[87], M. Kado[110], H. Kagan[119], M. Kagan[143], A. Kahn[41], A. Kahn[128], C. Kahra[100], T. Kaji[153], E. Kajomovitz[150], N. Kakati[169], I. Kalaitzidou[54], C.W. Kalderon[29], A. Kamenshchikov[155], N.J. Kang[136], D. Kar[33g], K. Karava[126], M.J. Kareem[156b], E. Karentzos[54], I. Karkanias[152], O. Karkout[114], S.N. Karpov[38], Z.M. Karpova[38], V. Kartvelishvili[91], A.N. Karyukhin[37], E. Kasimi[152], J. Katzy[48], S. Kaur[34], K. Kawade[140], M.P. Kawale[120], T. Kawamoto[135], E.F. Kay[36], F.I. Kaya[158], S. Kazakos[107], V.F. Kazanin[37], Y. Ke[145], J.M. Keaveney[33a], R. Keeler[165], G.V. Kehris[61], J.S. Keller[34], A.S. Kelly[96], J.J. Kempster[146], K.E. Kennedy[41], P.D. Kennedy[100], O. Kepka[131], B.P. Kerridge[167], S. Kersten[171], B.P. Kerševan[93], S. Keshri[66], L. Keszeghova[28a], S. Ketabchi Haghighat[155], M. Khandoga[127], A. Khanov[121], A.G. Kharlamov[37], T. Kharlamova[37], E.E. Khoda[138], T.J. Khoo[18], G. Khoriauli[166], J. Khubua[149b], Y.A.R. Khwaira[66], A. Kilgallon[123], D.W. Kim[47a,47b], Y.K. Kim[39], N. Kimura[96], A. Kirchhoff[55], C. Kirfel[24], F. Kirfel[24], J. Kirk[134], A.E. Kiryunin[110], C. Kitsaki[10], O. Kivernyk[24], M. Klassen[63a], C. Klein[34], L. Klein[166], M.H. Klein[106], M. Klein[92], S.B. Klein[56], U. Klein[92], P. Klimek[36], A. Klimentov[29], T. Klioutchnikova[36], P. Kluit[114], S. Kluth[110], E. Kneringer[79], T.M. Knight[155], A. Knue[49], R. Kobayashi[88], D. Kobylianskii[169], S.F. Koch[126], M. Kocian[143], P. Kodyš[133], D.M. Koeck[123], P.T. Koenig[24], T. Koffas[34], M. Kolb[135], I. Koletsou[4], T. Komarek[122], K. Köneke[54], A.X.Y. Kong[1], T. Kono[118], N. Konstantinidis[96], B. Konya[98], R. Kopeliansky[68], S. Koperny[86a], K. Korcyl[87], K. Kordas[152,f], G. Koren[151], A. Korn[96], S. Korn[55], I. Korolkov[13],

N. Korotkova[37], B. Kortman[114], O. Kortner[110], S. Kortner[110], W.H. Kostecka[115], V.V. Kostyukhin[141], A. Kotsokechagia[135], A. Kotwal[51], A. Koulouris[36], A. Kourkoumeli-Charalampidi[73a,73b], C. Kourkoumelis[9], E. Kourlitis[110,as], O. Kovanda[146], R. Kowalewski[165], W. Kozanecki[135], A.S. Kozhin[37], V.A. Kramarenko[37], G. Kramberger[93], P. Kramer[100], M.W. Krasny[127], A. Krasznahorkay[36], J.W. Kraus[171], J.A. Kremer[100], T. Kresse[50], J. Kretzschmar[92], K. Kreul[18], P. Krieger[155], S. Krishnamurthy[103], M. Krivos[133], K. Krizka[20], K. Kroeninger[49], H. Kroha[110], J. Kroll[131], J. Kroll[128], K.S. Krowpman[107], U. Kruchonak[38], H. Krüger[24], N. Krumnack[81], M.C. Kruse[51], J.A. Krzysiak[87], O. Kuchinskaia[37], S. Kuday[3a], S. Kuehn[36], R. Kuesters[54], T. Kuhl[48], V. Kukhtin[38], Y. Kulchitsky[37,a], S. Kuleshov[137d,137b], M. Kumar[33g], N. Kumari[48], A. Kupco[131], T. Kupfer[49], A. Kupich[37], O. Kuprash[54], H. Kurashige[85], L.L. Kurchaninov[156a], O. Kurdysh[66], Y.A. Kurochkin[37], A. Kurova[37], M. Kuze[154], A.K. Kvam[103], J. Kvita[122], T. Kwan[104], N.G. Kyriacou[106], L.A.O. Laatu[102], C. Lacasta[163], F. Lacava[75a,75b], H. Lacker[18], D. Lacour[127], N.N. Lad[96], E. Ladygin[38], B. Laforge[127], T. Lagouri[137e], F.Z. Lahbabi[35a], S. Lai[55], I.K. Lakomiec[86a], N. Lalloue[60], J.E. Lambert[165,o], S. Lammers[68], W. Lampl[7], C. Lampoudis[152,f], A.N. Lancaster[115], E. Lançon[29], U. Landgraf[54], M.P.J. Landon[94], V.S. Lang[54], R.J. Langenberg[103], O.K.B. Langrekken[125], A.J. Lankford[160], F. Lanni[36], K. Lantzsch[24], A. Lanza[73a], A. Lapertosa[57b,57a], J.F. Laporte[135], T. Lari[71a], F. Lasagni Manghi[23b], M. Lassnig[36], V. Latonova[131], A. Laudrain[100], A. Laurier[150], S.D. Lawlor[95], Z. Lawrence[101], M. Lazzaroni[71a,71b], B. Le[101], E.M. Le Boulicaut[51], B. Leban[93], A. Lebedev[81], M. LeBlanc[101,aq], F. Ledroit-Guillon[60], A.C.A. Lee[96], S.C. Lee[148], S. Lee[47a,47b], T.F. Lee[92], L.L. Leeuw[33c], H.P. Lefebvre[95], M. Lefebvre[165], C. Leggett[17a], G. Lehmann Miotto[36], M. Leigh[56], W.A. Leight[103], W. Leinonen[113], A. Leisos[152,ab], M.A.L. Leite[83c], C.E. Leitgeb[48], R. Leitner[133], K.J.C. Leney[44], T. Lenz[24], S. Leone[74a], C. Leonidopoulos[52], A. Leopold[144], C. Leroy[108], R. Les[107], C.G. Lester[32], M. Levchenko[37], J. Levêque[4], D. Levin[106], L.J. Levinson[169], M.P. Lewicki[87], D.J. Lewis[4], A. Li[5], B. Li[62b], C. Li[62a], C.-Q. Li[62c], H. Li[62a], H. Li[62b], H. Li[14c], H. Li[14b], H. Li[62b], K. Li[138], L. Li[62c], M. Li[14a,14e], Q.Y. Li[62a], S. Li[14a,14e], S. Li[62d,62c,e], T. Li[5,c], X. Li[104], Z. Li[126], Z. Li[104], Z. Li[92], Z. Li[14a,14e], S. Liang[14a,14e], Z. Liang[14a], M. Liberatore[135,ak], B. Liberti[76a], K. Lie[64c], J. Lieber Marin[83b], H. Lien[68], K. Lin[107], R.E. Lindley[7], J.H. Lindon[2], E. Lipeles[128], A. Lipniacka[16], A. Lister[164], J.D. Little[4], B. Liu[14a], B.X. Liu[142], D. Liu[62d,62c], J.B. Liu[62a], J.K.K. Liu[32], K. Liu[62d,62c], M. Liu[62a], M.Y. Liu[62a], P. Liu[14a], Q. Liu[62d,138,62c], X. Liu[62a], Y. Liu[14d,14e], Y.L. Liu[62b], Y.W. Liu[62a], J. Llorente Merino[142], S.L. Lloyd[94], E.M. Lobodzinska[48], P. Loch[7], S. Loffredo[76a,76b], T. Lohse[18], K. Lohwasser[139], E. Loiacono[48], M. Lokajicek[131,**], J.D. Lomas[20], J.D. Long[162], I. Longarini[160], L. Longo[70a,70b], R. Longo[162], I. Lopez Paz[67], A. Lopez Solis[48], J. Lorenz[109], N. Lorenzo Martinez[4], A.M. Lory[109], G. Löschcke Centeno[146], O. Loseva[37], X. Lou[47a,47b], X. Lou[14a,14e], A. Lounis[66], J. Love[6], P.A. Love[91], G. Lu[14a,14e], M. Lu[80], S. Lu[128], Y.J. Lu[65], H.J. Lubatti[138], C. Luci[75a,75b], F.L. Lucio Alves[14c], A. Lucotte[60], F. Luehring[68], I. Luise[145], O. Lukianchuk[66], O. Lundberg[144], B. Lund-Jensen[144], N.A. Luongo[123], M.S. Lutz[151], D. Lynn[29], H. Lyons[92], R. Lysak[131], E. Lytken[98], V. Lyubushkin[38], T. Lyubushkina[38], M.M. Lyukova[145], H. Ma[29], K. Ma[62a], L.L. Ma[62b], Y. Ma[121], D.M. Mac Donell[165], G. Maccarrone[53], J.C. MacDonald[100], R. Madar[40], W.F. Mader[50], T. Madula[96], J. Maeda[85], T. Maeno[29], M. Maerker[50], H. Maguire[139], V. Maiboroda[135], A. Maio[130a,130b,130d], K. Maj[86a], O. Majersky[48], S. Majewski[123], N. Makovec[66], V. Maksimovic[15], B. Malaescu[127], Pa. Malecki[87], V.P. Maleev[37], F. Malek[60], M. Mali[93], D. Malito[95,t], U. Mallik[80], S. Maltezos[10], S. Malyukov[38], J. Mamuzic[13], G. Mancini[53], G. Manco[73a,73b], J.P. Mandalia[94], I. Mandić[93], L. Manhaes de Andrade Filho[83a], I.M. Maniatis[169], J. Manjarres Ramos[102,al], D.C. Mankad[169], A. Mann[109], B. Mansoulie[135], S. Manzoni[36], A. Marantis[152,ab], G. Marchiori[5], M. Marcisovsky[131], C. Marcon[71a,71b], M. Marinescu[20], M. Marjanovic[120], E.J. Marshall[91], Z. Marshall[17a], S. Marti-Garcia[163], T.A. Martin[167], V.J. Martin[52], B. Martin dit Latour[16], L. Martinelli[75a,75b], M. Martinez[13,ac], P. Martinez Agullo[163], V.I. Martinez Outschoorn[103], P. Martinez Suarez[13], S. Martin-Haugh[134], V.S. Martoiu[27b], A.C. Martyniuk[96], A. Marzin[36], D. Mascione[78a,78b], L. Masetti[100], T. Mashimo[153], J. Masik[101], A.L. Maslennikov[37], L. Massa[23b], P. Massarotti[72a,72b], P. Mastrandrea[74a,74b], A. Mastroberardino[43b,43a], T. Masubuchi[153], T. Mathisen[161], J. Matousek[133], N. Matsuzawa[153], J. Maurer[27b], B. Maček[93], D.A. Maximov[37], R. Mazini[148], I. Maznas[152], M. Mazza[107], S.M. Mazza[136], E. Mazzeo[71a,71b], C. Mc Ginn[29], J.P. Mc Gowan[104], S.P. Mc Kee[106], E.F. McDonald[105], A.E. McDougall[114], J.A. Mcfayden[146], R.P. McGovern[128], G. Mchedlidze[149b], R.P. Mckenzie[33g], T.C. Mclachlan[48], D.J. Mclaughlin[96], K.D. McLean[165], S.J. McMahon[134], P.C. McNamara[105], C.M. Mcpartland[92], R.A. McPherson[165,ag], S. Mehlhase[109], A. Mehta[92], D. Melini[150], B.R. Mellado Garcia[33g], A.H. Melo[55], F. Meloni[48], A.M. Mendes Jacques Da Costa[101], H.Y. Meng[155], L. Meng[91], S. Menke[110], M. Mentink[36], E. Meoni[43b,43a], C. Merlassino[126], L. Merola[72a,72b], C. Meroni[71a,71b], G. Merz[106], O. Meshkov[37], J. Metcalfe[6], A.S. Mete[6], C. Meyer[68], J.-P. Meyer[135], R.P. Middleton[134], L. Mijović[52], G. Mikenberg[169], M. Mikestikova[131], M. Mikuž[93], H. Mildner[100], A. Milic[36], C.D. Milke[44], D.W. Miller[39], L.S. Miller[34], A. Milov[169], D.A. Milstead[47a,47b], T. Min[14c], A.A. Minaenko[37], I.A. Minashvili[149b], L. Mince[59], A.I. Mincer[117], B. Mindur[86a], M. Mineev[38], Y. Mino[88], L.M. Mir[13], M. Miralles Lopez[163], M. Mironova[17a], A. Mishima[153], M.C. Missio[113], A. Mitra[167], V.A. Mitsou[163], Y. Mitsumori[111], O. Miu[155], P.S. Miyagawa[94], T. Mkrtchyan[63a], M. Mlinarevic[96], T. Mlinarevic[96], M. Mlynarikova[36], S. Mobius[19], P. Moder[48], P. Mogg[109], A.F. Mohammed[14a,14e], S. Mohapatra[41], G. Mokgatitswane[33g], L. Moleri[169], B. Mondal[141], S. Mondal[132], G. Monig[146], K. Mönig[48], E. Monnier[102], L. Monsonis Romero[163], J. Montejo Berlingen[13], M. Montella[119], F. Montereali[77a,77b], F. Monticelli[90], S. Monzani[69a,69c], N. Morange[66], A.L. Moreira De Carvalho[130a], M. Moreno Llácer[163], C. Moreno Martinez[56], P. Morettini[57b], S. Morgenstern[36], M. Morii[61], M. Morinaga[153], A.K. Morley[36], F. Morodei[75a,75b], L. Morvaj[36], P. Moschovakos[36], B. Moser[36], M. Mosidze[149b], T. Moskalets[54], P. Moskvitina[113], J. Moss[31,q], E.J.W. Moyse[103], O. Mtintsilana[33g], S. Muanza[102], J. Mueller[129], D. Muenstermann[91], R. Müller[19], G.A. Mullier[161], A.J. Mullin[32], J.J. Mullin[128], D.P. Mungo[155], D. Munoz Perez[163], F.J. Munoz Sanchez[101], M. Murin[101], W.J. Murray[167,134], A. Murrone[71a,71b], J.M. Muse[120], M. Muškinja[17a], C. Mwewa[29], A.G. Myagkov[37,a], A.J. Myers[8], A.A. Myers[129], G. Myers[68], M. Myska[132], B.P. Nachman[17a], O. Nackenhorst[49], A. Nag[50], K. Nagai[126], K. Nagano[84], J.L. Nagle[29,aw], E. Nagy[102], A.M. Nairz[36], Y. Nakahama[84], K. Nakamura[84], K. Nakkalil[5], H. Nanjo[124], R. Narayan[44], E.A. Narayanan[112], I. Naryshkin[37], M. Naseri[34], S. Nasri[159], C. Nass[24], G. Navarro[22a], J. Navarro-Gonzalez[163], R. Nayak[151], A. Nayaz[18], P.Y. Nechaeva[37], F. Nechansky[48], L. Nedic[126], T.J. Neep[20], A. Negri[73a,73b], M. Negrini[23b], C. Nellist[114], C. Nelson[104], K. Nelson[106], S. Nemecek[131], M. Nessi[36,j], M.S. Neubauer[162], F. Neuhaus[100], J. Neundorf[48], R. Newhouse[164], P.R. Newman[20], C.W. Ng[129], Y.W.Y. Ng[48], B. Ngair[35e], H.D.N. Nguyen[108], R.B. Nickerson[126], R. Nicolaidou[135], J. Nielsen[136], M. Niemeyer[55], J. Niermann[55,36], N. Nikiforou[36], V. Nikolaenko[37,a], I. Nikolic-Audit[127], K. Nikolopoulos[20], P. Nilsson[29], I. Ninca[48], H.R. Nindhito[56], G. Ninio[151], A. Nisati[75a], N. Nishu[2], R. Nisius[110], J.-E. Nitschke[50], E.K. Nkadimeng[33g], S.J. Noacco Rosende[90], T. Nobe[153], D.L. Noel[32], T. Nommensen[147],

M.B. Norfolk[139], R.R.B. Norisam[96], B.J. Norman[34], J. Novak[93], T. Novak[48], L. Novotny[132], R. Novotny[112], L. Nozka[122], K. Ntekas[160], N.M.J. Nunes De Moura Junior[83b], E. Nurse[96], J. Ocariz[127], A. Ochi[85], I. Ochoa[130a], S. Oerdek[48,z], J.T. Offermann[39], A. Ogrodnik[133], A. Oh[101], C.C. Ohm[144], H. Oide[84], R. Oishi[153], M.L. Ojeda[48], M.W. O'Keefe[92], Y. Okumura[153], L.F. Oleiro Seabra[130a], S.A. Olivares Pino[137d], D. Oliveira Damazio[29], D. Oliveira Goncalves[83a], J.L. Oliver[160], A. Olszewski[87], Ö.O. Öncel[54], A.P. O'Neill[19], A. Onofre[130a,130e], P.U.E. Onyisi[11], M.J. Oreglia[39], G.E. Orellana[90], D. Orestano[77a,77b], N. Orlando[13], R.S. Orr[155], V. O'Shea[59], L.M. Osojnak[128], R. Ospanov[62a], G. Otero y Garzon[30], H. Otono[89], P.S. Ott[63a], G.J. Ottino[17a], M. Ouchrif[35d], J. Ouellette[29], F. Ould-Saada[125], M. Owen[59], R.E. Owen[134], K.Y. Oyulmaz[21a], V.E. Ozcan[21a], N. Ozturk[8], S. Ozturk[82], H.A. Pacey[32], A. Pacheco Pages[13], C. Padilla Aranda[13], G. Padovano[75a,75b], S. Pagan Griso[17a], G. Palacino[68], A. Palazzo[70a,70b], S. Palestini[36], J. Pan[172], T. Pan[64a], D.K. Panchal[11], C.E. Pandini[114], J.G. Panduro Vazquez[95], H.D. Pandya[1], H. Pang[14b], P. Pani[48], G. Panizzo[69a,69c], L. Paolozzi[56], C. Papadatos[108], S. Parajuli[44], A. Paramonov[6], C. Paraskevopoulos[10], D. Paredes Hernandez[64b], T.H. Park[155], M.A. Parker[32], F. Parodi[57b,57a], E.W. Parrish[115], V.A. Parrish[52], J.A. Parsons[41], U. Parzefall[54], B. Pascual Dias[108], L. Pascual Dominguez[151], E. Pasqualucci[75a], S. Passaggio[57b], F. Pastore[95], P. Pasuwan[47a,47b], P. Patel[87], U.M. Patel[51], J.R. Pater[101], T. Pauly[36], J. Pearkes[143], M. Pedersen[125], R. Pedro[130a], S.V. Peleganchuk[37], O. Penc[36], E.A. Pender[52], H. Peng[62a], K.E. Penski[109], M. Penzin[37], B.S. Peralva[83d], A.P. Pereira Peixoto[60], L. Pereira Sanchez[47a,47b], D.V. Perepelitsa[29,aw], E. Perez Codina[156a], M. Perganti[10], L. Perini[71a,71b,**], H. Pernegger[36], O. Perrin[40], K. Peters[48], R.F.Y. Peters[101], B.A. Petersen[36], T.C. Petersen[42], E. Petit[102], V. Petousis[132], C. Petridou[152,f], A. Petrukhin[141], M. Pettee[17a], N.E. Pettersson[36], A. Petukhov[37], K. Petukhova[133], R. Pezoa[137f], L. Pezzotti[36], G. Pezzullo[172], T.M. Pham[170], T. Pham[105], P.W. Phillips[134], G. Piacquadio[145], E. Pianori[17a], F. Piazza[71a,71b], R. Piegaia[30], D. Pietreanu[27b], A.D. Pilkington[101], M. Pinamonti[69a,69c], J.L. Pinfold[2], B.C. Pinheiro Pereira[130a], A.E. Pinto Pinoargote[135], L. Pintucci[69a,69c], K.M. Piper[146], A. Pirttikoski[56], D.A. Pizzi[34], L. Pizzimento[64b], A. Pizzini[114], M.-A. Pleier[29], V. Plesanovs[54], V. Pleskot[133], E. Plotnikova[38], G. Poddar[4], R. Poettgen[98], L. Poggioli[127], I. Pokharel[55], S. Polacek[133], G. Polesello[73a], A. Poley[142,156a], R. Polifka[132], A. Polini[23b], C.S. Pollard[167], Z.B. Pollock[119], V. Polychronakos[29], E. Pompa Pacchi[75a,75b], D. Ponomarenko[113], L. Pontecorvo[36], S. Popa[27a], G.A. Popeneciu[27d], A. Poreba[36], D.M. Portillo Quintero[156a], S. Pospisil[132], M.A. Postill[139], P. Postolache[27c], K. Potamianos[167], P.A. Potepa[86a], I.N. Potrap[38], C.J. Potter[32], H. Potti[1], T. Poulsen[48], J. Poveda[163], M.E. Pozo Astigarraga[36], A. Prades Ibanez[163], J. Pretel[54], D. Price[101], M. Primavera[70a], M.A. Principe Martin[99], R. Privara[122], T. Procter[59], M.L. Proffitt[138], N. Proklova[128], K. Prokofiev[64c], G. Proto[110], S. Protopopescu[29], J. Proudfoot[6], M. Przybycien[86a], W.W. Przygoda[86b], J.E. Puddefoot[139], D. Pudzha[37], D. Pyatiizbyantseva[37], J. Qian[106], D. Qichen[101], Y. Qin[101], T. Qiu[52], A. Quadt[55], M. Queitsch-Maitland[101], G. Quetant[56], R.P. Quinn[164], G. Rabanal Bolanos[61], D. Rafanoharana[54], F. Ragusa[71a,71b], J.L. Rainbolt[39], J.A. Raine[56], S. Rajagopalan[29], E. Ramakoti[37], K. Ran[48,14e], N.P. Rapheeha[33g], H. Rasheed[27b], V. Raskina[127], D.F. Rassloff[63a], S. Rave[100], B. Ravina[55], I. Ravinovich[169], M. Raymond[36], A.L. Read[125], N.P. Readioff[139], D.M. Rebuzzi[73a,73b], G. Redlinger[29], A.S. Reed[110], K. Reeves[26], J.A. Reidelsturz[171,aa], D. Reikher[151], A. Rej[141], C. Rembser[36], A. Renardi[48], M. Renda[27b], M.B. Rendel[110], F. Renner[48], A.G. Rennie[160], A.L. Rescia[48], S. Resconi[71a], M. Ressegotti[57b,57a], S. Rettie[36], J.G. Reyes Rivera[107], E. Reynolds[17a], O.L. Rezanova[37], P. Reznicek[133], N. Ribaric[91], E. Ricci[78a,78b], R. Richter[110], S. Richter[47a,47b], E. Richter-Was[86b], M. Ridel[127], S. Ridouani[35d], P. Rieck[117], P. Riedler[36], M. Rijssenbeek[145], A. Rimoldi[73a,73b], M. Rimoldi[48], L. Rinaldi[23b,23a], T.T. Rinn[29], M.P. Rinnagel[109], G. Ripellino[161], I. Riu[13], P. Rivadeneira[48], J.C. Rivera Vergara[165], F. Rizatdinova[121], E. Rizvi[94], B.A. Roberts[167], B.R. Roberts[17a], S.H. Robertson[104,ag], D. Robinson[32], C.M. Robles Gajardo[137f], M. Robles Manzano[100], A. Robson[59], A. Rocchi[76a,76b], C. Roda[74a,74b], S. Rodriguez Bosca[63a], Y. Rodriguez Garcia[22a], A. Rodriguez Rodriguez[54], A.M. Rodríguez Vera[156b], S. Roe[36], J.T. Roemer[160], A.R. Roepe-Gier[136], J. Roggel[171], O. Røhne[125], R.A. Rojas[103], C.P.A. Roland[68], J. Roloff[29], A. Romaniouk[37], E. Romano[73a,73b], M. Romano[23b], A.C. Romero Hernandez[162], N. Rompotis[92], L. Roos[127], S. Rosati[75a], B.J. Rosser[39], E. Rossi[126], E. Rossi[72a,72b], L.P. Rossi[57b], L. Rossini[54], R. Rosten[119], M. Rotaru[27b], B. Rottler[54], C. Rougier[102,al], D. Rousseau[66], D. Rousso[32], A. Roy[162], S. Roy-Garand[155], A. Rozanov[102], Y. Rozen[150], X. Ruan[33g], A. Rubio Jimenez[163], A.J. Ruby[92], V.H. Ruelas Rivera[18], T.A. Ruggeri[1], A. Ruggiero[126], A. Ruiz-Martinez[163], A. Rummler[36], Z. Rurikova[54], N.A. Rusakovich[38], H.L. Russell[165], G. Russo[75a,75b], J.P. Rutherfoord[7], S. Rutherford Colmenares[32], K. Rybacki[91], M. Rybar[133], E.B. Rye[125], A. Ryzhov[44], J.A. Sabater Iglesias[56], P. Sabatini[163], L. Sabetta[75a,75b], H.F.-W. Sadrozinski[136], F. Safai Tehrani[75a], B. Safarzadeh Samani[146], M. Safdari[143], S. Saha[165], M. Sahinsoy[110], M. Saimpert[135], M. Saito[153], T. Saito[153], D. Salamani[36], A. Salnikov[143], J. Salt[163], A. Salvador Salas[13], D. Salvatore[43b,43a], F. Salvatore[146], A. Salzburger[36], D. Sammel[54], D. Sampsonidis[152,f], D. Sampsonidou[123], J. Sánchez[163], A. Sanchez Pineda[4], V. Sanchez Sebastian[163], H. Sandaker[125], C.O. Sander[48], J.A. Sandesara[103], M. Sandhoff[171], C. Sandoval[22b], D.P.C. Sankey[134], T. Sano[88], A. Sansoni[53], L. Santi[75a,75b], C. Santoni[40], H. Santos[130a,130b], S.N. Santpur[17a], A. Santra[169], K.A. Saoucha[139], J.G. Saraiva[130a,130d], J. Sardain[7], O. Sasaki[84], K. Sato[157], C. Sauer[63b], F. Sauerburger[54], E. Sauvan[4], P. Savard[155,au], R. Sawada[153], C. Sawyer[134], L. Sawyer[97], I. Sayago Galvan[163], C. Sbarra[23b], A. Sbrizzi[23b,23a], T. Scanlon[96], J. Schaarschmidt[138], P. Schacht[110], D. Schaefer[39], U. Schäfer[100], A.C. Schaffer[66,44], D. Schaile[109], R.D. Schamberger[145], C. Scharf[18], M.M. Schefer[19], V.A. Schegelsky[37], D. Scheirich[133], F. Schenck[18], M. Schernau[160], C. Scheulen[55], C. Schiavi[57b,57a], E.J. Schioppa[70a,70b], M. Schioppa[43b,43a], B. Schlag[143,u], K.E. Schleicher[54], S. Schlenker[36], J. Schmeing[171], M.A. Schmidt[171], K. Schmieden[100], C. Schmitt[100], S. Schmitt[48], L. Schoeffel[135], A. Schoening[63b], P.G. Scholer[54], E. Schopf[126], M. Schott[100], J. Schovancova[36], S. Schramm[56], F. Schroeder[171], T. Schroer[56], H.-C. Schultz-Coulon[63a], M. Schumacher[54], B.A. Schumm[136], Ph. Schune[135], A.J. Schuy[138], H.R. Schwartz[136], A. Schwartzman[143], T.A. Schwarz[106], Ph. Schwemling[135], R. Schwienhorst[107], A. Sciandra[136], G. Sciolla[26], F. Scuri[74a], C.D. Sebastiani[92], K. Sedlaczek[115], P. Seema[18], S.C. Seidel[112], A. Seiden[136], B.D. Seidlitz[41], C. Seitz[48], J.M. Seixas[83b], G. Sekhniaidze[72a], S.J. Sekula[44], L. Selem[60], N. Semprini-Cesari[23b,23a], D. Sengupta[56], V. Senthilkumar[163], L. Serin[66], L. Serkin[69a,69b], M. Sessa[76a,76b], H. Severini[120], F. Sforza[57b,57a], A. Sfyrla[56], E. Shabalina[55], R. Shaheen[144], J.D. Shahinian[128], D. Shaked Renous[169], L.Y. Shan[14a], M. Shapiro[17a], A. Sharma[36], A.S. Sharma[164], P. Sharma[80], S. Sharma[48], P.B. Shatalov[37], K. Shaw[146], S.M. Shaw[101], A. Shcherbakova[37], Q. Shen[62c,5], P. Sherwood[96], L. Shi[96], X. Shi[14a], C.O. Shimmin[172], J.D. Shinner[95], I.P.J. Shipsey[126], S. Shirabe[56,j], M. Shiyakova[38,ae], J. Shlomi[169], M.J. Shochet[39], J. Shojaii[105], D.R. Shope[125], B. Shrestha[120], S. Shrestha[119,ax], E.M. Shrif[33g], M.J. Shroff[165], P. Sicho[131], A.M. Sickles[162], E. Sideras Haddad[33g], A. Sidoti[23b], F. Siegert[50], Dj. Sijacki[15], R. Sikora[86a], F. Sili[90], J.M. Silva[20], M.V. Silva Oliveira[29], S.B. Silverstein[47a], S. Simion[66], R. Simoniello[36], E.L. Simpson[59], H. Simpson[146], L.R. Simpson[106],

N.D. Simpson[98], S. Simsek[82], S. Sindhu[55], P. Sinervo[155], S. Singh[155], S. Sinha[48], S. Sinha[101], M. Sioli[23b,23a], I. Siral[36], E. Sitnikova[48], S.Yu. Sivoklokov[37,**], J. Sjölin[47a,47b], A. Skaf[55], E. Skorda[20,ap], P. Skubic[120], M. Slawinska[87], V. Smakhtin[169], B.H. Smart[134], J. Smiesko[36], S.Yu. Smirnov[37], Y. Smirnov[37], L.N. Smirnova[37,a], O. Smirnova[98], A.C. Smith[41], E.A. Smith[39], H.A. Smith[126], J.L. Smith[92], R. Smith[143], M. Smizanska[91], K. Smolek[132], A.A. Snesarev[37], S.R. Snider[155], H.L. Snoek[114], S. Snyder[29], R. Sobie[165,ag], A. Soffer[151], C.A. Solans Sanchez[36], E.Yu. Soldatov[37], U. Soldevila[163], A.A. Solodkov[37], S. Solomon[26], A. Soloshenko[38], K. Solovieva[54], O.V. Solovyanov[40], V. Solovyev[37], P. Sommer[36], A. Sonay[13], W.Y. Song[156b], J.M. Sonneveld[114], A. Sopczak[132], A.L. Sopio[96], F. Sopkova[28b], V. Sothilingam[63a], S. Sottocornola[68], R. Soualah[116b], Z. Soumaimi[35e], D. South[48], N. Soybelman[169], S. Spagnolo[70a,70b], M. Spalla[110], D. Sperlich[54], G. Spigo[36], S. Spinali[91], D.P. Spiteri[59], M. Spousta[133], E.J. Staats[34], A. Stabile[71a,71b], R. Stamen[63a], A. Stampekis[20], M. Standke[24], E. Stanecka[87], M.V. Stange[50], B. Stanislaus[17a], M.M. Stanitzki[48], B. Stapf[48], E.A. Starchenko[37], G.H. Stark[136], J. Stark[102,al], D.M. Starko[156b], P. Staroba[131], P. Starovoitov[63a], S. Stärz[104], R. Staszewski[87], G. Stavropoulos[46], J. Steentoft[161], P. Steinberg[29], B. Stelzer[142,156a], H.J. Stelzer[129], O. Stelzer-Chilton[156a], H. Stenzel[58], T.J. Stevenson[146], G.A. Stewart[36], J.R. Stewart[121], M.C. Stockton[36], G. Stoicea[27b], M. Stolarski[130a], S. Stonjek[110], A. Straessner[50], J. Strandberg[144], S. Strandberg[47a,47b], M. Strauss[120], T. Strebler[102], P. Strizenec[28b], R. Ströhmer[166], D.M. Strom[123], L.R. Strom[48], R. Stroynowski[44], A. Strubig[47a,47b], S.A. Stucci[29], B. Stugu[16], J. Stupak[120], N.A. Styles[48], D. Su[143], S. Su[62a], W. Su[62d], X. Su[62a,66], K. Sugizaki[153], V.V. Sulin[37], M.J. Sullivan[92], D.M.S. Sultan[78a,78b], L. Sultanaliyeva[37], S. Sultansoy[3b], T. Sumida[88], S. Sun[106], S. Sun[170], O. Sunneborn Gudnadottir[161], N. Sur[102], M.R. Sutton[146], H. Suzuki[157], M. Svatos[131], M. Swiatlowski[156a], T. Swirski[166], I. Sykora[28a], M. Sykora[133], T. Sykora[133], D. Ta[100], K. Tackmann[48,ad], A. Taffard[160], R. Tafirout[156a], J.S. Tafoya Vargas[66], E.P. Takeva[52], Y. Takubo[84], M. Talby[102], A.A. Talyshev[37], K.C. Tam[64b], N.M. Tamir[151], A. Tanaka[153], J. Tanaka[153], R. Tanaka[66], M. Tanasini[57b,57a], Z. Tao[164], S. Tapia Araya[137f], S. Tapprogge[100], A. Tarek Abouelfadl Mohamed[107], S. Tarem[150], K. Tariq[14a], G. Tarna[102,27b], G.F. Tartarelli[71a], P. Tas[133], M. Tasevsky[131], E. Tassi[43b,43a], A.C. Tate[162], G. Tateno[153], Y. Tayalati[35e,af], G.N. Taylor[105], W. Taylor[156b], H. Teagle[92], A.S. Tee[170], R. Teixeira De Lima[143], P. Teixeira-Dias[95], J.J. Teoh[155], K. Terashi[153], J. Terron[99], S. Terzo[13], M. Testa[53], R.J. Teuscher[155,ag], A. Thaler[79], O. Theiner[56], N. Themistokleous[52], T. Theveneaux-Pelzer[102], O. Thielmann[171], D.W. Thomas[95], J.P. Thomas[20], E.A. Thompson[17a], P.D. Thompson[20], E. Thomson[128], Y. Tian[55], V. Tikhomirov[37,a], Yu.A. Tikhonov[37], S. Timoshenko[37], D. Timoshyn[133], E.X.L. Ting[1], P. Tipton[172], S.H. Tlou[33g], A. Tnourji[40], K. Todome[154], S. Todorova-Nova[133], S. Todt[50], M. Togawa[84], J. Tojo[89], S. Tokár[28a], K. Tokushuku[84], O. Toldaiev[68], R. Tombs[32], M. Tomoto[84,111], L. Tompkins[143,u], K.W. Topolnicki[86b], E. Torrence[123], H. Torres[102,al], E. Torró Pastor[163], M. Toscani[30], C. Tosciri[39], M. Tost[11], D.R. Tovey[139], A. Traeet[16], I.S. Trandafir[27b], T. Trefzger[166], A. Tricoli[29], I.M. Trigger[156a], S. Trincaz-Duvoid[127], D.A. Trischuk[26], B. Trocmé[60], C. Troncon[71a], L. Truong[33c], M. Trzebinski[87], A. Trzupek[87], F. Tsai[145], M. Tsai[106], A. Tsiamis[152,f], P.V. Tsiareshka[37], S. Tsigaridas[156a], A. Tsirigotis[152,ab], V. Tsiskaridze[155], E.G. Tskhadadze[149a], M. Tsopoulou[152,f], Y. Tsujikawa[88], I.I. Tsukerman[37], V. Tsulaia[17a], S. Tsuno[84], O. Tsur[150], K. Tsuri[118], D. Tsybychev[145], Y. Tu[64b], A. Tudorache[27b], V. Tudorache[27b], A.N. Tuna[36], S. Turchikhin[38], I. Turk Cakir[3a], R. Turra[71a], T. Turtuvshin[38,ah], P.M. Tuts[41], S. Tzamarias[152,f], P. Tzanis[10], E. Tzovara[100], F. Ukegawa[157], P.A. Ulloa Poblete[137c,137b], E.N. Umaka[29], G. Unal[36], M. Unal[11], A. Undrus[29], G. Unel[160], J. Urban[28b], P. Urquijo[105], G. Usai[8], R. Ushioda[154], M. Usman[108], Z. Uysal[21b], L. Vacavant[102], V. Vacek[132], B. Vachon[104], K.O.H. Vadla[125], T. Vafeiadis[36], A. Vaitkus[96], C. Valderanis[109], E. Valdes Santurio[47a,47b], M. Valente[156a], S. Valentinetti[23b,23a], A. Valero[163], E. Valiente Moreno[163], A. Vallier[102,al], J.A. Valls Ferrer[163], D.R. Van Arneman[114], T.R. Van Daalen[138], A. Van Der Graaf[49], P. Van Gemmeren[6], M. Van Rijnbach[125,36], S. Van Stroud[96], I. Van Vulpen[114], M. Vanadia[76a,76b], W. Vandelli[36], M. Vandenbroucke[135], E.R. Vandewall[121], D. Vannicola[151], L. Vannoli[57b,57a], R. Vari[75a], E.W. Varnes[7], C. Varni[17b], T. Varol[148], D. Varouchas[66], L. Varriale[163], K.E. Varvell[147], M.E. Vasile[27b], L. Vaslin[40], G.A. Vasquez[165], A. Vasyukov[38], F. Vazeille[40], T. Vazquez Schroeder[36], J. Veatch[31], V. Vecchio[101], M.J. Veen[103], I. Veliscek[126], L.M. Veloce[155], F. Veloso[130a,130c], S. Veneziano[75a], A. Ventura[70a,70b], S. Ventura Gonzalez[135], A. Verbytskyi[110], M. Verducci[74a,74b], C. Vergis[24], M. Verissimo De Araujo[83b], W. Verkerke[114], J.C. Vermeulen[114], C. Vernieri[143], M. Vessella[103], M.C. Vetterli[142,au], A. Vgenopoulos[152,f], N. Viaux Maira[137f], T. Vickey[139], O.E. Vickey Boeriu[139], G.H.A. Viehhauser[126], L. Vigani[63b], M. Villa[23b,23a], M. Villaplana Perez[163], E.M. Villhauer[52], E. Vilucchi[53], M.G. Vincter[34], G.S. Virdee[20], A. Vishwakarma[52], A. Visibile[114], C. Vittori[36], I. Vivarelli[146], V. Vladimirov[167], E. Voevodina[110], F. Vogel[109], P. Vokac[132], Yu. Volkotrub[86a], J. Von Ahnen[48], E. Von Toerne[24], B. Vormwald[36], V. Vorobel[133], K. Vorobev[37], M. Vos[163], K. Voss[141], J.H. Vossebeld[92], M. Vozak[114], L. Vozdecky[94], N. Vranjes[15], M. Vranjes Milosavljevic[15], M. Vreeswijk[114], N.K. Vu[62d], R. Vuillermet[36], O. Vujinovic[100], I. Vukotic[39], S. Wada[157], C. Wagner[103], J.M. Wagner[17a], W. Wagner[171], S. Wahdan[171], H. Wahlberg[90], M. Wakida[111], J. Walder[134], R. Walker[109], W. Walkowiak[141], A. Wall[128], T. Wamorkar[6], A.Z. Wang[170], C. Wang[100], C. Wang[62c], H. Wang[17a], J. Wang[64a], R.-J. Wang[100], R. Wang[61], R. Wang[6], S.M. Wang[148], S. Wang[62b], T. Wang[62a], W.T. Wang[80], W. Wang[14a], X. Wang[14c], X. Wang[162], X. Wang[62c], Y. Wang[62d], Y. Wang[14c], Z. Wang[106], Z. Wang[62d,51,62c], Z. Wang[106], A. Warburton[104], R.J. Ward[20], N. Warrack[59], A.T. Watson[20], H. Watson[59], M.F. Watson[20], E. Watton[59,134], G. Watts[138], B.M. Waugh[96], C. Weber[29], H.A. Weber[18], M.S. Weber[19], S.M. Weber[63a], C. Wei[62a], Y. Wei[126], A.R. Weidberg[126], E.J. Weik[117], J. Weingarten[49], M. Weirich[100], C. Weiser[54], C.J. Wells[48], T. Wenaus[29], B. Wendland[49], T. Wengler[36], N.S. Wenke[110], N. Wermes[24], M. Wessels[63a], A.M. Wharton[91], A.S. White[61], A. White[8], M.J. White[1], D. Whiteson[160], L. Wickremasinghe[124], W. Wiedenmann[170], C. Wiel[50], M. Wielers[134], C. Wiglesworth[42], D.J. Wilbern[120], H.G. Wilkens[36], D.M. Williams[41], H.H. Williams[128], S. Williams[32], S. Willocq[103], B.J. Wilson[101], P.J. Windischhofer[39], F.I. Winkel[30], F. Winklmeier[123], B.T. Winter[54], J.K. Winter[101], M. Wittgen[143], M. Wobisch[97], Z. Wolffs[114], R. Wölker[126], J. Wollrath[160], M.W. Wolter[87], H. Wolters[130a,130c], A.F. Wongel[48], S.D. Worm[48], B.K. Wosiek[87], K.W. Woźniak[87], S. Wozniewski[55], K. Wraight[59], C. Wu[20], J. Wu[14a,14e], M. Wu[64a], M. Wu[113], S.L. Wu[170], X. Wu[56], Y. Wu[62a], Z. Wu[135], J. Wuerzinger[110,as], T.R. Wyatt[101], B.M. Wynne[52], S. Xella[42], L. Xia[14c], M. Xia[14b], J. Xiang[64c], M. Xie[62a], X. Xie[62a], S. Xin[14a,14e], J. Xiong[17a], D. Xu[14a], H. Xu[62a], L. Xu[62a], R. Xu[128], T. Xu[106], Y. Xu[14b], Z. Xu[52], Z. Xu[14a], B. Yabsley[147], S. Yacoob[33a], Y. Yamaguchi[154], E. Yamashita[153], H. Yamauchi[157], T. Yamazaki[17a], Y. Yamazaki[85], J. Yan[62c], S. Yan[126], Z. Yan[25], H.J. Yang[62c,62d], H.T. Yang[62a], S. Yang[62a], T. Yang[64c], X. Yang[62a], X. Yang[14a], Y. Yang[44], Y. Yang[62a], Z. Yang[62a], W.-M. Yao[17a], Y.C. Yap[48], H. Ye[14c], H. Ye[55], J. Ye[44], S. Ye[29], X. Ye[62a], Y. Yeh[96], I. Yeletskikh[38], B.K. Yeo[17b], M.R. Yexley[96], P. Yin[41], K. Yorita[168], S. Younas[27b], C.J.S. Young[36], C. Young[143], Y. Yu[62a], M. Yuan[106], R. Yuan[62b,m], L. Yue[96], M. Zaazoua[62a], B. Zabinski[87], E. Zaid[52],

T. Zakareishvili[149b], N. Zakharchuk[34], S. Zambito[56], J.A. Zamora Saa[137d,137b], J. Zang[153], D. Zanzi[54], O. Zaplatilek[132], C. Zeitnitz[171], H. Zeng[14a], J.C. Zeng[162], D.T. Zenger Jr[26], O. Zenin[37], T. Ženiš[28a], S. Zenz[94], S. Zerradi[35a], D. Zerwas[66], M. Zhai[14a,14e], B. Zhang[14c], D.F. Zhang[139], J. Zhang[62b], J. Zhang[6], K. Zhang[14a,14e], L. Zhang[14c], P. Zhang[14a,14e], R. Zhang[170], S. Zhang[106], T. Zhang[153], X. Zhang[62c], X. Zhang[62b], Y. Zhang[62c,5], Y. Zhang[96], Z. Zhang[17a], Z. Zhang[66], H. Zhao[138], P. Zhao[51], T. Zhao[62b], Y. Zhao[136], Z. Zhao[62a], A. Zhemchugov[38], J. Zheng[14c], K. Zheng[162], X. Zheng[62a], Z. Zheng[143], D. Zhong[162], B. Zhou[106], H. Zhou[7], N. Zhou[62c], Y. Zhou[7], C.G. Zhu[62b], J. Zhu[106], Y. Zhu[62c], Y. Zhu[62a], X. Zhuang[14a], K. Zhukov[37], V. Zhulanov[37], N.I. Zimine[38], J. Zinsser[63b], M. Ziolkowski[141], L. Živković[15], A. Zoccoli[23b,23a], K. Zoch[56], T.G. Zorbas[139], O. Zormpa[46], W. Zou[41], L. Zwalinski[36]

[1] *Department of Physics, University of Adelaide, Adelaide, Australia*
[2] *Department of Physics, University of Alberta, Edmonton, AB, Canada*
[3a] *Department of Physics, Ankara University, Ankara, Türkiye*
[3b] *Division of Physics, TOBB University of Economics and Technology, Ankara, Türkiye*
[4] *LAPP, Université Savoie Mont Blanc, CNRS/IN2P3, Annecy, France*
[5] *APC, Université Paris Cité, CNRS/IN2P3, Paris, France*
[6] *High Energy Physics Division, Argonne National Laboratory, Argonne, IL, United States of America*
[7] *Department of Physics, University of Arizona, Tucson, AZ, United States of America*
[8] *Department of Physics, University of Texas at Arlington, Arlington, TX, United States of America*
[9] *Physics Department, National and Kapodistrian University of Athens, Athens, Greece*
[10] *Physics Department, National Technical University of Athens, Zografou, Greece*
[11] *Department of Physics, University of Texas at Austin, Austin, TX, United States of America*
[12] *Institute of Physics, Azerbaijan Academy of Sciences, Baku, Azerbaijan*
[13] *Institut de Física d'Altes Energies (IFAE), Barcelona Institute of Science and Technology, Barcelona, Spain*
[14a] *Institute of High Energy Physics, Chinese Academy of Sciences, Beijing*
[14b] *Physics Department, Tsinghua University, Beijing*
[14c] *Department of Physics, Nanjing University, Nanjing*
[14d] *School of Science, Shenzhen Campus of Sun Yat-sen University*
[14e] *University of Chinese Academy of Science (UCAS), Beijing*
[15] *Institute of Physics, University of Belgrade, Belgrade, Serbia*
[16] *Department for Physics and Technology, University of Bergen, Bergen, Norway*
[17a] *Physics Division, Lawrence Berkeley National Laboratory, Berkeley, CA, United States of America*
[17b] *University of California, Berkeley, CA, United States of America*
[18] *Institut für Physik, Humboldt Universität zu Berlin, Berlin, Germany*
[19] *Albert Einstein Center for Fundamental Physics and Laboratory for High Energy Physics, University of Bern, Bern, Switzerland*
[20] *School of Physics and Astronomy, University of Birmingham, Birmingham, United Kingdom*
[21a] *Department of Physics, Bogazici University, Istanbul, Türkiye*
[21b] *Department of Physics Engineering, Gaziantep University, Gaziantep, Türkiye*
[21c] *Department of Physics, Istanbul University, Istanbul, Türkiye*
[22a] *Facultad de Ciencias y Centro de Investigaciónes, Universidad Antonio Nariño, Bogotá, Colombia*
[22b] *Departamento de Física, Universidad Nacional de Colombia, Bogotá, Colombia*
[23a] *Dipartimento di Fisica e Astronomia A. Righi, Università di Bologna, Bologna, Italy*
[23b] *INFN Sezione di Bologna, Italy*
[24] *Physikalisches Institut, Universität Bonn, Bonn, Germany*
[25] *Department of Physics, Boston University, Boston, MA, United States of America*
[26] *Department of Physics, Brandeis University, Waltham, MA, United States of America*
[27a] *Transilvania University of Brasov, Brasov, Romania*
[27b] *Horia Hulubei National Institute of Physics and Nuclear Engineering, Bucharest, Romania*
[27c] *Department of Physics, Alexandru Ioan Cuza University of Iasi, Iasi, Romania*
[27d] *National Institute for Research and Development of Isotopic and Molecular Technologies, Physics Department, Cluj-Napoca, Romania*
[27e] *National University of Science and Technology Politechnica, Bucharest, Romania*
[27f] *West University in Timisoara, Timisoara, Romania*
[27g] *Faculty of Physics, University of Bucharest, Bucharest, Romania*
[28a] *Faculty of Mathematics, Physics and Informatics, Comenius University, Bratislava, Slovak Republic*
[28b] *Department of Subnuclear Physics, Institute of Experimental Physics of the Slovak Academy of Sciences, Kosice, Slovak Republic*
[29] *Physics Department, Brookhaven National Laboratory, Upton, NY, United States of America*
[30] *Universidad de Buenos Aires, Facultad de Ciencias Exactas y Naturales, Departamento de Física, y CONICET, Instituto de Física de Buenos Aires (IFIBA), Buenos Aires, Argentina*
[31] *California State University, CA, United States of America*
[32] *Cavendish Laboratory, University of Cambridge, Cambridge, United Kingdom*
[33a] *Department of Physics, University of Cape Town, Cape Town, South Africa*
[33b] *iThemba Labs, Western Cape, South Africa*
[33c] *Department of Mechanical Engineering Science, University of Johannesburg, Johannesburg, South Africa*
[33d] *National Institute of Physics, University of the Philippines Diliman (Philippines)*
[33e] *University of South Africa, Department of Physics, Pretoria, South Africa*
[33f] *University of Zululand, KwaDlangezwa, South Africa*
[33g] *School of Physics, University of the Witwatersrand, Johannesburg, South Africa*
[34] *Department of Physics, Carleton University, Ottawa, ON, Canada*
[35a] *Faculté des Sciences Ain Chock, Réseau Universitaire de Physique des Hautes Energies - Université Hassan II, Casablanca, Morocco*
[35b] *Faculté des Sciences, Université Ibn-Tofail, Kénitra, Morocco*
[35c] *Faculté des Sciences Semlalia, Université Cadi Ayyad, LPHEA-Marrakech, Morocco*
[35d] *LPMR, Faculté des Sciences, Université Mohamed Premier, Oujda, Morocco*
[35e] *Faculté des sciences, Université Mohammed V, Rabat, Morocco*
[35f] *Institute of Applied Physics, Mohammed VI Polytechnic University, Ben Guerir, Morocco*
[36] *CERN, Geneva, Switzerland*
[37] *Affiliated with an institute covered by a cooperation agreement with CERN*
[38] *Affiliated with an international laboratory covered by a cooperation agreement with CERN*
[39] *Enrico Fermi Institute, University of Chicago, Chicago, IL, United States of America*
[40] *LPC, Université Clermont Auvergne, CNRS/IN2P3, Clermont-Ferrand, France*
[41] *Nevis Laboratory, Columbia University, Irvington, NY, United States of America*
[42] *Niels Bohr Institute, University of Copenhagen, Copenhagen, Denmark*

[43a] Dipartimento di Fisica, Università della Calabria, Rende, Italy
[43b] INFN Gruppo Collegato di Cosenza, Laboratori Nazionali di Frascati, Italy
[44] Physics Department, Southern Methodist University, Dallas, TX, United States of America
[45] Physics Department, University of Texas at Dallas, Richardson, TX, United States of America
[46] National Centre for Scientific Research "Demokritos", Agia Paraskevi, Greece
[47a] Department of Physics, Stockholm University, Sweden
[47b] Oskar Klein Centre, Stockholm, Sweden
[48] Deutsches Elektronen-Synchrotron DESY, Hamburg and Zeuthen, Germany
[49] Fakultät Physik, Technische Universität Dortmund, Dortmund, Germany
[50] Institut für Kern-und Teilchenphysik, Technische Universität Dresden, Dresden, Germany
[51] Department of Physics, Duke University, Durham, NC, United States of America
[52] SUPA-School of Physics and Astronomy, University of Edinburgh, Edinburgh, United Kingdom
[53] INFN e Laboratori Nazionali di Frascati, Frascati, Italy
[54] Physikalisches Institut, Albert-Ludwigs-Universität Freiburg, Freiburg, Germany
[55] II. Physikalisches Institut, Georg-August-Universität Göttingen, Göttingen, Germany
[56] Département de Physique Nucléaire et Corpusculaire, Université de Genève, Genève, Switzerland
[57a] Dipartimento di Fisica, Università di Genova, Genova, Italy
[57b] INFN Sezione di Genova, Italy
[58] II. Physikalisches Institut, Justus-Liebig-Universität Giessen, Giessen, Germany
[59] SUPA-School of Physics and Astronomy, University of Glasgow, Glasgow, United Kingdom
[60] LPSC, Université Grenoble Alpes, CNRS/IN2P3, Grenoble INP, Grenoble, France
[61] Laboratory for Particle Physics and Cosmology, Harvard University, Cambridge, MA, United States of America
[62a] Department of Modern Physics and State Key Laboratory of Particle Detection and Electronics, University of Science and Technology of China, Hefei
[62b] Institute of Frontier and Interdisciplinary Science and Key Laboratory of Particle Physics and Particle Irradiation (MOE), Shandong University, Qingdao
[62c] School of Physics and Astronomy, Shanghai Jiao Tong University, Key Laboratory for Particle Astrophysics and Cosmology (MOE), SKLPPC, Shanghai
[62d] Tsung-Dao Lee Institute, Shanghai
[63a] Kirchhoff-Institut für Physik, Ruprecht-Karls-Universität Heidelberg, Heidelberg, Germany
[63b] Physikalisches Institut, Ruprecht-Karls-Universität Heidelberg, Heidelberg, Germany
[64a] Department of Physics, Chinese University of Hong Kong, Shatin, N. T., Hong Kong
[64b] Department of Physics, University of Hong Kong, Hong Kong
[64c] Department of Physics and Institute for Advanced Study, Hong Kong University of Science and Technology, Clear Water Bay, Kowloon, Hong Kong
[65] Department of Physics, National Tsing Hua University, Hsinchu
[66] IJCLab, Université Paris-Saclay, CNRS/IN2P3, 91405, Orsay, France
[67] Centro Nacional de Microelectrónica (IMB-CNM-CSIC), Barcelona, Spain
[68] Department of Physics, Indiana University, Bloomington, IN, United States of America
[69a] INFN Gruppo Collegato di Udine, Sezione di Trieste, Udine, Italy
[69b] ICTP, Trieste, Italy
[69c] Dipartimento Politecnico di Ingegneria e Architettura, Università di Udine, Udine, Italy
[70a] INFN Sezione di Lecce, Italy
[70b] Dipartimento di Matematica e Fisica, Università del Salento, Lecce, Italy
[71a] INFN Sezione di Milano, Italy
[71b] Dipartimento di Fisica, Università di Milano, Milano, Italy
[72a] INFN Sezione di Napoli, Italy
[72b] Dipartimento di Fisica, Università di Napoli, Napoli, Italy
[73a] INFN Sezione di Pavia, Italy
[73b] Dipartimento di Fisica, Università di Pavia, Pavia, Italy
[74a] INFN Sezione di Pisa, Italy
[74b] Dipartimento di Fisica E. Fermi, Università di Pisa, Pisa, Italy
[75a] INFN Sezione di Roma, Italy
[75b] Dipartimento di Fisica, Sapienza Università di Roma, Roma, Italy
[76a] INFN Sezione di Roma Tor Vergata, Italy
[76b] Dipartimento di Fisica, Università di Roma Tor Vergata, Roma, Italy
[77a] INFN Sezione di Roma Tre, Italy
[77b] Dipartimento di Matematica e Fisica, Università Roma Tre, Roma, Italy
[78a] INFN-TIFPA, Italy
[78b] Università degli Studi di Trento, Trento, Italy
[79] Universität Innsbruck, Department of Astro and Particle Physics, Innsbruck, Austria
[80] University of Iowa, Iowa City, IA, United States of America
[81] Department of Physics and Astronomy, Iowa State University, Ames, IA, United States of America
[82] Istinye University, Sariyer, Istanbul, Türkiye
[83a] Departamento de Engenharia Elétrica, Universidade Federal de Juiz de Fora (UFJF), Juiz de Fora, Brazil
[83b] Universidade Federal do Rio De Janeiro COPPE/EE/IF, Rio de Janeiro, Brazil
[83c] Instituto de Física, Universidade de São Paulo, São Paulo, Brazil
[83d] Rio de Janeiro State University, Rio de Janeiro, Brazil
[84] KEK, High Energy Accelerator Research Organization, Tsukuba, Japan
[85] Graduate School of Science, Kobe University, Kobe, Japan
[86a] AGH University of Krakow, Faculty of Physics and Applied Computer Science, Krakow, Poland
[86b] Marian Smoluchowski Institute of Physics, Jagiellonian University, Krakow, Poland
[87] Institute of Nuclear Physics Polish Academy of Sciences, Krakow, Poland
[88] Faculty of Science, Kyoto University, Kyoto, Japan
[89] Research Center for Advanced Particle Physics and Department of Physics, Kyushu University, Fukuoka, Japan
[90] Instituto de Física La Plata, Universidad Nacional de La Plata and CONICET, La Plata, Argentina
[91] Physics Department, Lancaster University, Lancaster, United Kingdom
[92] Oliver Lodge Laboratory, University of Liverpool, Liverpool, United Kingdom
[93] Department of Experimental Particle Physics, Jožef Stefan Institute and Department of Physics, University of Ljubljana, Ljubljana, Slovenia
[94] School of Physics and Astronomy, Queen Mary University of London, London, United Kingdom
[95] Department of Physics, Royal Holloway University of London, Egham, United Kingdom
[96] Department of Physics and Astronomy, University College London, London, United Kingdom
[97] Louisiana Tech University, Ruston, LA, United States of America
[98] Fysiska institutionen, Lunds universitet, Lund, Sweden
[99] Departamento de Física Teorica C-15 and CIAFF, Universidad Autónoma de Madrid, Madrid, Spain

[100] Institut für Physik, Universität Mainz, Mainz, Germany
[101] School of Physics and Astronomy, University of Manchester, Manchester, United Kingdom
[102] CPPM, Aix-Marseille Université, CNRS/IN2P3, Marseille, France
[103] Department of Physics, University of Massachusetts, Amherst, MA, United States of America
[104] Department of Physics, McGill University, Montreal, QC, Canada
[105] School of Physics, University of Melbourne, Victoria, Australia
[106] Department of Physics, University of Michigan, Ann Arbor, MI, United States of America
[107] Department of Physics and Astronomy, Michigan State University, East Lansing, MI, United States of America
[108] Group of Particle Physics, University of Montreal, Montreal, QC, Canada
[109] Fakultät für Physik, Ludwig-Maximilians-Universität München, München, Germany
[110] Max-Planck-Institut für Physik (Werner-Heisenberg-Institut), München, Germany
[111] Graduate School of Science and Kobayashi-Maskawa Institute, Nagoya University, Nagoya, Japan
[112] Department of Physics and Astronomy, University of New Mexico, Albuquerque, NM, United States of America
[113] Institute for Mathematics, Astrophysics and Particle Physics, Radboud University/Nikhef, Nijmegen, Netherlands
[114] Nikhef National Institute for Subatomic Physics and University of Amsterdam, Amsterdam, Netherlands
[115] Department of Physics, Northern Illinois University, DeKalb, IL, United States of America
[116a] New York University Abu Dhabi, Abu Dhabi, United Arab Emirates
[116b] University of Sharjah, Sharjah, United Arab Emirates
[117] Department of Physics, New York University, New York, NY, United States of America
[118] Ochanomizu University, Otsuka, Bunkyo-ku, Tokyo, Japan
[119] Ohio State University, Columbus, OH, United States of America
[120] Homer L. Dodge Department of Physics and Astronomy, University of Oklahoma, Norman, OK, United States of America
[121] Department of Physics, Oklahoma State University, Stillwater, OK, United States of America
[122] Palacký University, Joint Laboratory of Optics, Olomouc, Czech Republic
[123] Institute for Fundamental Science, University of Oregon, Eugene, OR, United States of America
[124] Graduate School of Science, Osaka University, Osaka, Japan
[125] Department of Physics, University of Oslo, Oslo, Norway
[126] Department of Physics, Oxford University, Oxford, United Kingdom
[127] LPNHE, Sorbonne Université, Université Paris Cité, CNRS/IN2P3, Paris, France
[128] Department of Physics, University of Pennsylvania, Philadelphia, PA, United States of America
[129] Department of Physics and Astronomy, University of Pittsburgh, Pittsburgh, PA, United States of America
[130a] Laboratório de Instrumentação e Física Experimental de Partículas - LIP, Lisboa, Portugal
[130b] Departamento de Física, Faculdade de Ciências, Universidade de Lisboa, Lisboa, Portugal
[130c] Departamento de Física, Universidade de Coimbra, Coimbra, Portugal
[130d] Centro de Física Nuclear da Universidade de Lisboa, Lisboa, Portugal
[130e] Departamento de Física, Universidade do Minho, Braga, Portugal
[130f] Departamento de Física Teórica y del Cosmos, Universidad de Granada, Granada, Spain
[130g] Departamento de Física, Instituto Superior Técnico, Universidade de Lisboa, Lisboa, Portugal
[131] Institute of Physics of the Czech Academy of Sciences, Prague, Czech Republic
[132] Czech Technical University in Prague, Prague, Czech Republic
[133] Charles University, Faculty of Mathematics and Physics, Prague, Czech Republic
[134] Particle Physics Department, Rutherford Appleton Laboratory, Didcot, United Kingdom
[135] IRFU, CEA, Université Paris-Saclay, Gif-sur-Yvette, France
[136] Santa Cruz Institute for Particle Physics, University of California Santa Cruz, Santa Cruz, CA, United States of America
[137a] Departamento de Física, Pontificia Universidad Católica de, Chile, Santiago, Chile
[137b] Millennium Institute for Subatomic physics at high energy frontier (SAPHIR), Santiago, Chile
[137c] Instituto de Investigación Multidisciplinario en Ciencia y Tecnología, y Departamento de Física, Universidad de La Serena, Chile
[137d] Universidad Andres Bello, Department of Physics, Santiago, Chile
[137e] Instituto de Alta Investigación, Universidad de Tarapacá, Arica, Chile
[137f] Departamento de Física, Universidad Técnica Federico Santa María, Valparaíso, Chile
[138] Department of Physics, University of Washington, Seattle, WA, United States of America
[139] Department of Physics and Astronomy, University of Sheffield, Sheffield, United Kingdom
[140] Department of Physics, Shinshu University, Nagano, Japan
[141] Department Physik, Universität Siegen, Siegen, Germany
[142] Department of Physics, Simon Fraser University, Burnaby, BC, Canada
[143] SLAC National Accelerator Laboratory, Stanford, CA, United States of America
[144] Department of Physics, Royal Institute of Technology, Stockholm, Sweden
[145] Departments of Physics and Astronomy, Stony Brook University, Stony Brook, NY, United States of America
[146] Department of Physics and Astronomy, University of Sussex, Brighton, United Kingdom
[147] School of Physics, University of Sydney, Sydney, Australia
[148] Institute of Physics, Academia Sinica, Taipei
[149a] E. Andronikashvili Institute of Physics, Iv. Javakhishvili Tbilisi State University, Tbilisi, Georgia
[149b] High Energy Physics Institute, Tbilisi State University, Tbilisi, Georgia
[149c] University of Georgia, Tbilisi, Georgia
[150] Department of Physics, Technion, Israel Institute of Technology, Haifa, Israel
[151] Raymond and Beverly Sackler School of Physics and Astronomy, Tel Aviv University, Tel Aviv, Israel
[152] Department of Physics, Aristotle University of Thessaloniki, Thessaloniki, Greece
[153] International Center for Elementary Particle Physics and Department of Physics, University of Tokyo, Tokyo, Japan
[154] Department of Physics, Tokyo Institute of Technology, Tokyo, Japan
[155] Department of Physics, University of Toronto, Toronto, ON, Canada
[156a] TRIUMF, Vancouver, BC, Canada
[156b] Department of Physics and Astronomy, York University, Toronto, ON, Canada
[157] Division of Physics and Tomonaga Center for the History of the Universe, Faculty of Pure and Applied Sciences, University of Tsukuba, Tsukuba, Japan
[158] Department of Physics and Astronomy, Tufts University0, Medford, MA, United States of America
[159] United Arab Emirates University, Al Ain, United Arab Emirates

[160] Department of Physics and Astronomy, University of California Irvine, Irvine, CA, United States of America
[161] Department of Physics and Astronomy, University of Uppsala, Uppsala, Sweden
[162] Department of Physics, University of Illinois, Urbana, IL, United States of America
[163] Instituto de Física Corpuscular (IFIC), Centro Mixto Universidad de Valencia - CSIC, Valencia, Spain
[164] Department of Physics, University of British Columbia, Vancouver, BC, Canada
[165] Department of Physics and Astronomy, University of Victoria, Victoria, BC, Canada
[166] Fakultät für Physik und Astronomie, Julius-Maximilians-Universität Würzburg, Würzburg, Germany
[167] Department of Physics, University of Warwick, Coventry, United Kingdom
[168] Waseda University, Tokyo, Japan
[169] Department of Particle Physics and Astrophysics, Weizmann Institute of Science, Rehovot, Israel
[170] Department of Physics, University of Wisconsin, Madison, WI, United States of America
[171] Fakultät für Mathematik und Naturwissenschaften, Fachgruppe Physik, Bergische Universität Wuppertal, Wuppertal, Germany
[172] Department of Physics, Yale University, New Haven, CT, United States of America
[a] Also Affiliated with an institute covered by a cooperation agreement with CERN
[b] Also at An-Najah National University, Nablus, Palestine
[c] Also at APC, Université Paris Cité, CNRS/IN2P3, Paris, France
[d] Also at Borough of Manhattan Community College, City University of New York, New York, NY, United States of America
[e] Also at Center for High Energy Physics, Peking University, Beijing
[f] Also at Center for Interdisciplinary Research and Innovation (CIRI-AUTH), Thessaloniki, Greece
[g] Also at Centro Studi e Ricerche Enrico Fermi, Italy
[h] Also at CERN Tier-0, Switzerland
[i] Also at CERN, Geneva, Switzerland
[j] Also at Département de Physique Nucléaire et Corpusculaire, Université de Genève, Genève, Switzerland
[k] Also at Departament de Fisica de la Universitat Autonoma de Barcelona, Barcelona, Spain
[l] Also at Department of Financial and Management Engineering, University of the Aegean, Chios, Greece
[m] Also at Department of Physics and Astronomy, Michigan State University, East Lansing, MI, United States of America
[n] Also at Department of Physics and Astronomy, University of Sheffield, Sheffield, United Kingdom
[o] Also at Department of Physics and Astronomy, University of Victoria, Victoria, BC, Canada
[p] Also at Department of Physics, Ben Gurion University of the Negev, Beer Sheva, Israel
[q] Also at Department of Physics, California State University, Sacramento, United States of America
[r] Also at Department of Physics, King's College London, London, United Kingdom
[s] Also at Department of Physics, Oxford University, Oxford, United Kingdom
[t] Also at Department of Physics, Royal Holloway University of London, Egham, United Kingdom
[u] Also at Department of Physics, Stanford University, Stanford, CA, United States of America
[v] Also at Department of Physics, University of Fribourg, Fribourg, Switzerland
[w] Also at Department of Physics, University of Massachusetts, Amherst, MA, United States of America
[x] Also at Department of Physics, University of Thessaly, Greece
[y] Also at Department of Physics, Westmont College, Santa Barbara, United States of America
[z] Also at Institut für Experimentalphysik, Universität Hamburg, Hamburg, Germany
[aa] Also at Fakultät für Mathematik und Naturwissenschaften, Fachgruppe Physik, Bergische Universität Wuppertal, Wuppertal, Germany
[ab] Also at Hellenic Open University, Patras, Greece
[ac] Also at Institucio Catalana de Recerca i Estudis Avancats, ICREA, Barcelona, Spain
[ad] Also at Institut für Experimentalphysik, Universität Hamburg, Hamburg, Germany
[ae] Also at Institute for Nuclear Research and Nuclear Energy (INRNE) of the Bulgarian Academy of Sciences, Sofia, Bulgaria
[af] Also at Institute of Applied Physics, Mohammed VI Polytechnic University, Ben Guerir, Morocco
[ag] Also at Institute of Particle Physics (IPP), Canada
[ah] Also at Institute of Physics and Technology, Ulaanbaatar, Mongolia
[ai] Also at Institute of Physics, Azerbaijan Academy of Sciences, Baku, Azerbaijan
[aj] Also at Institute of Theoretical Physics, Ilia State University, Tbilisi, Georgia
[ak] Also at IRFU, CEA, Université Paris-Saclay, Gif-sur-Yvette, France
[al] Also at L2IT, Université de Toulouse, CNRS/IN2P3, UPS, Toulouse, France
[am] Also at Lawrence Livermore National Laboratory, Livermore, United States of America
[an] Also at National Institute of Physics, University of the Philippines Diliman (Philippines), Philippines
[ao] Also at Ochanomizu University, Otsuka, Bunkyo-ku, Tokyo, Japan
[ap] Also at School of Physics and Astronomy, University of Birmingham, Birmingham, United Kingdom
[aq] Also at School of Physics and Astronomy, University of Manchester, Manchester, United Kingdom
[ar] Also at SUPA - School of Physics and Astronomy, University of Glasgow, Glasgow, United Kingdom
[as] Also at Technical University of Munich, Munich, Germany
[at] Also at The Collaborative Innovation Center of Quantum Matter (CICQM), Beijing
[au] Also at TRIUMF, Vancouver, BC, Canada
[av] Also at Università di Napoli Parthenope, Napoli, Italy
[aw] Also at University of Colorado Boulder, Department of Physics, Colorado, United States of America
[ax] Also at Washington College, Chestertown, MD, United States of America
[ay] Also at Yeditepe University, Physics Department, Istanbul, Türkiye

[**] Deceased